

AFIT/GA/ENY/92D-05

**AD-A259 143**



**AN ELECTROMAGNETICALLY-CONTROLLED  
PRECISION ORBITAL TRACKING VEHICLE  
(POTV)**

**THESIS**

**Richard E. Lawrence Jr.  
Captain, USAF**

**AFIT/GA/ENY/92D-05**

**DTIC  
ELECTE  
JAN 1 1993  
S E D**

**Approved for public release; distribution unlimited**

**93-00042**

**93 1 04 117**

**AFIT/GA/ENY/92D-05**

**AN ELECTROMAGNETICALLY-CONTROLLED  
PRECISION ORBITAL TRACKING VEHICLE  
(POTV)**

**THESIS**

**Presented to the Faculty of the School of Engineering  
of the Air Force Institute of Technology  
Air University  
In Partial Fulfillment of the  
Requirements for the Degree of  
Master of Science in Astronautical Engineering**

**Richard E. Lawrence Jr., B.S.  
Captain, USAF**

**December, 1992**

**Approved for public release; distribution unlimited**

### *Acknowledgements*

I thank my thesis advisor, Dr. Curtis Spenny, for his ideas, patience, and enthusiastic support of this research. His office door was always open. I thank my committee members Dr. W. Wiesel, Dr. W. Bailey, and Capt C. Hall, for their respective assistance in the areas of orbits, geomagnetism, and dynamics. I also appreciate the personal interest that Dr. B. Liebst took in the control aspects of this research. This effort is dedicated to my dear wife Stephanie.

Richard E. Lawrence Jr.

Accession For	
NTIS	<input checked="checked" type="checkbox"/> CRA&I
DTIC	<input type="checkbox"/> TAB
Unannounced	<input type="checkbox"/>
Justification .....	
By .....	
Distribution /	
Availability Codes	
Dist	Avail and / or Special
A-1	

DTIC QUALITY INSPECTED 5

## *Table of Contents*

	Page
Acknowledgements . . . . .	ii
Table of Contents . . . . .	iii
List of Figures . . . . .	vi
Abstract . . . . .	vii
 I. Introduction . . . . .	 1-1
 II. Derivation of Equations of Motion . . . . .	 2-1
2.1 Coordinate Frames . . . . .	2-1
2.1.1 Coordinate Frame Description . . . . .	2-1
2.1.2 Rotation Matrices . . . . .	2-1
2.2 Unforced Equations of Motion . . . . .	2-6
2.2.1 Translational Equations . . . . .	2-6
2.2.2 Rotational Equations . . . . .	2-11
 III. Magnetic Forces and Moments . . . . .	 3-1
3.1 Geomagnetic Field Description . . . . .	3-1
3.2 Transformation to the Orbital Reference Frame . . . . .	3-2
3.3 Magnetic Forces and Moments for Design # 1 . . . . .	3-7
3.3.1 Magnetic Forces . . . . .	3-8
3.3.2 Magnetic Moments . . . . .	3-9
3.3.3 Complete Equations of Motion . . . . .	3-12
3.4 Magnetic Forces and Moments for Design # 2 . . . . .	3-12
3.4.1 Magnetic Forces . . . . .	3-13
3.4.2 Magnetic Moments . . . . .	3-14
3.4.3 Complete Equations of Motion . . . . .	3-15

	Page
IV. Tracking and Control Issues . . . . .	4-1
4.1 State Space Representation of Equations of Motion . . . . .	4-1
4.1.1 Eigenvalues and Stability . . . . .	4-5
4.1.2 Equilibrium Points . . . . .	4-6
4.1.3 Controllability . . . . .	4-6
4.2 Controller Design and Performance . . . . .	4-10
4.2.1 Stability Robustness . . . . .	4-14
4.2.2 Steady-State Controllability . . . . .	4-15
V. Steady-State Tracking and Docking Performance . . . . .	5-1
5.1 Vertical In-Plane Conductor Sizing for Orbit Transfer . . . . .	5-1
5.2 Steady-State Tracking Performance . . . . .	5-4
5.3 General Non-Steady-State Tracking Performance . . . . .	5-6
5.4 Docking Examples . . . . .	5-7
5.4.1 R-BAR . . . . .	5-7
5.4.2 V-BAR . . . . .	5-8
5.4.3 Z-BAR . . . . .	5-9
VI. Conclusions and Recommendations . . . . .	6-1
Appendix A. Plots of the Geomagnetic Field in the Orbital Reference Frame	A-1
Appendix B. Aerodynamic and Earth Oblateness Effects in Low Earth Orbit	B-1
Appendix C. Electrodynamic Propulsion Power Requirements . . . . .	C-1
Appendix D. Approximate Mass and Moments of Inertia for the POTV . .	D-1
Appendix E. Controller Design Program Results . . . . .	E-1
E.1 Steady-State Tracking Example . . . . .	E-1
E.2 R-BAR Docking Approach Example . . . . .	E-14
E.3 V-BAR Docking Approach Example . . . . .	E-27

	Page
Appendix F.      Controller Design Program Listing . . . . .	F-1
Bibliography . . . . .	BIB-1
Vita . . . . .	VITA-1

## *List of Figures*

Figure	Page
2.1. Coordinate Frames and Position Vectors . . . . .	2-2
3.1. Magnetic Dipole Moment Vector in the Greenwich Frame . . . . .	3-2
3.2. Design # 1 Conductor Configuration . . . . .	3-7
3.3. Design # 2 Conductor Configuration . . . . .	3-13
4.1. Closed-Loop System Block Diagram . . . . .	4-11
C.1. Electrical Model of the Conductor in Thruster Mode . . . . .	C-2
D.1. Truss Assembly for Conductor Towers . . . . .	D-2
E.1. R-BAR Tracking Vehicle Trajectory in the X-Y Plane . . . . .	E-26
E.2. V-BAR Tracking Vehicle Trajectory in the X-Y Plane . . . . .	E-39

*Abstract*

A propulsion configuration is defined for a precision orbital tracking vehicle (POTV) that employs electrodynamic forces to control vehicle attitude and position with respect to another spacecraft. A pair of electrically powered thrusters assist the POTV in position control. The vehicle can maintain continuous standoff at close range from another spacecraft in any direction, has docking capability, and has gross orbital transfer capability. These capabilities and the specific design derived for the POTV have been defined by the requirements of a postulated space facility (ASSET) that salvages structural aluminum from the external fuel tank of the Space Shuttle. Precision control of the POTV is achieved by an electrical conductor configuration that makes current-produced thrust continuously available for independent control of components of vehicle attitude and translation. A robust tracking controller is designed which guarantees stability and compensates for geomagnetic field modeling error. This concept is applicable for vehicles with mass and power capabilities differing from the particular design described herein and has application in the areas of attitude control, satellite retrieval, and free-flying platforms.



# AN ELECTROMAGNETICALLY-CONTROLLED PRECISION ORBITAL TRACKING VEHICLE (POTV)

## *I. Introduction*

The use of the earth's magnetic field as a source of spacecraft propulsion was first proposed in 1965 by Drell, Foley, and Ruderman in their ground-breaking paper "Drag and Propulsion of Large Satellites in the Ionosphere: An Alfvén Propulsion Engine in Space." (2). Their idea has been used to design electrodynamic *tethers* for various uses in earth orbit. Tethers have many non-electrodynamic uses, including payload orbital transfer, orbital rendezvous, docking, artificial gravity, and gravity-gradient stabilization. These and many other applications are detailed in NASA's Tethers in Space Handbook (15). Electrically conducting tethers can be used for power generation and storage, very low frequency communication, orbital braking, and most importantly for our purposes, propulsion. In this thesis we design a spacecraft which uses the electrodynamic forces arising from the interaction of electrical currents with the geomagnetic field to precisely track other space vehicles at close range, dock with other spacecraft, and perform gross orbital maneuvers.

There are two important differences between the *conductors* the POTV uses to conduct electricity and the electrodynamic tethers extensively written about in the literature. First, there are multiple conductors attached to the POTV whereas the literature generally discusses electrodynamic tethers singly. Secondly, the POTV conductors are supported by "rigid" towers whose dynamic behavior is much simpler than that of flexible "strings". The rigidity is provided by lightweight structural webbing that connects all the conductors. The POTV conductors are also much shorter than the electrodynamic tethers commonly encountered in the literature. POTV conductors are expected to be less than one kilometer in length. A twenty kilometer long electrodynamic flexible tether was supposed to have been

deployed in August of 1992 from the space shuttle. The Tethered Satellite System (TSS-1) experiment failed for reasons unrelated to the electrical characteristics of the tether.

How do the POTV conductors use the geomagnetic field to produce thrust? We review the pertinent electromagnetic theory: The force on a current conductor in a magnetic field is given by the Lorentz equation (15:131):

$$\underline{F}_B = I \underline{L} \times \underline{B} \quad (1.1)$$

where  $\underline{F}$  is the force exerted on the conductor by the magnetic field,  $I$  is the current flowing through the conductor,  $\underline{L}$  is a vector with magnitude equal to the conductor length which points in the direction of positive current flow, and  $\underline{B}$  is the magnetic field vector. For our application,  $\underline{B}$  is the geomagnetic field vector. The Lorentz equation is fundamental to the thesis work.

The POTV conductors must make electrical contact with the plasma in the earth's ionosphere in order to close the current loop. Three basic methods for accomplishing this are presented by Penzo and Ammann (15:120-121):

- A passive large-area conductor at both conductor ends.
- A passive large-area conductor at one end and an electron gun at the other end.
- A plasma-generating hollow cathode (PMG) at both ends.

The first two methods are dependent upon the density of the surrounding ionospheric plasma. We use PMGs for the POTV because this technology is the most promising for high current densities. The power requirements inherent in electrodynamic propulsion are discussed in appendix C.

Since the POTV conductors rely upon the geomagnetic field to produce thrust, the magnetic field strength produced by the current flowing through any one conductor at another conductor should not be a significant fraction of the geomagnetic field strength. The magnetic field (scalar) due to a current flowing through a wire is (6:243):

$$B = \frac{\mu I}{2\pi\rho} \quad (1.2)$$

where  $\mu$  is the magnetic permeability of free space,  $I$  is the current flowing through the wire, and  $\rho$  is the radial distance from the wire. This equation should be checked when designing the current capacity of the conductors and the physical separation between conductors.

An electrodynamic propulsion systems is fundamentally different from a conventional reaction systems in that it produces thrust which is not dependent upon the expulsion of mass. Any thrust arising from the PMG's ejection of electrons/ions is assumed to be negligible. Unfortunately, a major finding of this thesis is that it is not physically possible to independently control all components of vehicle position and attitude with electrodynamic thrusters (conductors) alone. Thus we add a single pair of electromagnetic plasma thrusters to provide needed position control capability. We choose high specific impulse electrically-powered thrusters over conventional chemical thrusters to minimize fuel consumption. Jahn (8:197) states that plasma thrusters should be able to deliver high thrust in conjunction with high exhaust velocities.

The POTV is capable of gross orbital maneuvers as well as close-range precision tracking. Penzo and Ammann (15:168-169) show how an electrodynamic system like the POTV can be used to change all of the classical orbital elements. Thus we will not go into detail about large orbital change. We assume that the POTV has enough gross orbital maneuvering capability to move close enough to a target vehicle for the precision control system to handle close-range target tracking and docking.

Docking using purely electrodynamic forces has the advantage over reaction systems of not imparting any momentum to the target vehicle from the exhaust products of the tracking vehicle. We neglect the possible effects that the ionospheric currents have upon the target vehicle. There are different approaches to docking in the literature. Two in-plane methods, V-BAR and R-BAR, are described by Hall (5). We will investigate these methods as well as an out-of-plane approach (Z-BAR) to see which approach is "best" for the POTV.

In this chapter we have discussed how the POTV can use the earth's geomagnetic field as a source of propulsion. Chapter two covers the derivation of the relative translational and rotational equations of motion for the POTV. In chapter three we describe

the geomagnetic field and express it in terms of an orbital frame of reference. Chapter three also covers magnetic forces and moments. Chapter four covers the design of a POTV closed-loop controller. Chapter five goes into detail about tracking behavior, docking strategies, and conductor-sizing. The final chapter summarizes important results and makes recommendations for further research. The appendices contain geomagnetic field plots, a description of forces not included in the equations of motion, a controller design program listing, and plots corresponding to different docking approaches.

## II. Derivation of Equations of Motion

In this chapter we derive the relative translational and rotational equations of motion for the POTV. The equations of motion derived herein include only forces and moments due to gravity. Magnetic forces and moments are described in chapter three. We describe the coordinate frames necessary for the derivation and the rotation matrices that relate the coordinate systems. We also perform a steady-state analysis of the equations of motion.

### 2.1 Coordinate Frames

**2.1.1 Coordinate Frame Description** Figure 2.1 shows the coordinate frames that are used in the derivation of the relative equations of motion of the tracking vehicle (POTV). A description of each coordinate frame follows:

- **Geocentric Equatorial Frame ( $\hat{i}$ ):** The origin of the  $\hat{i}$  frame is at the center of the earth. The  $\hat{i}_1$  unit vector is defined to point in the vernal equinox direction. The  $\hat{i}_3$  unit vector is collinear with the earth's rotation axis and points out of the earth's geographic north pole. The  $\hat{i}_2$  unit vector completes the right-handed orthogonal set. An excellent description of this "inertial" frame is found in Bate (1:55).
- **Orbital Reference Frame ( $\hat{c}$ ):** The origin of the  $\hat{c}$  frame is at a point on a reference orbit. This point usually, but not necessarily, coincides with the center of mass of a target vehicle.  $\hat{c}_1$  points radially outward along a line connecting the center of the earth and the  $\hat{c}$  frame origin.  $\hat{c}_2$  points along the orbital velocity vector of the target vehicle.  $\hat{c}_3$  points "northward" out of the orbital plane.
- **Body-Fixed Reference Frame ( $\hat{b}$ ):** The origin of the  $\hat{b}$  frame is at the tracking vehicle's center of mass. The coordinate frame unit vectors coincide with the principal axes of inertia of the tracking vehicle. This frame is referred to as the *body frame* henceforth.

**2.1.2 Rotation Matrices** A rotation matrix is a special type of matrix that allows a vector defined in terms of the unit vectors of a coordinate system to be expressed in terms of the unit vectors of another coordinate system. We will derive the rotation matrix

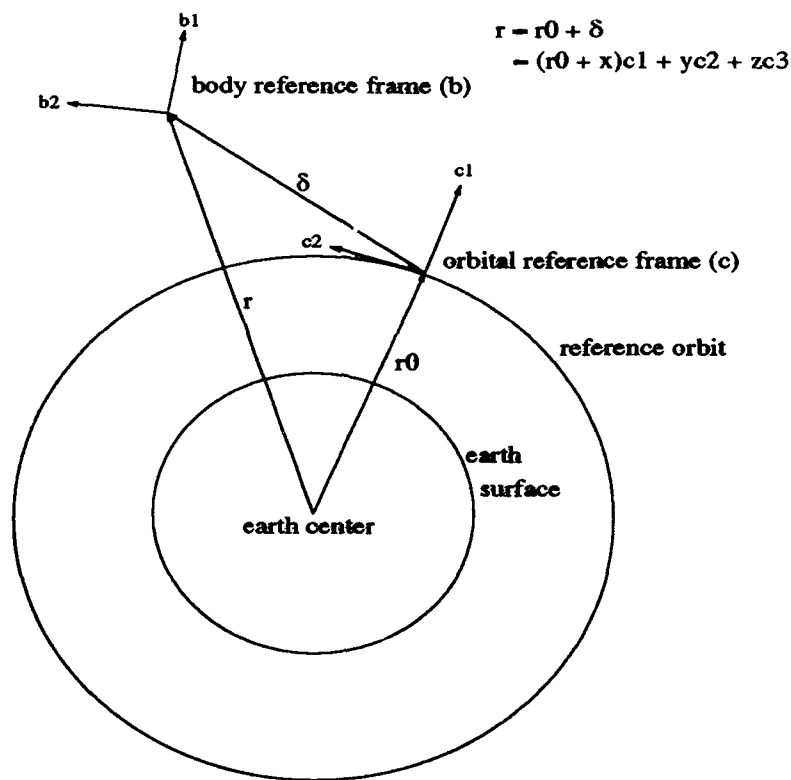


Figure 2.1. Coordinate Frames and Position Vectors

$\mathcal{R}^{ic}$  that allows a vector expressed in inertial coordinates to be expressed in terms of orbital reference frame coordinates. We say that the matrix  $\mathcal{R}^{ic}$  transforms the vector from the  $\hat{i}$  coordinate system to the  $\hat{c}$  coordinate system. This matrix is of use in section 3.2 where we derive an expression for the geomagnetic field in terms of orbital reference frame coordinates.

The size, shape, and inertial orientation of the reference orbit and the location of the target vehicle within the reference orbit must be known in order to derive  $\mathcal{R}^{ic}$ . This information is contained in a set of six orbital elements defined by Bate (1:58–60):

- The semi-major axis  $a$ .
- The eccentricity  $e$ .
- The orbital inclination angle  $i$ .
- The right ascension of the ascending node  $\Omega$ .

- The argument of periapsis  $\omega$ .
- The argument of latitude at epoch  $u_0$ .

We assume that the reference orbit is circular in order to simplify the derivation of the relative equations of motion. Thus the eccentricity  $e$  equals zero and the argument of periapsis  $\omega$  is undefined. The orbital radius  $r_0$  ( $r_0 \equiv a$ ) specifies the size of the circular reference orbit. The right ascension of the ascending node  $\Omega$  and the inclination  $i$  completely determine the orientation of the orbit in inertial space. Note for future reference that  $i$  is zero and that  $\Omega$  is undefined for an equatorial orbit. The argument of latitude at epoch angle  $u_0$  locates the target vehicle within the reference orbit at initial time (epoch)  $t_0$ . We define a new angle  $u$  that locates the target vehicle within the reference orbit at any later time  $t$ . The concept of orbital mean motion  $n$  is used to write:

$$u(t) = u_0 + n(t - t_0) \quad (2.1)$$

where

$$n = \sqrt{\frac{GM_{\oplus}}{r_0^3}}$$

where  $G$  is the universal gravitational constant and  $M_{\oplus}$  is the mass of the earth. The angular velocity  $\underline{\omega}^{\hat{c}}$  of the  $\hat{c}$  frame with respect to the  $\hat{i}$  frame is simply  $n\hat{c}_3$ .

Thomson (22:33-36) derives the rotation matrix  $\mathcal{R}^{ic}$  that transforms from the inertial frame to the orbital reference frame. The process of rotating from the  $\hat{i}$  frame to the  $\hat{c}$  frame is described by rotating an angle  $\Omega$  about the inertial  $\hat{z}$  axis, then rotating an angle  $i$  about the new  $\hat{x}$  axis, and finally rotating an angle  $u$  about the newest  $\hat{z}$  axis. The angles  $\Omega$ ,  $i$ ,  $u$  are often referred to as a 3-1-3 Euler angle set. The rotation matrix  $\mathcal{R}^{ic}$  is formed by the product of three intermediate rotation matrices:

$$\mathcal{R}^{ic} = \mathcal{R}_z(u)\mathcal{R}_x(i)\mathcal{R}_z(\Omega)$$

where

$$\mathcal{R}_z(u) = \begin{bmatrix} \cos u & \sin u & 0 \\ -\sin u & \cos u & 0 \\ 0 & 0 & 1 \end{bmatrix}$$

$$\mathcal{R}_x(i) = \begin{bmatrix} 1 & 0 & 0 \\ 0 & \cos i & \sin i \\ 0 & -\sin i & \cos i \end{bmatrix}$$

$$\mathcal{R}_z(\Omega) = \begin{bmatrix} \cos \Omega & \sin \Omega & 0 \\ -\sin \Omega & \cos \Omega & 0 \\ 0 & 0 & 1 \end{bmatrix}$$

The resulting rotation matrix  $\mathcal{R}^{ic}$  is calculated to be:

$$\begin{bmatrix} \cos \Omega \cos u - \sin \Omega \cos i \sin u & \sin \Omega \cos u + \cos \Omega \cos i \sin u & \sin i \sin u \\ -\cos \Omega \sin u - \sin \Omega \cos i \cos u & -\sin \Omega \sin u + \cos \Omega \cos i \cos u & \sin i \cos u \\ \sin \Omega \sin i & -\cos \Omega \sin i & \cos i \end{bmatrix} \quad (2.2)$$

Another important coordinate transformation is that relating the orbital reference frame to the body frame. The rotation matrix  $\mathcal{R}^{cb}$  we derive is important in section 3.3 where an expression for magnetically-induced moment is derived. Here we use the concept of yaw, roll, and pitch angles to represent the rotational angles needed to relate the frames. These angles are collectively referred to as orientation or attitude angles. The process of rotating from the  $\hat{c}$  frame to the  $\hat{b}$  frame is described by rotating an angle  $\psi_1$  about the  $\hat{x}$  axis, then rotating an angle  $\psi_2$  about the new  $\hat{y}$  axis, and finally rotating an angle  $\psi_3$  about the newest  $\hat{z}$  axis. Rimrott (18:329-330) refers to these angles with this particular sequence of angular rotations as "Cardan angles of the first kind". The rotation matrix  $\mathcal{R}^{cb}$  is formed by the product of three intermediate rotation matrices:

$$\mathcal{R}^{cb} = \mathcal{R}_z(\psi_3)\mathcal{R}_y(\psi_2)\mathcal{R}_x(\psi_1)$$



where

$$\mathcal{R}_x(\psi_1) = \begin{bmatrix} 1 & 0 & 0 \\ 0 & \cos \psi_1 & \sin \psi_1 \\ 0 & -\sin \psi_1 & \cos \psi_1 \end{bmatrix}$$

$$\mathcal{R}_y(\psi_2) = \begin{bmatrix} \cos \psi_2 & 0 & -\sin \psi_2 \\ 0 & 1 & 0 \\ \sin \psi_2 & 0 & \cos \psi_2 \end{bmatrix}$$

$$\mathcal{R}_z(\psi_3) = \begin{bmatrix} \cos \psi_3 & \sin \psi_3 & 0 \\ -\sin \psi_3 & \cos \psi_3 & 0 \\ 0 & 0 & 1 \end{bmatrix}$$

The resulting rotation matrix  $\mathcal{R}^{cb}$  is calculated to be:

$$\begin{bmatrix} \cos \psi_2 \cos \psi_3 & \cos \psi_1 \sin \psi_3 + \sin \psi_1 \sin \psi_2 \cos \psi_3 & \sin \psi_1 \sin \psi_3 - \cos \psi_1 \sin \psi_2 \cos \psi_3 \\ -\cos \psi_2 \sin \psi_3 & \cos \psi_1 \cos \psi_3 - \sin \psi_1 \sin \psi_2 \sin \psi_3 & \sin \psi_1 \cos \psi_3 + \cos \psi_1 \sin \psi_2 \sin \psi_3 \\ \sin \psi_2 & -\sin \psi_1 \cos \psi_2 & \cos \psi_1 \cos \psi_2 \end{bmatrix}$$

If we assume that the orientation angles are "small", then we can use small-angle assumptions to linearize the  $\mathcal{R}^{cb}$  matrix. For small angle  $\theta$ :

$$\sin \theta \approx \theta$$

$$\cos \theta \approx 1$$

The products of small angles are assumed to be negligible and are not included in the linearized form of the matrix. Thus for small angles  $\psi_1, \psi_2, \psi_3$ , the linearized form of  $\mathcal{R}^{cb}$  is:

$$\mathcal{R}^{cb} = \begin{bmatrix} 1 & \psi_3 & -\psi_2 \\ -\psi_3 & 1 & \psi_1 \\ \psi_2 & -\psi_1 & 1 \end{bmatrix} \quad (2.3)$$

We assume that "small" angles are less than  $15^\circ$  for the purposes of this research.

Rotation matrices are orthogonal. The inverse of an orthogonal matrix is equal to its transpose. Thus it is easy to form the linearized version of  $\mathcal{R}^{bc}$ :

$$\mathcal{R}^{bc} = \mathcal{R}^{cb^T} = \begin{bmatrix} 1 & -\psi_3 & \psi_2 \\ \psi_3 & 1 & -\psi_1 \\ -\psi_2 & \psi_1 & 1 \end{bmatrix} \quad (2.4)$$

## 2.2 Unforced Equations of Motion

The translational equations of motion of the tracking vehicle relative to the target vehicle are derived by Wiesel (24:78-80) and by Kaplan (9:108-111). The derivation of the small-angle relative rotational equations of motion in section 2.2.2 is believed to be partially original.

**2.2.1 Translational Equations** The complete derivation of the relative translational equations of motion is not shown by Wiesel or Kaplan. All steps of the derivation are explicitly shown here to illustrate linearization techniques used later in the thesis.

We want to derive an expression for the inertial acceleration of the tracking vehicle and expressions for the forces acting on it. These expressions will be substituted into Newton's second law to give the translational equations of motion:

$$\sum \underline{F} = M_t \underline{a} \quad (2.5)$$

where  $\sum \underline{F}$  is the sum all external forces,  $M_t$  is the mass of the tracking vehicle, and  $\underline{a}$  is the inertial acceleration of the tracking vehicle.

We derive the inertial acceleration first. Refer to the position vectors shown in figure 2.1. The inertial position vector of the tracking vehicle is:

$$\underline{r} = \underline{r}_0 + \underline{\delta} = (r_0 + x)\hat{c}_1 + y\hat{c}_2 + z\hat{c}_3 \quad (2.6)$$

where  $r_0$  is the distance from the center of the earth to the  $\hat{c}$  frame origin and  $x, y, z$  are the  $\hat{c}$  frame components of the relative position vector  $\underline{r}$ . The inertial velocity is:

$$\begin{aligned}
 \underline{v} &= \dot{\underline{r}} \\
 &= \frac{d}{dt}\underline{r} + \underline{\omega}^{ci} \times \underline{r} \\
 &= (\dot{x}\hat{c}_1 + \dot{y}\hat{c}_2 + \dot{z}\hat{c}_3) + n\hat{c}_3 \times ((r_0 + x)\hat{c}_1 + y\hat{c}_2 + z\hat{c}_3) \\
 &= (\dot{x} - ny)\hat{c}_1 + (\dot{y} + nr_0 + nx)\hat{c}_2 + \dot{z}\hat{c}_3
 \end{aligned} \tag{2.7}$$

The inertial acceleration is:

$$\begin{aligned}
 \underline{a} &= \frac{d}{dt}(\dot{\underline{r}}) \\
 &= \frac{d}{dt}(\dot{\underline{r}}) + \underline{\omega}^{ci} \times (\dot{\underline{r}}) \\
 &= ((\ddot{x} - n\dot{y})\hat{c}_1 + (\ddot{y} + n\dot{x})\hat{c}_2 + \ddot{z}\hat{c}_3) + n\hat{c}_3 \times ((\dot{x} - ny)\hat{c}_1 + (\dot{y} + nr_0 + nx)\hat{c}_2 + \dot{z}\hat{c}_3) \\
 &= (\ddot{x} - 2n\dot{y} - n^2r_0 - n^2x)\hat{c}_1 + (\ddot{y} + 2n\dot{x} - n^2y)\hat{c}_2 + \ddot{z}\hat{c}_3
 \end{aligned} \tag{2.8}$$

We have derived the acceleration part of Newton's second law. Now we decide which external forces to include in the equations of motion. There are several types of external forces that could act on the tracking vehicle. The largest of these in magnitude for low earth orbits are gravitational force, magnetic force, and aerodynamic drag. In section 3.3 a linearized expression for magnetic force is derived. Aerodynamic drag is described in appendix B. Now we derive a linearized expression for the gravitational force  $\underline{F}_g$ . The general formula for the gravitational force on the tracking vehicle is:

$$\underline{F}_g = \frac{-GM_\oplus M_t}{r^3} \underline{r}$$

Substituting  $\underline{r} = (r_0 + x)\hat{c}_1 + y\hat{c}_2 + z\hat{c}_3$  into this formula yields:

$$\underline{F}_g = \frac{-GM_\oplus M_t((r_0 + x)\hat{c}_1 + y\hat{c}_2 + z\hat{c}_3)}{(r_0^2 + 2r_0x + x^2 + y^2 + z^2)^{\frac{3}{2}}} \tag{2.9}$$

The tracking vehicle must be able to track the target vehicle at "close" range. We assume that "close" means that  $x \ll r_0$ ,  $y \ll r_0$ , and  $z \ll r_0$ . The expression for gravitational force (eq. 2.9) is simplified (linearized) by making these assumptions. The following steps are used in the linearization of the gravitational force expression:

- A partial binomial series expansion is used.
- Products of "small" relative position components  $x$ ,  $y$ , and  $z$  are neglected.

The binomial formula (19:110) states that an expression of the form  $(a + b)^n$ , where  $b < a$ , is equivalent to the series:

$$(a + b)^n = a^n + na^{n-1}b + \dots \text{ (higher order terms)}$$

Using this idea to simplify the denominator of equation 2.9:

$$\begin{aligned} (r_0^2 + 2r_0x + x^2 + y^2 + z^2)^{-\frac{3}{2}} &\simeq (r_0^2 + 2r_0x)^{-\frac{3}{2}} \\ &\simeq r_0^{-3} - 3r_0^{-4}x \end{aligned}$$

Substituting this result into equation 2.9 and remembering  $n = \sqrt{GM_\oplus/r^3}$ :

$$\begin{aligned} \underline{F}_g &\simeq -GM_\oplus M_t ((r_0 + x)\hat{c}_1 + y\hat{c}_2 + z\hat{c}_3)(r_0^{-3} - r_0^{-4}x) \\ &\simeq \frac{-GM_\oplus M_t}{r_0^3} ((r_0 - 2x)\hat{c}_1 + y\hat{c}_2 + z\hat{c}_3) \\ &\simeq -M_t n^2 ((r_0 - 2x)\hat{c}_1 + y\hat{c}_2 + z\hat{c}_3) \end{aligned} \tag{2.10}$$

Now, substituting the inertial acceleration (eq. 2.8) and the gravitational force (eq. 2.10) into  $\sum \underline{F} = M_t \underline{a}$ , we obtain the relative translational equations of motion:

$$\ddot{x} - 2n\dot{y} - 3n^2x = \frac{F_{x_{other}}}{M_t} \quad (2.11)$$

$$\ddot{y} + 2n\dot{x} = \frac{F_{y_{other}}}{M_t} \quad (2.12)$$

$$\ddot{z} + n^2z = \frac{F_{z_{other}}}{M_t} \quad (2.13)$$

where  $F_{x_{other}}, F_{y_{other}}, F_{z_{other}}$  are the  $\hat{c}$  frame components of the sum of all non-gravitational forces acting on the tracking vehicle. Wiesel (24:78) calls this set of equations the Clohessy-Wiltshire equations. These differential equations are linear, coupled, and have constant coefficients. When  $\underline{F}_{other} = 0$ , we call these equations the *unforced* relative translational equations of motion.

**2.2.1.1 Solution to the Unforced Equations** The unforced equations can be solved in closed form (24:80-81) to yield:

$$x(t) = -\left(\frac{2}{n}\dot{y}(0) + 3x(0)\right)\cos nt + \frac{1}{n}\dot{x}(0)\sin nt + 4x(0) + \frac{2}{n}\dot{y}(0) \quad (2.14)$$

$$y(t) = y(0) - (3\dot{y}(0) + 6nx(0))t + \left(\frac{4}{n}\dot{y}(0) + 6x(0)\right)\sin nt + \frac{2}{n}\dot{x}(0)\cos nt - \frac{2}{n}\dot{x}(0) \quad (2.15)$$

$$z(t) = z(0)\cos nt + \frac{1}{n}\dot{z}(0)\sin nt \quad (2.16)$$

We note that  $x(t)$  contains only sinusoidal and constant terms.  $z(t)$  contains purely sinusoidal terms. Interestingly,  $y(t)$  contains the linear term  $(3\dot{y}(0) + 6nx(0))t$  that grows with time as well as sinusoidal terms and constant terms. This means that the tracking vehicle will move steadily away from the target vehicle in the  $y$  direction if  $x(0)$  and/or  $\dot{y}(0)$  is non-zero. We see in section 2.2.2.1 how the solutions  $x(t), y(t), z(t)$  affect the solutions of the relative small-angle rotational equations of motion.

The unforced relative translational motion of the tracking vehicle is solely dependent upon its initial relative position and relative velocity. Except for two special cases, the

tracker will never stay at its initial relative position. One trivial case occurs when all the relative positions and velocities are zero. The origin of the body frame and the origin of the orbital reference frame are then coincident. In the absence of any perturbing forces, the tracker will stay at this zero reference state. A more interesting special case occurs when the relative velocities are all zero, the relative positions  $x(0)$ ,  $z(0)$  are zero, and  $y(0)$  is any non-zero value. Then the tracker will remain at a distance  $y(0)$  ahead or behind the target vehicle in the same orbit.

**2.2.1.2 Steady-State Behavior** Eventually we would like to design a position controller for the tracking vehicle which will allow it to track steady-state values of  $x$ ,  $y$ , and  $z$ . We refer to these steady-state values as  $x_{ss}$ ,  $y_{ss}$ , and  $z_{ss}$ . Now we examine the steady-state forces required to maintain steady-state position tracking. In the steady-state,  $\dot{x} = \ddot{x} = \dot{y} = \ddot{y} = \dot{z} = \ddot{z} \equiv 0$ . The relative translational equations of motion (eqs. 2.11, 2.12, 2.13) in the steady-state become:

$$F_{x_{ss}} = -3n^2 M_t x_{ss} \quad (2.17)$$

$$F_{y_{ss}} = 0 \quad (2.18)$$

$$F_{z_{ss}} = n^2 M_t z_{ss} \quad (2.19)$$

So the steady-state force required for the tracker to standoff a fixed  $x$  (vertical) and/or  $z$  (out-of-plane) distance from the target vehicle is directly proportional to the standoff distance, the tracking vehicle mass, and the square of the orbital mean motion. We note that three times as much force is required to maintain the  $x$  component of the standoff distance as is required to maintain the  $z$  component. This fact makes out-of-plane standoff less "costly" than vertical in-plane standoff. No steady-state force is required to maintain the  $y$  component of the standoff distance. We note that a force in the negative  $x$  direction (down) is needed to maintain a constant positive (up)  $x$  component of the standoff distance. We also observe that the required steady-state force for a given standoff distance becomes smaller as the reference orbital radius  $r_0$  increases since  $n^2 = GM_\oplus/r_0^3$ .

**2.2.2 Rotational Equations** Kaplan (9:201–202) and Wiesel (24:145–148) derive the small-angle rotational equations of motion of the gravity-gradient satellite for the purpose of studying attitude stability. The body attitude angles that these authors use are defined with respect to an orbital reference frame attached to the body. The important difference in the following derivation is that the orientation angles are defined with respect to an orbital reference frame attached to *another* body (the target vehicle). The equations we derive are the rotational equivalent of the Clohessy-Wiltshire translational equations of motion.

We start with Euler's general rotational equations of motion:

$$\begin{aligned} A\dot{\omega}_1 + (C - B)\omega_2\omega_3 &= M_1 \\ B\dot{\omega}_2 + (A - C)\omega_1\omega_3 &= M_2 \\ C\dot{\omega}_3 + (B - A)\omega_1\omega_2 &= M_3 \end{aligned} \quad (2.20)$$

where  $A$ ,  $B$ ,  $C$  are the principal moments of inertia,  $\omega_1$ ,  $\omega_2$ ,  $\omega_3$  are the body frame components of the inertial angular velocity vector  $\underline{\omega}$ , and  $M_1$ ,  $M_2$ ,  $M_3$  are the body frame components of the sum of all external moments. We need to express the inertial angular velocity  $\underline{\omega}$  and the external moment  $\underline{M}$  in terms of the orientation angles  $\psi_1$ ,  $\psi_2$ , and  $\psi_3$ .

There are several possible external moment sources acting on the tracking vehicle. Only the gravitational moment  $\underline{M}_g$  is examined in this section. In section 3.3 an expression for magnetic moment is derived. Any moment arising from aerodynamic drag is assumed to be negligible.

Wiesel (24:145–147) derives the gravitational moment in body frame coordinates:

$$\begin{aligned} M_{g1} &= \frac{3GM_\oplus}{r^5} YZ(C - B) \\ M_{g2} &= \frac{3GM_\oplus}{r^5} XZ(A - C) \\ M_{g3} &= \frac{3GM_\oplus}{r^5} XY(B - A) \end{aligned} \quad (2.21)$$

where  $X$ ,  $Y$ ,  $Z$  are the body frame components of the position vector  $\underline{r}$ . Here the derivation diverges from that of Wiesel and Kaplan because our position vector  $\underline{r}$  includes the relative

position components  $x, y, z$ . We need to express the given gravitational moment in terms of the orientation angles. We begin by expressing  $\underline{r}$  in body frame coordinates:

$$\hat{\underline{r}} = \mathcal{R}^{cb} \hat{\underline{c}}_{\underline{r}}$$

where the linearized form of  $\mathcal{R}^{cb}$  is used (eq. 2.3) because the orientation angles are assumed to be small. Neglecting the products of small variables  $x, y, z, \psi_1, \psi_2$ , and  $\psi_3$  we get:

$$\hat{\underline{r}} \simeq (r_0 + x)\hat{b}_1 + (-\psi_3 r_0 + y)\hat{b}_2 + (\psi_2 r_0 + z)\hat{b}_3$$

which can also be stated:

$$\hat{\underline{r}} = X\hat{b}_1 + Y\hat{b}_2 + Z\hat{b}_3$$

where

$$X \simeq r_0 + x$$

$$Y \simeq -\psi_3 r_0 + y$$

$$Z \simeq \psi_2 r_0 + z$$

Again neglecting the products of small variables, the terms  $YZ, XZ, XY$  are evaluated:

$$YZ \simeq 0$$

$$XZ \simeq r_0^2 \psi_2 + r_0 z \quad (2.22)$$

$$XY \simeq -r_0^2 \psi_3 + r_0 y$$

The denominator  $r^{-5}$  of the moment terms is linearized:

$$\begin{aligned} r^{-5} &= (r_0^2 + 2r_0 x + x^2 + y^2 + z^2)^{-\frac{5}{2}} \\ &\simeq (r_0^2 + 2r_0 x)^{-\frac{5}{2}} \\ &\simeq r_0^{-5} - 5r_0^{-6} x \end{aligned} \quad (2.23)$$



Finally substituting equations 2.22 and 2.23 into the gravitational moment equations (eq. 2.21), we get the linearized form of  $\underline{M}_g$ :

$$\begin{aligned} M_{g1} &\simeq 0 \\ M_{g2} &\simeq 3n^2(\psi_2 + \frac{z}{r_0})(A - C) \\ M_{g3} &\simeq 3n^2(-\psi_3 + \frac{y}{r_0})(B - A) \end{aligned}$$

We now have the gravitational moment part of the small-angle rotational equations of motion. Now we derive the inertial angular velocity:

$$\begin{aligned} \underline{\omega} &= n\hat{c}_3 + \dot{\psi}_1\hat{b}_1 + \dot{\psi}_2\hat{b}_2 + \dot{\psi}_3\hat{b}_3 \\ &= \sqrt{\frac{GM_\oplus}{r^3}}\hat{c}_3 + \dot{\psi}_1\hat{b}_1 + \dot{\psi}_2\hat{b}_2 + \dot{\psi}_3\hat{b}_3 \end{aligned}$$

where the linearized form of  $\sqrt{GM_\oplus/r^3}$  is:

$$\begin{aligned} \sqrt{\frac{GM_\oplus}{r^3}} &= (GM_\oplus)^{\frac{1}{2}}(r)^{-\frac{3}{2}} \\ &= (GM_\oplus)^{\frac{1}{2}}(r_0^2 + 2r_0x + x^2 + y^2 + z^2)^{-\frac{3}{2}} \\ &\simeq (GM_\oplus)^{\frac{1}{2}}(r_0^{-\frac{3}{2}} - \frac{3}{2}r_0^{-\frac{5}{2}}x) \end{aligned}$$

Then the inertial angular velocity becomes:

$$\underline{\omega} = (GM_\oplus)^{\frac{1}{2}}(r_0^{-\frac{3}{2}} - \frac{3}{2}r_0^{-\frac{5}{2}}x)\hat{c}_3 + \dot{\psi}_1\hat{b}_1 + \dot{\psi}_2\hat{b}_2 + \dot{\psi}_3\hat{b}_3$$

Using the linearized rotation matrix  $\mathcal{R}^{cb}$  (eq. 2.3) to transform the  $\hat{c}_3$  term into the  $\hat{b}$  frame (again neglecting the products of small variables) we derive the linearized form of the inertial angular velocity:

$$\underline{\omega} = (-n\psi_2 + \dot{\psi}_1)\hat{b}_1 + (n\psi_1 + \dot{\psi}_2)\hat{b}_2 + (n + \dot{\psi}_3 - \frac{3nx}{2r_0})\hat{b}_3 \quad (2.24)$$

We use equation 2.24 to find  $\dot{\omega}_1, \dot{\omega}_2, \dot{\omega}_3$ :

$$\frac{d}{dt}\underline{\omega} = (\ddot{\psi}_1 - n\dot{\psi}_2)\hat{b}_1 + (\ddot{\psi}_2 + n\dot{\psi}_1)\hat{b}_2 + (\ddot{\psi}_3 - \frac{3n\dot{x}}{2r_0})\hat{b}_3$$

and the products  $\omega_2\omega_3, \omega_1\omega_3, \omega_1\omega_2$ :

$$\omega_2\omega_3 = (\dot{\psi}_2 + n\psi_1)(\dot{\psi}_3 + n - \frac{3n\dot{x}}{2r_0}) \simeq n\dot{\psi}_2 + n^2\psi_1$$

$$\omega_1\omega_3 = (\dot{\psi}_1 - n\psi_2)(\dot{\psi}_3 + n - \frac{3n\dot{x}}{2r_0}) \simeq n\dot{\psi}_1 - n^2\psi_2$$

$$\omega_1\omega_2 = (\dot{\psi}_1 - n\psi_2)(\dot{\psi}_2 + n\psi_1) \simeq 0$$

Substituting these results into the general rotational equations of motion (eq. 2.20), we obtain the small-angle relative rotational equations of motion:

$$A(\ddot{\psi}_1 - n\dot{\psi}_2) + (C - B)(n\dot{\psi}_2 + n^2\psi_1) = 0 \quad (2.25)$$

$$B(\ddot{\psi}_2 + n\dot{\psi}_1) + (A - C)(n\dot{\psi}_1 - 4n^2\psi_2 - \frac{3n^2\dot{z}}{r_0}) = 0 \quad (2.26)$$

$$C(\ddot{\psi}_3 - \frac{3n\dot{x}}{2r_0}) + (B - A)(3n^2\psi_3 - \frac{3n^2\dot{y}}{r_0}) = 0 \quad (2.27)$$

These differential equations are linear, constant-coefficient, and coupled. The  $-3n^2z/r_0$  term in the second equation and the  $-3n\dot{x}/2r_0$  and  $-3n^2y/r_0$  terms in the third equation do not appear in the rotational equations of motions derived by Kaplan and Wiesel. These "extra" terms arise from the definition of the body orientation angles. These angles were defined with respect to an orbital reference frame attached to another body (the target vehicle) instead of an orbital reference frame attached to the tracking vehicle.

**2.2.2.1 Unforced Equation Observations** The solutions  $x(t), y(t), z(t)$  (eqs. 2.14, 2.15, 2.16) to the relative translational equations of motion can be inserted into the "extra" terms in the relative rotational equations of motion to yield:

$$A(\ddot{\psi}_1 - n\dot{\psi}_2) + (C - B)(n\dot{\psi}_2 + n^2\psi_1) = 0$$

$$B(\ddot{\psi}_2 + n\dot{\psi}_1) + (A - C)(n\dot{\psi}_1 - 4n^2\psi_2 - \frac{3n^2(z(0) \cos nt + \frac{1}{n}\dot{z}(0) \sin nt)}{r_0}) = 0$$

$$C(\ddot{\psi}_3 - \frac{3n((2\dot{y}(0) + 3nx(0)) \sin nt + \dot{x}(0) \cos nt)}{2r_0}) + (B - A)(3n^2\psi_3 - \frac{3n^2(y(0) - (3\dot{y}(0) + 6nx(0))t + (\frac{4}{n}\dot{y}(0) + 6x(0)) \sin nt + \frac{2}{n}\dot{x}(0) \cos nt - \frac{2}{n}\dot{x}(0))}{r_0}) = 0$$

Note that these equations become the equations shown in Wiesel's text (24:148) when the relative positions and velocities are zero. We call the equations that we have derived here the "unforced" equations because we assume no forces other than gravitational are acting on the tracking vehicle. In another sense we could think of these equations as the rotational equations shown in Wiesel's text with added forcing functions which result from non-zero initial relative positions and velocities. Wiesel shows that the solutions to the unforced equations are oscillatory in nature as long as the condition  $C > B > A$  is satisfied.

Although we do not explicitly solve the relative rotational equations of motion for  $\psi_1(t)$ ,  $\psi_2(t)$ ,  $\psi_3(t)$ , we can make general comments about the nature of the solutions. We assume that  $C > B > A$ . Then  $\psi_1(t)$  is purely sinusoidal.  $\psi_2(t)$  is also sinusoidal because the forcing function  $z(t)$  is sinusoidal.  $\psi_3(t)$  is more interesting because while  $\dot{x}(t)$  is sinusoidal,  $y(t)$  contains linear and constant terms in addition to sinusoidal terms. Therefore if  $x(0)$  is non-zero,  $\psi_3(t)$  grows larger with time until the small-angle assumption becomes invalid. Then the linearized equation in  $\psi_3(t)$  does not apply to the non-linear behavior of  $\psi_3(t)$ .

**2.2.2.2 Steady State Behavior** We want to eventually design an attitude control system for the tracking vehicle which will allow it to regulate the steady-state values of  $\psi_1$ ,  $\psi_2$ , and  $\psi_3$  to zero. We refer to these steady-state values as  $\psi_{1..}$ ,  $\psi_{2..}$ , and  $\psi_{3..}$ . Now we examine what moments are required to maintain steady-state attitude regulation. In the steady-state, all the orientation angle rates and position rates go to zero. Note that the relative position variables are allowed to be non-zero in the steady state. The small-angle relative rotational equations of motion (eqs. 2.25, 2.26, 2.27) in the steady-state become:

$$M_{x..} = n^2(C - B)\psi_{1..} \quad (2.28)$$

$$M_{y..} = -4n^2(A - C)\psi_{2..} - \frac{3n^2(A - C)}{r_0}z_{..} \quad (2.29)$$

$$M_{z,,} = 3n^2(B - A)\psi_{3,,} - \frac{3n^2(B - A)}{r_0}y_{,,} \quad (2.30)$$

We usually want  $\psi_{1,,}$ ,  $\psi_{2,,}$ , and  $\psi_{3,,}$  to be equal to zero to avoid rotational inertia during a docking maneuver. From these equations we then expect that  $M_{x,,}$  is equal to zero,  $M_{y,,}$  is constant and proportional to the steady-state  $z$  component of position, and  $M_{z,,}$  is constant and proportional to the steady-state  $y$  component of position. We expect that the forces required to generate these steady-state moments are much smaller than the forces required for steady-state position standoff when  $\psi_{1,,}$ ,  $\psi_{2,,}$ , and  $\psi_{3,,}$  are zero.

### III. Magnetic Forces and Moments

In this chapter we complete the linearized relative translational and rotational equations of motion by deriving expressions for magnetic force and moment.

#### 3.1 Geomagnetic Field Description

The geomagnetic field strength  $\underline{B}$  is equal to the negative gradient of the scalar magnetic potential  $\Phi_m$  (14:2.22):

$$\underline{B} = -\nabla \Phi_m$$

The  $\Phi_m$  that one chooses for analysis purposes depends upon the level of accuracy one wants and the complexity that one is willing to tolerate. Unfortunately, the more accurate of a model desired, the more complex  $\Phi_m$  becomes. The most accurate model is the multipole expansion model (also known as the spherical harmonic analysis model) (7:41). The scalar magnetic potential for this model is:

$$\Phi_m = r_\oplus \sum_{n=1}^N \left(\frac{r_\oplus}{n}\right)^{n+1} \sum_{m=0}^n (g_n^m \cos m\lambda + h_n^m \sin m\lambda) P_n^m(\sin \delta) \quad (3.1)$$

where  $r_\oplus$  is the radius of the earth,  $\delta$  is the magnetic co-latitude,  $\lambda$  is longitude, and  $P_n^m(\sin \delta)$  is the associated Legendre function of order  $m$  and degree  $n$  (19:149). The coefficients  $g_n^m$  and  $h_n^m$  are known as the Schmidt coefficients. Several are tabulated in NASA TM 82478 (14:2.23).

We will instead use the simple dipole model (21:33-34) to represent the geomagnetic field. The scalar magnetic potential for this model is equivalent to the first term of the scalar magnetic potential expression of the multipole expansion model (eq. 3.1). The farther one moves from the earth, the more accurate the simple dipole model becomes because the higher order multipole terms decrease in magnitude more quickly than the dominant dipole term. The scalar magnetic potential for the simple dipole model is:

$$\Phi_m = \frac{\underline{m} \cdot \underline{r}}{r^3} \quad (3.2)$$

$$\lambda = 111$$

$$\delta = -78.5$$

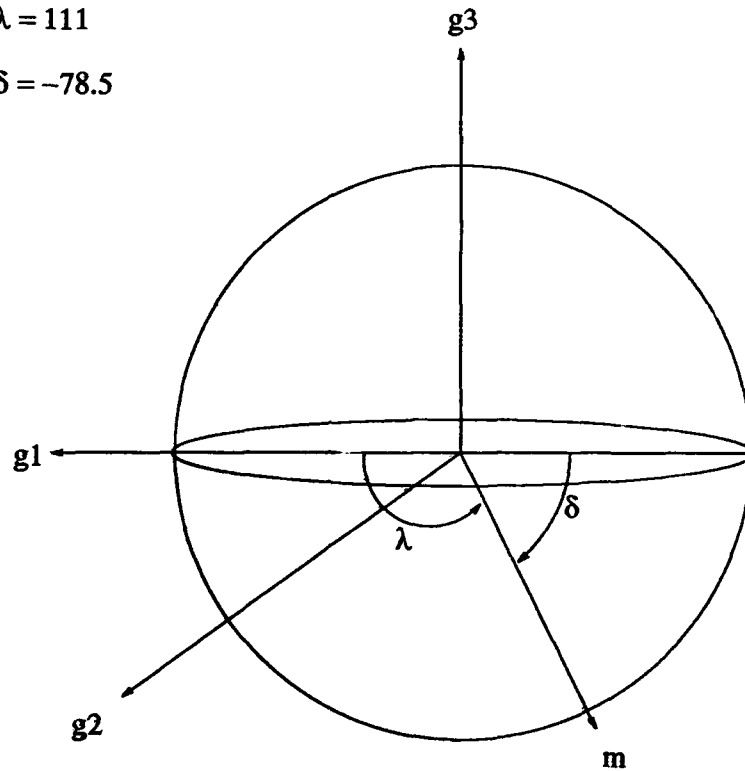


Figure 3.1. Magnetic Dipole Moment Vector in the Greenwich Frame

where  $\underline{m}$  denotes the magnetic dipole moment of the earth and  $\underline{r}$  is the position vector from the center of the earth to the tracking vehicle. The  $\underline{m}$  vector originates at the center of the earth and passes through the earth's surface at the austral magnetic pole in the southern hemisphere. This model may give a magnetic field magnitude error of up to 30% at the earth's surface according to Hess (7:39).

### 3.2 Transformation to the Orbital Reference Frame

The relative translational equations of motion (eqs. 2.11, 2.12, 2.13) were derived in orbital reference frame ( $\hat{c}$ ) coordinates. An expression for the magnetic force  $\underline{B}$  in  $\hat{c}$  frame coordinates is derived in this section. This allows the convenient derivation of the magnetic forces acting on the tracking vehicle through the use of the Lorentz equation (eq. 1.1).

Using the simple dipole model, the geomagnetic field is expressed:

$$\begin{aligned}\underline{B} &= -\nabla \Phi_m \\ &= -\nabla \left( \frac{\underline{m} \cdot \underline{r}}{r^3} \right)\end{aligned}\quad (3.3)$$

In order to derive  ${}^c\underline{B}$  we must:

- Express  $\underline{m}$  in the  $\hat{c}$  frame ( ${}^c\underline{m}$ ).
- Perform the dot product  $\underline{m} \cdot \underline{r}$ .
- Apply the gradient operator  $\nabla$ .

This particular method of deriving the magnetic field in terms of orbital reference frame coordinates was suggested by Wiesel (25).

The magnetic dipole moment vector is easily visualized in a coordinate frame we designate the *greenwich frame* (see figure 3.1). The  $\hat{g}$  frame differs from the inertial geocentric equatorial frame ( $\hat{i}$ ) by a single rotation about the inertial z-axis ( $\hat{i}_3$ ). The angle of rotation  $\theta_g$  locates the greenwich prime meridian with respect to the inertial x-axis ( $\hat{i}_1$ ). This angle is called the sidereal time and is calculated using the following simple formula (1:99):

$$\theta_g = \theta_{g_0} + \omega_{\oplus}(t - t_0) \quad (3.4)$$

where  $\theta_{g_0}$  is the value of  $\theta_g$  at reference time  $t_0$  and  $\omega_{\oplus}$  is the angular velocity of the earth's rotation. The American Ephemeris and Nautical Almanac can be used to determine  $\theta_{g_0}$ . The angles  $\delta$  and  $\lambda$  shown in figure 3.1 are the latitude and longitude, respectively, of the austral magnetic pole. These angles completely determine the direction of the magnetic dipole moment vector  $\underline{m}$  in the greenwich frame:

$${}^g\underline{m} = m \cos \delta \cos \lambda \hat{g}_1 + m \cos \delta \sin \lambda \hat{g}_2 + m \sin \delta \hat{g}_3 \quad (3.5)$$

where the magnitude of the magnetic dipole moment  $m$  is approximately  $8.1 \cdot 10^{15}$  tesla-meter<sup>3</sup>. For the austral pole  $\delta \simeq -78.5^\circ$  and  $\lambda \simeq 111^\circ$ .

How is  $\underline{m}$  transformed from the  $\hat{g}$  frame to the  $\hat{c}$  frame? In section 2.1.2 we derived the rotation matrix  $\mathcal{R}^{ic}$  (eq. 2.2) that transforms from the inertial frame to the orbital reference frame. Thus  ${}^{\hat{c}}\underline{m}$  is represented:

$$\begin{aligned} {}^{\hat{c}}\underline{m} &= \mathcal{R}^{jc} {}^{\hat{j}}\underline{m} \\ &= \mathcal{R}^{ic} \mathcal{R}_z(\theta_g) {}^{\hat{j}}\underline{m} \end{aligned}$$

where

$$\mathcal{R}_z(\theta_g) = \begin{bmatrix} \cos \theta_g & -\sin \theta_g & 0 \\ \sin \theta_g & \cos \theta_g & 0 \\ 0 & 0 & 1 \end{bmatrix}$$

Then we calculate the elements of  $\mathcal{R}^{jc}$ :

$$\begin{aligned} \mathcal{R}_{11} &= \cos(\Omega - \theta_g) \cos u - \sin(\Omega - \theta_g) \cos i \sin u \\ \mathcal{R}_{12} &= \sin(\Omega - \theta_g) \cos u + \cos(\Omega - \theta_g) \cos i \sin u \\ \mathcal{R}_{13} &= \sin i \sin u \\ \mathcal{R}_{21} &= -\cos(\Omega - \theta_g) \sin u - \sin(\Omega - \theta_g) \cos i \cos u \\ \mathcal{R}_{22} &= -\sin(\Omega - \theta_g) \sin u + \cos(\Omega - \theta_g) \cos i \cos u \\ \mathcal{R}_{23} &= \sin i \cos u \\ \mathcal{R}_{31} &= \sin(\Omega - \theta_g) \sin i \\ \mathcal{R}_{32} &= -\cos(\Omega - \theta_g) \sin i \\ \mathcal{R}_{33} &= \cos i \end{aligned}$$



The transformation of  $\underline{m}$  from the  $\hat{g}$  frame to the  $\hat{c}$  frame yields the  $\hat{c}$  frame components of  $\underline{m}$ :

$$\begin{aligned}
 m_1 &= m(\cos \delta \cos \lambda (\cos (\Omega - \theta_g) \cos u - \sin (\Omega - \theta_g) \cos i \sin u) \\
 &\quad + \cos \delta \sin \lambda (\sin (\Omega - \theta_g) \cos u + \cos (\Omega - \theta_g) \cos i \sin u) \\
 &\quad + \sin \delta \sin i \sin u) \\
 m_2 &= m(\cos \delta \cos \lambda (-\cos (\Omega - \theta_g) \sin u - \sin (\Omega - \theta_g) \cos i \cos u) \\
 &\quad + \cos \delta \sin \lambda (-\sin (\Omega - \theta_g) \sin u + \cos (\Omega - \theta_g) \cos i \cos u) \\
 &\quad + \sin \delta \sin i \cos u) \\
 m_3 &= m(\cos \delta \cos \lambda \sin (\Omega - \theta_g) \sin i \\
 &\quad - \cos \delta \sin \lambda \cos (\Omega - \theta_g) \sin i \\
 &\quad + \sin \delta \cos i)
 \end{aligned}$$

which when simplified by the trigonometric identities:

$$\begin{aligned}
 \sin (A \pm B) &= \sin A \cos B \pm \cos A \sin B \\
 \cos (A \pm B) &= \cos A \cos B \mp \sin A \sin B
 \end{aligned} \tag{3.6}$$

become:

$$\begin{aligned}
 m_1 &= m(\cos \delta \cos u \cos (\Omega - \theta_g - \lambda) - \cos i \cos \delta \sin u \sin (\Omega - \theta_g - \lambda) + \sin i \sin \delta \sin u) \\
 m_2 &= m(-\cos \delta \sin u \cos (\Omega - \theta_g - \lambda) - \cos i \cos \delta \cos u \sin (\Omega - \theta_g - \lambda) + \sin i \sin \delta \cos u) \\
 m_3 &= m(\sin i \cos \delta \sin (\Omega - \theta_g - \lambda) + \cos i \sin \delta)
 \end{aligned}$$

We introduce some simplifying notation before performing the dot product ( $\underline{m} \cdot \underline{r}$ ).

Let

$$\begin{aligned}\alpha &= \cos \delta \cos u \cos (\Omega - \theta_g - \lambda) - \cos i \cos \delta \sin u \sin (\Omega - \theta_g - \lambda) + \sin i \sin \delta \sin u \\ \beta &= -\cos \delta \sin u \cos (\Omega - \theta_g - \lambda) - \cos i \cos \delta \cos u \sin (\Omega - \theta_g - \lambda) + \sin i \sin \delta \cos u \\ \gamma &= \sin i \cos \delta \sin (\Omega - \theta_g - \lambda) + \cos i \sin \delta\end{aligned}$$

where we note for future reference that  $\alpha, \beta$  are composed of purely sinusoidal components while  $\gamma$  includes the constant term  $\cos i \sin \delta$  as well as a sinusoidal component.

Now we can write  $\underline{\hat{e}}\underline{m} = m(\alpha\hat{c}_1 + \beta\hat{c}_2 + \gamma\hat{c}_3)$ . Remembering:

$$\underline{\hat{e}}\underline{r} = (r_0 + x)\hat{c}_1 + y\hat{c}_2 + z\hat{c}_3$$

the dot product  $\underline{m} \cdot \underline{r}$  becomes:

$$\underline{m} \cdot \underline{r} = m(\alpha(r_0 + x) + \beta y + \gamma z)$$

The remaining hurdle in the evaluation of the magnetic field  $\underline{B}$  in  $\hat{c}$  frame coordinates is the application of the gradient operator:

$$\underline{B} = -\nabla \left( m \frac{(\alpha(r_0 + x) + \beta y + \gamma z)}{(r_0^2 + 2r_0x + x^2 + y^2 + z^2)^{\frac{3}{2}}} \right)$$

which can also be expressed:

$$\underline{B} = -\left( \frac{\partial}{\partial x}\hat{c}_1 + \frac{\partial}{\partial y}\hat{c}_2 + \frac{\partial}{\partial z}\hat{c}_3 \right) \left( m \frac{(\alpha(r_0 + x) + \beta y + \gamma z)}{(r_0^2 + 2r_0x + x^2 + y^2 + z^2)^{\frac{3}{2}}} \right)$$

Performing the partial differentiation, making a binomial approximation to the resulting denominators, and neglecting the products of the small relative position components  $x, y, z$ , we arrive at the linearized expression for the magnetic field in orbital reference frame

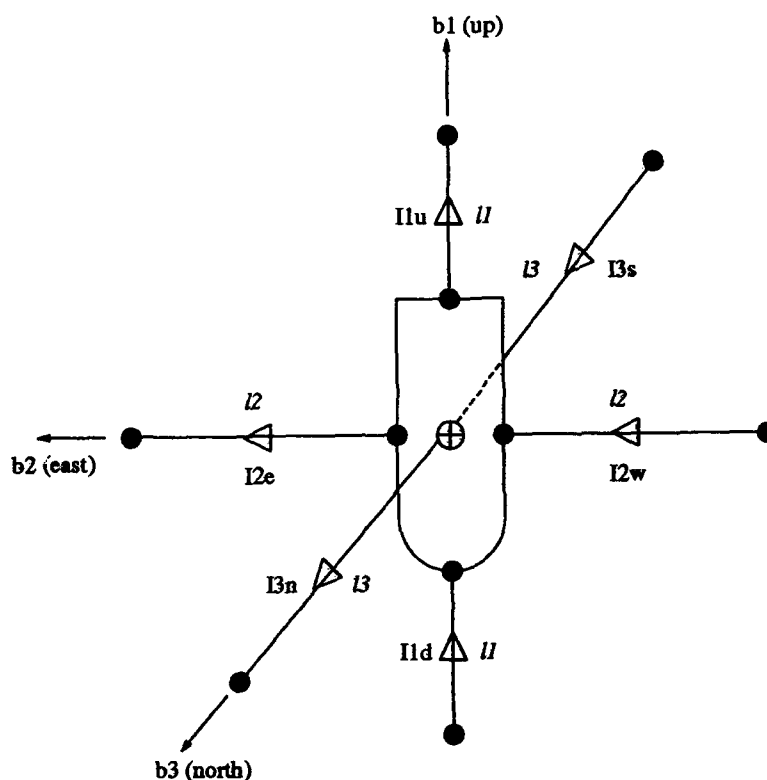


Figure 3.2. Design # 1 Conductor Configuration

coordinates:

$$\underline{\underline{\epsilon B}} = \frac{m}{r_0^4} ((2\alpha r_0 - 6\alpha x + 3\beta y + 3\gamma z)\hat{c}_1 + (-\beta r_0 + 3\beta x + 3\alpha y)\hat{c}_2 + (-\gamma r_0 + 3\gamma x + 3\alpha z)\hat{c}_3) \quad (3.7)$$

Appendix A shows plots of these orbital frame components of the magnetic field as functions of time assuming the relative position components  $x$ ,  $y$ ,  $z$  are all zero. The plots are done for a 400 km orbit at several different inclination angles. From these plots the reader can see that components disappear at certain times in the orbit. Both in-plane components or the out-of-plane component disappear entirely at some inclinations. This becomes important in the next chapter where we investigate the subject of controllability.

### 3.3 Magnetic Forces and Moments for Design # 1

An electrical conductor configuration is desired that allows independent control over every component of tracking vehicle position and attitude. Two designs are proposed in

this section to accomplish that goal. In chapter four we show that the second design is more controllable than the first design. Design # 1 is shown in figure 3.2. There are a total of six conductors: two on the in-plane body x-axis (one "up" and one "down"), two on the in-plane body y-axis (one "east" and one "west"), and two on the out-of-plane z-axis (one "north" and one "south"). Lightweight structural webbing exists between the conductors to provide rigidity. The filled-in circles at the ends of the conductors shown in figure 3.2 represent the plasma generators (PMGs) mentioned in chapter one.

**3.3.1 Magnetic Forces** The conductor lengths and currents are labeled in figure 3.2. Each conductor current is controlled independently of the other currents. The Lorentz equation (eq. 1.1) is used to determine the force on each conductor:

$$\underline{F}_B = I \underline{L} \times \underline{B} \quad (3.8)$$

We remind ourselves that the length vector  $\underline{L}$  is defined to point in the direction of positive current flow. The individual forces on each conductor are summed to determine the overall magnetic force on the tracking vehicle:

$${}^c \underline{F}_B = \sum (I {}^c \underline{L} \times {}^c \underline{B})$$

The summation  $\sum I \underline{L}$  is conveniently expressed in the body frame:

$$\begin{aligned} \sum I {}^b \underline{L} &= I_{1_u} l_1 \hat{b}_1 + I_{1_d} l_1 \hat{b}_1 + I_{2_e} l_2 \hat{b}_2 + I_{2_w} l_2 \hat{b}_2 + I_{3_n} l_3 \hat{b}_3 + I_{3_s} l_3 \hat{b}_3 \\ &= l_1 (I_{1_u} + I_{1_d}) \hat{b}_1 + l_2 (I_{2_e} + I_{2_w}) \hat{b}_2 + l_3 (I_{3_n} + I_{3_s}) \hat{b}_3 \end{aligned}$$

Using the linearized form of the rotation matrix  $\mathcal{R}^{bc}$  (eq. 2.4) to transform to the  $\hat{c}$  frame we get:

$$\begin{aligned}\sum I^{\hat{c}} \underline{L} = & (l_1(I_{1_u} + I_{1_d}) - \psi_3 l_2(I_{2_e} + I_{2_w}) + \psi_2 l_3(I_{3_n} + I_{3_s})) \hat{c}_1 \\ & + (\psi_3 l_1(I_{1_u} + I_{1_d}) + l_2(I_{2_e} + I_{2_w}) - \psi_1 l_3(I_{3_n} + I_{3_s})) \hat{c}_2 \\ & + (-\psi_2 l_1(I_{1_u} + I_{1_d}) + \psi_1 l_2(I_{2_e} + I_{2_w}) + l_3(I_{3_n} + I_{3_s})) \hat{c}_3\end{aligned}$$

We derived an expression for  ${}^{\hat{c}}\underline{B}$  in the previous section where we linearized with respect to the "small" position and attitude variables  $x, y, z, \psi_1, \psi_2$ , and  $\psi_3$ . In the next chapter we use control terminology to define these variables as the *states* of the tracking vehicle system. When we perform the cross product in the present derivation we will linearize with respect to the *controls* as well as with respect to the states. The tracking vehicle controls are the conductor currents. The products of states and the products of states and controls are neglected. This assumption greatly simplifies the cross product  ${}^{\hat{c}}\underline{F}_B = \sum (I^{\hat{c}} \underline{L} \times {}^{\hat{c}}\underline{B})$ . We calculate the total linearized magnetic force on Design # 1:

$$\begin{aligned}{}^{\hat{c}}\underline{F}_B = & m \left( -\frac{\gamma l_2(I_{2_e} + I_{2_w})}{r_0^3} + \frac{\beta l_3(I_{3_n} + I_{3_s})}{r_0^3} \right) \hat{c}_1 \\ & + m \left( \frac{2\alpha l_3(I_{3_n} + I_{3_s})}{r_0^3} + \frac{\gamma l_1(I_{1_u} + I_{1_d})}{r_0^3} \right) \hat{c}_2 \\ & + m \left( -\frac{\beta l_1(I_{1_u} + I_{1_d})}{r_0^3} - \frac{2\alpha l_2(I_{2_e} + I_{2_w})}{r_0^3} \right) \hat{c}_3\end{aligned}\tag{3.9}$$

**3.3.2 Magnetic Moments** We use the following general expression to evaluate the magnetic moment on the tracking vehicle:

$${}^{\hat{b}}\underline{M} = \sum ({}^{\hat{b}}\underline{r} \times (I^{\hat{b}} \underline{L} \times {}^{\hat{b}}\underline{B}))$$

where  ${}^{\hat{b}}\underline{r}$  represents the moment arm from the tracking vehicle center of mass to the center of applied magnetic force for each conductor. We assume that the conductors are short

enough so that we can reasonably assume that the center of magnetic force of a conductor coincides with the geometric center of that conductor.

The magnetic field in  $\hat{c}$  frame coordinates is known (eq. 3.7). We want to calculate the magnetic moment in terms of body frame coordinates in order to easily insert the resulting expression into the small-angle relative rotational equations of motion. Using the linearized form of  $\mathcal{R}^{cb}$  (eq. 2.3) to transform  $\underline{B}$  to the  $\hat{b}$  frame yields:

$$\begin{aligned} {}^b\underline{B} = & \frac{m}{r_0^4}((2\alpha r_0 - \alpha x + 3\beta y + 3\gamma z + \gamma\psi_2 - \beta\psi_3)\hat{b}_1 \\ & + (-\beta r_0 + 3\beta x + 3\alpha y - \gamma\psi_1 - 2\alpha\psi_3)\hat{b}_2 \\ & + (-\gamma r_0 + 3\gamma x + 3\alpha z + \beta\psi_1 + 2\alpha\psi_2)\hat{b}_3) \end{aligned} \quad (3.10)$$

where again we have neglected the products of relative position and attitude components. Then  ${}^b\underline{M}$  is expressed:

$$\begin{aligned} {}^b\underline{M} = & \frac{l_1}{2}\hat{b}_1 \times (I_{1*}l_1\hat{b}_1 \times {}^b\underline{B}) - \frac{l_1}{2}\hat{b}_1 \times (I_{1*}l_1\hat{b}_1 \times {}^b\underline{B}) \\ & + \frac{l_2}{2}\hat{b}_2 \times (I_{2*}l_2\hat{b}_2 \times {}^b\underline{B}) - \frac{l_2}{2}\hat{b}_2 \times (I_{2*}l_2\hat{b}_2 \times {}^b\underline{B}) \\ & + \frac{l_3}{2}\hat{b}_3 \times (I_{3*}l_3\hat{b}_3 \times {}^b\underline{B}) - \frac{l_3}{2}\hat{b}_3 \times (I_{3*}l_3\hat{b}_3 \times {}^b\underline{B}) \end{aligned}$$

which simplifies to:

$$\begin{aligned} {}^b\underline{M} = & \frac{l_1^2}{2}\hat{b}_1 \times ((I_{1*} - I_{1*})\hat{b}_1 \times {}^b\underline{B}) \\ & + \frac{l_2^2}{2}\hat{b}_2 \times ((I_{2*} - I_{2*})\hat{b}_2 \times {}^b\underline{B}) \\ & + \frac{l_3^2}{2}\hat{b}_3 \times ((I_{3*} - I_{3*})\hat{b}_3 \times {}^b\underline{B}) \end{aligned}$$

Performing the cross products and linearizing with respect to the states and the controls we find the total linearized magnetic moment acting on the tracking vehicle:

$$\begin{aligned}
 {}^i\mathbf{M} = & \left( -\frac{m\alpha l_2^2}{r_0^3}(I_{2s} - I_{2u}) - \frac{m\alpha l_3^2}{r_0^3}(I_{3s} - I_{3u}) \right) \hat{b}_1 \\
 & + \left( \frac{m\beta l_1^2}{2r_0^3}(I_{1s} - I_{1u}) + \frac{m\beta l_3^2}{2r_0^3}(I_{3s} - I_{3u}) \right) \hat{b}_2 \\
 & + \left( \frac{m\gamma l_1^2}{2r_0^3}(I_{1s} - I_{1u}) + \frac{m\gamma l_2^2}{2r_0^3}(I_{2s} - I_{2u}) \right) \hat{b}_3
 \end{aligned} \tag{3.11}$$

**3.3.3 Complete Equations of Motion** Now that we possess expressions for the total magnetic force (eq. 3.9) and moment (eq. 3.11), we can write the complete relative translational and rotational equations of motion for Design # 1. The translational equations of motion are:

$$\ddot{x} - 2n\dot{y} - 3n^2x = -\frac{m\gamma l_2(I_{2e} + I_{2w})}{M_t r_0^3} + \frac{m\beta l_3(I_{3n} + I_{3s})}{M_t r_0^3} \quad (3.12)$$

$$\ddot{y} + 2n\dot{x} = \frac{2m\alpha l_3(I_{3n} + I_{3s})}{M_t r_0^3} + \frac{m\gamma l_1(I_{1n} + I_{1s})}{M_t r_0^3} \quad (3.13)$$

$$\ddot{z} + n^2z = -\frac{m\beta l_1(I_{1n} + I_{1s})}{M_t r_0^3} - \frac{2m\alpha l_2(I_{2e} + I_{2w})}{M_t r_0^3} \quad (3.14)$$

The rotational equations of motion are:

$$\ddot{\psi}_1 + \frac{n(-A - B + C)}{A}\dot{\psi}_2 + \frac{n^2(C - B)}{A}\psi_1 = -\frac{m\alpha l_2^2}{A r_0^3}(I_{2e} - I_{2w}) - \frac{m\alpha l_3^2}{A r_0^3}(I_{3n} - I_{3s}) \quad (3.15)$$

$$\ddot{\psi}_2 + \frac{n(A + B - C)}{B}\dot{\psi}_1 - \frac{4n^2(A - C)}{B}\psi_2 - \frac{3n^2(A - C)}{B r_0}z = \frac{m\beta l_1^2}{2B r_0^3}(I_{1n} - I_{1s}) + \frac{m\beta l_3^2}{2B r_0^3}(I_{3n} - I_{3s}) \quad (3.16)$$

$$\ddot{\psi}_3 - \frac{3n}{2r_0}\dot{x} + \frac{3n^2(B - A)}{C}\psi_3 - \frac{3n^2(B - A)}{C r_0}y = \frac{m\gamma l_1^2}{2C r_0^3}(I_{1n} - I_{1s}) + \frac{m\gamma l_2^2}{2C r_0^3}(I_{2e} - I_{2w}) \quad (3.17)$$

where  $\alpha$ ,  $\beta$ , and  $\gamma$  were defined on page 3-6. We observe that these equations are highly coupled with respect to the controls as well as the states. We also note that the  $\psi_1$  and  $\psi_2$  equations for this design have purely sinusoidal forcing functions on the right hand side. When these terms become zero in either of these equations, "control authority" has been lost in that equation. This behavior is a first hint that Design# 1 may be inferior.

### 3.4 Magnetic Forces and Moments for Design # 2

Design # 2 is shown in figure 3.3. There are a total of eight conductors: two on the in-plane body x-axis, two on the in-plane body y-axis, two that form the out-of-plane northern cross, and another two that form the southern cross.



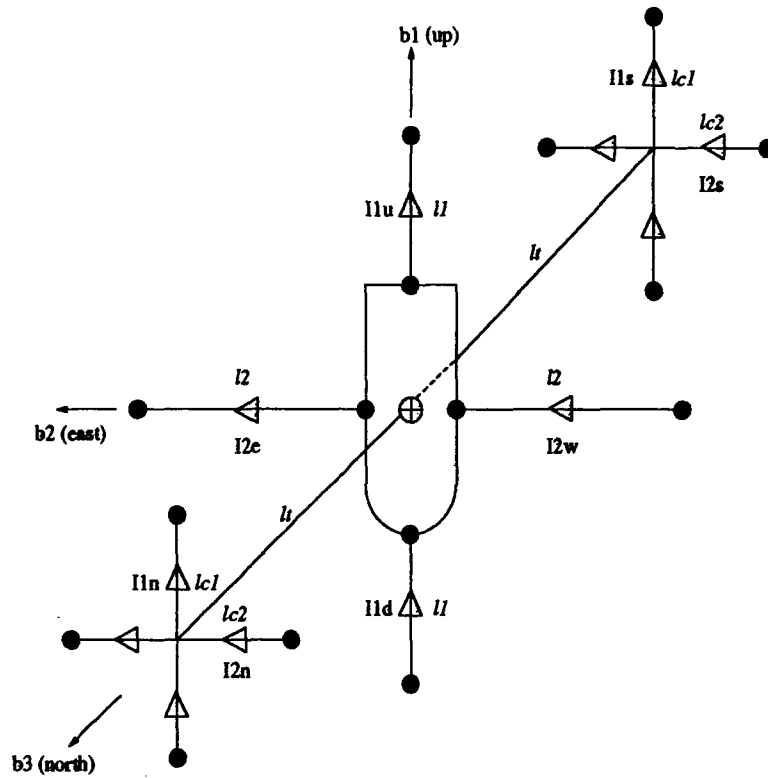


Figure 3.3. Design # 2 Conductor Configuration

**3.4.1 Magnetic Forces** Each conductor length and current is labeled in figure 3.3. The Lorentz equation (eq. 1.1) is used again to determine the force on each conductor:

$$\underline{F}_B = I \underline{L} \times \underline{B} \quad (3.18)$$

The individual forces on each conductor are summed to determine the overall magnetic force on the tracking vehicle:

$${}^c \underline{F}_B = \sum (I {}^c \underline{L} \times {}^c \underline{B})$$

The summation  $\sum I \underline{L}$  is conveniently expressed in the body frame:

$$\begin{aligned} \sum I {}^b \underline{L} &= I_{1u} l_1 \hat{b}_1 + I_{1d} l_1 \hat{b}_1 + I_{2e} l_2 \hat{b}_2 + I_{2w} l_2 \hat{b}_2 + I_{1s} l_{c1} \hat{b}_1 + I_{1n} l_{c1} \hat{b}_1 + I_{2s} l_{c2} \hat{b}_2 + I_{2n} l_{c2} \hat{b}_2 \\ &= (l_1 (I_{1u} + I_{1d}) + l_{c1} (I_{1s} + I_{1n})) \hat{b}_1 + (l_2 (I_{2e} + I_{2w}) + l_{c2} (I_{2s} + I_{2n})) \hat{b}_2 \end{aligned}$$

Using the linearized form of the rotation matrix  $\mathcal{R}^{bc}$  (eq. 2.4) to transform the current-length product to the  $\hat{c}$  frame we get:

$$\begin{aligned}\sum I^{\hat{c}} \underline{L} = & (l_1(I_{1_n} + I_{1_s}) + l_{c_1}(I_{1_n} + I_{1_s}) - \psi_3 l_2(I_{2_n} + I_{2_w}) - \psi_3 l_{c_2}(I_{2_n} + I_{2_s})) \hat{c}_1 \\ & + (\psi_3 l_1(I_{1_n} + I_{1_s}) + \psi_3 l_{c_1}(I_{1_n} + I_{1_s}) + l_2(I_{2_n} + I_{2_w}) + l_{c_2}(I_{2_n} + I_{2_s})) \hat{c}_2 \\ & + (-\psi_2 l_1(I_{1_n} + I_{1_s}) - \psi_2 l_{c_1}(I_{1_n} + I_{1_s}) + \psi_1 l_2(I_{2_n} + I_{2_w}) + \psi_1 l_{c_2}(I_{2_n} + I_{2_s})) \hat{c}_3\end{aligned}$$

Performing the cross product  ${}^{\hat{c}}\underline{F}_B = \sum(I^{\hat{c}} \underline{L} \times {}^{\hat{c}}\underline{B})$  and linearizing we calculate the total linearized magnetic force on Design # 2:

$$\begin{aligned}{}^{\hat{c}}\underline{F}_B = & m \left( -\frac{\gamma l_2(I_{2_n} + I_{2_w})}{r_0^3} - \frac{\gamma l_{c_2}(I_{2_n} + I_{2_s})}{r_0^3} \right) \hat{c}_1 \\ & + m \left( \frac{\gamma l_1(I_{1_n} + I_{1_s})}{r_0^3} + \frac{\gamma l_{c_1}(I_{1_n} + I_{1_s})}{r_0^3} \right) \hat{c}_2 \\ & + m \left( -\frac{\beta l_1(I_{1_n} + I_{1_s})}{r_0^3} - \frac{\beta l_{c_1}(I_{1_n} + I_{1_s})}{r_0^3} - \frac{2\alpha l_2(I_{2_n} + I_{2_w})}{r_0^3} - \frac{2\alpha l_{c_2}(I_{2_n} + I_{2_s})}{r_0^3} \right) \hat{c}_3\end{aligned}\quad (3.19)$$

**3.4.2 Magnetic Moments** As for Design # 1 we use the following general expression to evaluate the magnetic moment on the tracking vehicle:

$${}^{\hat{b}}\underline{M} = \sum({}^{\hat{b}}\underline{r} \times (I^{\hat{b}} \underline{L} \times {}^{\hat{b}}\underline{B}))$$

where  ${}^{\hat{b}}\underline{B}$  was calculated in equation 3.10. Then  ${}^{\hat{b}}\underline{M}$  is expressed:

$$\begin{aligned}{}^{\hat{b}}\underline{M} = & \frac{l_1}{2} \hat{b}_1 \times (I_{1_n} l_1 \hat{b}_1 \times {}^{\hat{b}}\underline{B}) - \frac{l_1}{2} \hat{b}_1 \times (I_{1_s} l_1 \hat{b}_1 \times {}^{\hat{b}}\underline{B}) \\ & + \frac{l_2}{2} \hat{b}_2 \times (I_{2_n} l_2 \hat{b}_2 \times {}^{\hat{b}}\underline{B}) - \frac{l_2}{2} \hat{b}_2 \times (I_{2_w} l_2 \hat{b}_2 \times {}^{\hat{b}}\underline{B}) \\ & + l_1 \hat{b}_3 \times (I_{1_n} l_{c_1} \hat{b}_1 \times {}^{\hat{b}}\underline{B}) + l_1 \hat{b}_3 \times (I_{2_n} l_{c_2} \hat{b}_2 \times {}^{\hat{b}}\underline{B}) \\ & - l_1 \hat{b}_3 \times (I_{1_s} l_{c_1} \hat{b}_1 \times {}^{\hat{b}}\underline{B}) - l_1 \hat{b}_3 \times (I_{2_s} l_{c_2} \hat{b}_2 \times {}^{\hat{b}}\underline{B})\end{aligned}$$

which simplifies to:

$$\begin{aligned} {}^i \underline{M} = & \frac{l_1^2}{2} \hat{b}_1 \times ((I_{1_n} - I_{1_s}) \hat{b}_1 \times {}^i \underline{B}) \\ & + \frac{l_2^2}{2} \hat{b}_2 \times ((I_{2_n} - I_{2_s}) \hat{b}_2 \times {}^i \underline{B}) \\ & + l_1 l_{c_1} \hat{b}_3 \times ((I_{1_n} - I_{1_s}) \hat{b}_1 \times {}^i \underline{B}) \\ & + l_1 l_{c_2} \hat{b}_3 \times ((I_{2_n} - I_{2_s}) \hat{b}_2 \times {}^i \underline{B}) \end{aligned}$$

Performing the cross products and linearizing with respect to the states and the controls we find the total linearized magnetic moment acting on the tracking vehicle:

$$\begin{aligned} {}^i \underline{M} = & \left( -\frac{m \alpha l_2^2}{r_0^3} (I_{2_n} - I_{2_s}) - \frac{m \gamma l_1 l_{c_1}}{r_0^3} (I_{1_n} - I_{1_s}) \right) \hat{b}_1 \\ & + \left( \frac{m \beta l_1^2}{2 r_0^3} (I_{1_n} - I_{1_s}) - \frac{m \gamma l_1 l_{c_2}}{r_0^3} (I_{2_n} - I_{2_s}) \right) \hat{b}_2 \\ & + \left( \frac{m \gamma l_1^2}{2 r_0^3} (I_{1_n} - I_{1_s}) + \frac{m \gamma l_2^2}{2 r_0^3} (I_{2_n} - I_{2_s}) \right) \hat{b}_3 \end{aligned} \quad (3.20)$$

**3.4.3 Complete Equations of Motion** Now that we possess expressions for the total magnetic force (eq. 3.9) and moment (eq. 3.11), we can write the complete relative translational and rotational equations of motion for Design # 2. The translational equations of motion are:

$$\ddot{x} - 2n\dot{y} - 3n^2 x = -\frac{m \gamma l_2 (I_{2_n} + I_{2_s})}{M_t r_0^3} - \frac{m \gamma l_{c_2} (I_{2_n} + I_{2_s})}{M_t r_0^3} \quad (3.21)$$

$$\ddot{y} + 2n\dot{x} = \frac{m \gamma l_1 (I_{1_n} + I_{1_s})}{M_t r_0^3} + \frac{m \gamma l_{c_1} (I_{1_n} + I_{1_s})}{M_t r_0^3} \quad (3.22)$$

$$\begin{aligned} \ddot{z} + n^2 z = & -\frac{m \beta l_1 (I_{1_n} + I_{1_s})}{M_t r_0^3} - \frac{m \beta l_{c_1} (I_{1_n} + I_{1_s})}{M_t r_0^3} \\ & - \frac{2 m \alpha l_2 (I_{2_n} + I_{2_s})}{M_t r_0^3} - \frac{2 m \alpha l_{c_2} (I_{2_n} + I_{2_s})}{M_t r_0^3} \end{aligned} \quad (3.23)$$

The rotational equations of motion are:

$$\ddot{\psi}_1 + \frac{n(-A - B + C)}{A} \dot{\psi}_2 + \frac{n^2(C - B)}{A} \psi_1 = \quad (3.24)$$

$$\ddot{\psi}_2 + \frac{n(A+B-C)}{B}\dot{\psi}_1 - \frac{4n^2(A-C)}{B}\psi_2 - \frac{3n^2(A-C)}{Br_0}z = -\frac{m\alpha l_2^2}{Ar_0^3}(I_{2e} - I_{2w}) - \frac{m\gamma l_1 l_{c1}}{Ar_0^3}(I_{1n} - I_{1s}) \quad (3.25)$$

$$\ddot{\psi}_3 - \frac{3n}{2r_0}\dot{x} + \frac{3n^2(B-A)}{C}\psi_3 - \frac{3n^2(B-A)}{Cr_0}y = \frac{m\beta l_1^2}{2Br_0^3}(I_{1n} - I_{1s}) - \frac{m\gamma l_1 l_{c2}}{Br_0^3}(I_{2n} - I_{2s})$$

$$\frac{m\gamma l_1^2}{2Cr_0^3}(I_{1n} - I_{1s}) + \frac{m\gamma l_2^2}{2Cr_0^3}(I_{2e} - I_{2w}) \quad (3.26)$$

where  $\alpha$ ,  $\beta$ , and  $\gamma$  were defined on page 3-6. We note the presence of  $\gamma$  terms in the  $\psi_1$  and  $\psi_2$  equations. Unlike Design# 1, control authority in low inclination orbits does not appear to be lost in these equations due to the constant term contained in the definition of  $\gamma$ .

94

#### IV. Tracking and Control Issues

This chapter explores the issue of controller design for the tracking vehicle. The controller is designed to allow the tracking vehicle to stay a fixed distance away from and maintain a constant attitude with respect to a target vehicle. Design # 2 is shown to be more controllable at certain points in low-inclination orbits than Design #1. A MATLAB (16) program (CONTROLLER.M - see appendix F) is written for controller design and evaluation. Also a new control theory concept we call *steady-state controllability* is defined and explored.

##### 4.1 State Space Representation of Equations of Motion

We use a state space representation to model the POTV's electrodynamic interaction with the geomagnetic field. The state space model lends itself to the understanding of system behavior and controller design. Our linearized system is time-varying. The state space model takes the form (3:363):

$$\begin{aligned}\dot{\underline{x}} &= F\underline{x} + G(t)\underline{u} \\ \underline{y} &= H\underline{x}\end{aligned}$$

where the *state vector*  $\underline{x}$  consists of the relative positions, attitude angles, and their rates. The number of states in a system is the system order  $N$ . Our system is twelfth-order.

$$\underline{x} = \begin{bmatrix} x & \dot{x} & y & \dot{y} & z & \dot{z} & \psi_1 & \dot{\psi}_1 & \psi_2 & \dot{\psi}_2 & \psi_3 & \dot{\psi}_3 \end{bmatrix}^T$$

The *output vector*  $\underline{y}$  consists of the system variables we are interested in controlling, namely, the relative position and attitude states. The dimension of  $\underline{y}$  is  $6 \times 1$ .

$$\underline{y} = \begin{bmatrix} x & y & z & \psi_1 & \psi_2 & \psi_3 \end{bmatrix}^T$$

The *control vector*  $\underline{u}$  consists of the conductor currents. The dimension of  $\underline{u}_1$  for Design # 1 is  $6 \times 1$ . The dimension of  $\underline{u}_2$  for Design # 2 is  $8 \times 1$ .

$$\underline{u}_1 = \begin{bmatrix} I_{1u} & I_{1d} & I_{2e} & I_{2w} & I_{3n} & I_{3s} \end{bmatrix}^T$$

$$\underline{u}_2 = \begin{bmatrix} I_{1u} & I_{1d} & I_{2e} & I_{2w} & I_{1n} & I_{1s} & I_{2n} & I_{2s} \end{bmatrix}^T$$

$F$  is the  $12 \times 12$  *system matrix*. This matrix is the same for both designs. The solution  $\underline{x}(t)$  of  $\dot{\underline{x}} = F\underline{x}$  represents the unforced behavior of the system.  $G(t)$  is the time-varying input matrix. It shows how the controls enter the system to affect the states. For Design # 1,  $G$  is  $12 \times 6$ . For Design # 2,  $G$  is  $12 \times 8$ .  $H$  is the  $6 \times 12$  output matrix.  $H$  selects the states we wish to control.

The six second order differential equations of motion for each design (eqs. 3.12–3.17 and eqs. 3.21–3.26) must be rewritten as a system of twelve first order equations in order to use the state space model. This process is described by Waltman (23:2,88). The resulting state space matrices are:

the system matrix  $F$ :

$$\begin{bmatrix} 0 & 1 & 0 & 0 & 0 & 0 & 0 & 0 & 0 & 0 & 0 & 0 \\ 3n^2 & 0 & 0 & 2n & 0 & 0 & 0 & 0 & 0 & 0 & 0 & 0 \\ 0 & 0 & 0 & 1 & 0 & 0 & 0 & 0 & 0 & 0 & 0 & 0 \\ 0 & -2n & 0 & 0 & 0 & 0 & 0 & 0 & 0 & 0 & 0 & 0 \\ 0 & 0 & 0 & 0 & 0 & 1 & 0 & 0 & 0 & 0 & 0 & 0 \\ 0 & 0 & 0 & 0 & -n^2 & 0 & 0 & 0 & 0 & 0 & 0 & 0 \\ 0 & 0 & 0 & 0 & 0 & 0 & 0 & 1 & 0 & 0 & 0 & 0 \\ 0 & 0 & 0 & 0 & 0 & 0 & -\frac{n^2(C-B)}{A} & 0 & 0 & -\frac{n(-A-B+C)}{A} & 0 & 0 \\ 0 & 0 & 0 & 0 & 0 & 0 & 0 & 0 & 0 & 1 & 0 & 0 \\ 0 & 0 & 0 & 0 & \frac{3n^2(A-C)}{Br_0} & 0 & 0 & -\frac{n(A+B-C)}{B} & \frac{4n^2(A-C)}{B} & 0 & 0 & 0 \\ 0 & 0 & 0 & 0 & 0 & 0 & 0 & 0 & 0 & 0 & 0 & 1 \\ 0 & \frac{3n}{2r_0} & \frac{3n^2(B-A)}{Cr_0} & 0 & 0 & 0 & 0 & 0 & 0 & 0 & -\frac{3n^2(B-A)}{C} & 0 \end{bmatrix} \quad (4.1)$$

the input matrix  $G_1(t)$  for Design # 1:

$$\begin{bmatrix}
 0 & 0 & 0 & 0 & 0 & 0 \\
 0 & 0 & -\frac{m\gamma l_2}{M_t r_0^3} & -\frac{m\gamma l_2}{M_t r_0^3} & \frac{m\beta l_2}{M_t r_0^3} & \frac{m\beta l_2}{M_t r_0^3} \\
 0 & 0 & 0 & 0 & 0 & 0 \\
 \frac{m\gamma l_1}{M_t r_0^3} & \frac{m\gamma l_1}{M_t r_0^3} & 0 & 0 & \frac{2m\alpha l_2}{M_t r_0^3} & \frac{2m\alpha l_2}{M_t r_0^3} \\
 0 & 0 & 0 & 0 & 0 & 0 \\
 -\frac{m\beta l_1}{M_t r_0^3} & -\frac{m\beta l_1}{M_t r_0^3} & -\frac{2m\alpha l_2}{M_t r_0^3} & -\frac{2m\alpha l_2}{M_t r_0^3} & 0 & 0 \\
 0 & 0 & 0 & 0 & 0 & 0 \\
 0 & 0 & -\frac{m\alpha l_2^2}{A r_0^3} & \frac{m\alpha l_2^2}{A r_0^3} & -\frac{m\alpha l_2^2}{A r_0^3} & \frac{m\alpha l_2^2}{A r_0^3} \\
 0 & 0 & 0 & 0 & 0 & 0 \\
 \frac{m\beta l_1^2}{2B r_0^3} & -\frac{m\beta l_1^2}{2B r_0^3} & 0 & 0 & \frac{m\beta l_1^2}{2B r_0^3} & -\frac{m\beta l_1^2}{2B r_0^3} \\
 0 & 0 & 0 & 0 & 0 & 0 \\
 \frac{m\gamma l_1^2}{2C r_0^3} & -\frac{m\gamma l_1^2}{2C r_0^3} & \frac{m\gamma l_2^2}{2C r_0^3} & -\frac{m\gamma l_2^2}{2C r_0^3} & 0 & 0
 \end{bmatrix} \quad (4.2)$$

the input matrix  $G_2(t)$  for Design # 2:

$$\begin{bmatrix}
 0 & 0 & 0 & 0 & 0 & 0 & 0 & 0 \\
 0 & 0 & -\frac{m\gamma l_2}{M_t r_0^3} & -\frac{m\gamma l_2}{M_t r_0^3} & 0 & 0 & -\frac{m\gamma l_{c2}}{M_t r_0^3} & -\frac{m\gamma l_{c2}}{M_t r_0^3} \\
 0 & 0 & 0 & 0 & 0 & 0 & 0 & 0 \\
 \frac{m\gamma l_1}{M_t r_0^3} & \frac{m\gamma l_1}{M_t r_0^3} & 0 & 0 & \frac{m\gamma l_{c1}}{M_t r_0^3} & \frac{m\gamma l_{c1}}{M_t r_0^3} & 0 & 0 \\
 0 & 0 & 0 & 0 & 0 & 0 & 0 & 0 \\
 -\frac{m\beta l_1}{M_t r_0^3} & -\frac{m\beta l_1}{M_t r_0^3} & -\frac{2m\alpha l_2}{M_t r_0^3} & -\frac{2m\alpha l_2}{M_t r_0^3} & -\frac{m\beta l_{c1}}{M_t r_0^3} & -\frac{m\beta l_{c1}}{M_t r_0^3} & -\frac{2m\alpha l_{c2}}{M_t r_0^3} & -\frac{2m\alpha l_{c2}}{M_t r_0^3} \\
 0 & 0 & 0 & 0 & 0 & 0 & 0 & 0 \\
 0 & 0 & -\frac{m\alpha l_2^2}{A r_0^3} & \frac{m\alpha l_2^2}{A r_0^3} & -\frac{m\gamma l_1 l_{c1}}{A r_0^3} & \frac{m\gamma l_1 l_{c1}}{A r_0^3} & 0 & 0 \\
 0 & 0 & 0 & 0 & 0 & 0 & 0 & 0 \\
 \frac{m\beta l_1^2}{2B r_0^3} & -\frac{m\beta l_1^2}{2B r_0^3} & 0 & 0 & 0 & 0 & -\frac{m\gamma l_1 l_{c2}}{B r_0^3} & \frac{m\gamma l_1 l_{c2}}{B r_0^3} \\
 0 & 0 & 0 & 0 & 0 & 0 & 0 & 0 \\
 \frac{m\gamma l_1^2}{2C r_0^3} & -\frac{m\gamma l_1^2}{2C r_0^3} & \frac{m\gamma l_2^2}{2C r_0^3} & -\frac{m\gamma l_2^2}{2C r_0^3} & 0 & 0 & 0 & 0
 \end{bmatrix} \quad (4.3)$$

and the output matrix  $H$ :

$$\begin{bmatrix}
 1 & 0 & 0 & 0 & 0 & 0 & 0 & 0 & 0 & 0 & 0 & 0 \\
 0 & 0 & 1 & 0 & 0 & 0 & 0 & 0 & 0 & 0 & 0 & 0 \\
 0 & 0 & 0 & 0 & 1 & 0 & 0 & 0 & 0 & 0 & 0 & 0 \\
 0 & 0 & 0 & 0 & 0 & 0 & 1 & 0 & 0 & 0 & 0 & 0 \\
 0 & 0 & 0 & 0 & 0 & 0 & 0 & 0 & 1 & 0 & 0 & 0 \\
 0 & 0 & 0 & 0 & 0 & 0 & 0 & 0 & 0 & 0 & 1 & 0
 \end{bmatrix} \quad (4.4)$$

Note that the rank of the input matrices  $G_1^{12 \times 6}(t)$ ,  $G_2^{12 \times 8}(t)$  can never be greater than five.

Six of the rows are comprised of zeros. Rows two, four, and six are linearly dependent:

$$\frac{-2\alpha}{\gamma}(\text{Row}_2) + \frac{\beta}{\gamma}(\text{Row}_4) + \text{Row}_6 = \underline{0}$$

These rows are comprised of the control terms in the relative translational equations of motion. This relationship among rows two, four, and six holds for any orbital inclination.



**4.1.1 Eigenvalues and Stability** The eigenvalues of the  $F$  matrix are the system poles. They characterize the natural, unforced behavior of the system. A pole with an imaginary component produces oscillatory behavior. A pole with a positive real part causes system instability. We define instability to mean that if system is displaced from an equilibrium state (defined in next section), the system will not return to that equilibrium state and remain. Mathematica (12) is used to determine the eigenvalues ( $\lambda_i$ ) of  $F$  (twelve total):

$$\begin{aligned}\lambda_i = & 0, 0, \\ & \pm jn, \pm jn \\ & \pm n\left[\frac{3(A-B)}{C}\right]^{\frac{1}{2}}, \\ & \pm n[3A^2 - 2AB - 2AC + BC - C^2 \\ & \quad \pm [9A^4 - 12A^3B - 12A^2B^2 - 12A^3C + 30A^2BC + 12AB^2C \\ & \quad - 2A^2C^2 - 16ABC^2 + B^2C^2 + 4AC^3 - 2BC^3 + C^4]^{\frac{1}{2}}/2AB]^{\frac{1}{2}}\end{aligned}$$

We note here that absence or presence of three particular entries of the  $F$  system matrix has no effect upon the eigenvalues of  $F$ . These terms are  $-3n^2z/r_0$ ,  $-3n\dot{x}/2r_0$  and  $-3n^2y/r_0$ . These are the so-called "extra" terms whose origin and effect upon the equations of motion were discussed in section 2.2.2.1.

The repeated poles at zero are the source of the constant and linear terms in the solution to the coupled  $x$  and  $y$  translational equations of motion. They make the system unstable in  $x$  and  $y$ . The four purely imaginary poles lead to oscillatory behavior. One pair is associated with the coupled  $x$  and  $y$  equations and the other pair is associated with the  $z$  equation. The poles  $\pm n[3(A-B)/C]^{\frac{1}{2}}$  cause  $\psi_3$  oscillatory behavior if  $B > A$ . Otherwise the  $\psi_3$  equation is exponentially unstable. The last four complicated-looking poles are associated with the coupled  $\psi_1$ ,  $\psi_2$  equations. They cause oscillatory behavior when  $C > B > A$ . Otherwise these poles seem to cause instability. The POTV should always be designed to have  $C > B > A$  for passive attitude stability. There may exist combinations of  $A$ ,  $B$ ,  $C$  where the condition  $C > B > A$  does not hold where the resulting poles are stable. This possibility was not investigated.

**4.1.2 Equilibrium Points** System equilibrium points are values of the state vector  $\underline{x}$  which make  $\dot{\underline{x}} = F\underline{x} = 0$ . The solutions  $\underline{x}_{eq}$  of  $F\underline{x} = 0$  lie in the nullspace of the matrix  $F$ . One equilibrium point is the trivial solution  $\underline{x}_{eq} = \underline{0}$ . We note that the nullspace of  $F$  can not solely consist of the zero vector since rows one and four of  $F$  are linearly dependent. Thus the rank of the  $12 \times 12$  matrix  $F$  is eleven. The Mathematica "NullSpace" command is used to calculate the resulting equilibrium point:

$$\underline{x}_{eq} = c \begin{bmatrix} 0 & 0 & r_0 & 0 & 0 & 0 & 0 & 0 & 0 & 1 & 0 & 0 \end{bmatrix}^T$$

where  $c$  is any constant. We expect this equilibrium point to exist because in chapter two we saw that a tracking vehicle ahead or behind the target vehicle in the same orbit would stay at that relative position without any expenditure of control effort. The pitch angle  $\psi_3$  is equal to  $y/r_0$  at this equilibrium point.

**4.1.3 Controllability** Thus far we have explored the unforced behavior of the system. The unforced system has been shown to be unstable. Control effort must be expended to maintain the system in a non-equilibrium state. This section addresses the issue of controllability. We find that Design # 1 is actually uncontrollable at certain times in an equatorial orbit. Design # 2 is found to be fully controllable at all times in an equatorial orbit.

A system is said to be completely controllable if in a finite time span  $(t - t_0)$ , any desired system state  $\underline{x}(t)$  can be reached through some control history  $\underline{u}(t)$  (3:384-385). The assessment of the controllability of a linear time-invariant system is a simple process. Unfortunately our system is linear and *time-varying*. We will make a simplification to the system that will allow us to make a time-invariant controllability analysis of both designs in an equatorial orbit.

How is the controllability of a linear time-invariant system determined? Begin by forming the controllability matrix  $M_c$ :

$$M_c = [G | FG | \dots | F^{n-1}G]$$

If the rank of  $M_c$  is equal to the system order  $N$ , then the system is completely controllable. Incidentally, the observability matrix  $M_o$  can be formed in an analogous fashion but we do not concern ourselves with this because the combination of the system matrix  $F$  and the chosen output matrix  $H$  always assure complete observability.

Mathematica can be used to evaluate the rank of  $M_c$  when  $F$  and  $G$  are constant matrices. Our  $F$  is a constant matrix. The non-constant input matrices  $G_1$  and  $G_2$  for the two designs contain the time-varying expressions  $\alpha$ ,  $\beta$ , and  $\gamma$ . The definitions of  $\alpha$ ,  $\beta$ ,  $\gamma$  are repeated here for convenience:

$$\begin{aligned}\alpha &= \cos \delta \cos u \cos (\Omega - \theta_g - \lambda) - \cos i \cos \delta \sin u \sin (\Omega - \theta_g - \lambda) + \sin i \sin \delta \sin u \\ \beta &= -\cos \delta \sin u \cos (\Omega - \theta_g - \lambda) - \cos i \cos \delta \cos u \sin (\Omega - \theta_g - \lambda) + \sin i \sin \delta \cos u \\ \gamma &= \sin i \cos \delta \sin (\Omega - \theta_g - \lambda) + \cos i \sin \delta\end{aligned}$$

where the time dependence of these expressions comes from the quantities  $\theta_g$  and  $u$  (see eqs. 3.4 and 2.1):

$$\begin{aligned}\theta_g &= \theta_{g_0} + \omega_{\oplus}(t - t_0) \\ u &= u_0 + n(t - t_0)\end{aligned}$$

We note that the quantities  $\alpha$ ,  $\beta$  are composed of trigonometric functions with frequencies  $n$  and  $\omega_{\oplus}$ . The orbital frequency  $n$  is approximately fifteen times larger than the earth's rotational frequency  $\omega_{\oplus}$  for a 400 km orbit.

We use the "gain-scheduling" concept proposed by Ridgely (17) to perform a "time-invariant" analysis of the controllability of our system. This method "freezes" a time-varying system at an instant in time, then a time-invariant controllability analysis is performed for that time instant. If the system is completely controllable at all time instants, then the time-varying system is completely controllable. The method becomes tractable when the time-varying system is periodic. Then the values of all entries in the input matrix  $G$  are known at any future time  $t$ . Fortunately our system is periodic for any inclination angle. This can be seen from the periodic plots of the magnetic field in the orbital frame

(appendix A). The gain-scheduling method is used in this section as well as in section 4.2 where it is used to discuss the design of a time-varying controller.

The periodicity of the magnetic field in orbital frame coordinates is conceptually simplest when the tracking vehicle is traveling in an equatorial orbit. Then the in-plane  $\hat{c}_1$  and  $\hat{c}_2$  components of the  $\underline{B}$  field are single-frequency sinusoids and the out-of-plane  $\hat{c}_3$  component is constant (see appendix A). The orbital inclination angle  $i$  is zero and the right ascension of the ascending node  $\Omega$  is undefined for an equatorial orbit. For our purposes, we pick  $\Omega$  to be zero. After the application of the trigonometric identity (eq. 3.6), the expressions  $\alpha, \beta, \gamma$  for the equatorial orbit become:

$$\begin{aligned}\alpha_0 &= \cos \delta \cos (u - \theta_g - \lambda) \\ \beta_0 &= -\cos \delta \sin (u - \theta_g - \lambda) \\ \gamma_0 &= \sin \delta\end{aligned}$$

Inserting these expressions for  $\alpha, \beta, \gamma$ , the input matrices  $G(t)$  become:

Design # 1  $G_1(t)$ :

$$\begin{bmatrix} 0 & 0 & 0 & 0 & 0 & 0 \\ 0 & 0 & -\frac{ml_2 s \delta}{M_1 r_0^3} & -\frac{ml_2 s \delta}{M_1 r_0^3} & -\frac{ml_2 c \delta s \theta}{M_1 r_0^3} & -\frac{ml_2 c \delta s \theta}{M_1 r_0^3} \\ 0 & 0 & 0 & 0 & 0 & 0 \\ \frac{ml_1 s \delta}{M_1 r_0^3} & \frac{ml_1 s \delta}{M_1 r_0^3} & 0 & 0 & \frac{2ml_2 c \delta c \theta}{M_1 r_0^3} & \frac{2ml_2 c \delta c \theta}{M_1 r_0^3} \\ 0 & 0 & 0 & 0 & 0 & 0 \\ \frac{ml_1 c \delta s \theta}{M_1 r_0^3} & \frac{ml_1 c \delta s \theta}{M_1 r_0^3} & -\frac{2ml_2 c \delta c \theta}{M_1 r_0^3} & -\frac{2ml_2 c \delta c \theta}{M_1 r_0^3} & 0 & 0 \\ 0 & 0 & 0 & 0 & 0 & 0 \\ 0 & 0 & -\frac{ml_2^2 c \delta c \theta}{Ar_0^3} & \frac{ml_2^2 c \delta c \theta}{Ar_0^3} & -\frac{ml_2^2 c \delta c \theta}{Ar_0^3} & \frac{ml_2^2 c \delta c \theta}{Ar_0^3} \\ 0 & 0 & 0 & 0 & 0 & 0 \\ \frac{ml_1^2 c \delta s \theta}{2Br_0^3} & \frac{ml_1^2 c \delta s \theta}{2Br_0^3} & 0 & 0 & -\frac{ml_2^2 c \delta s \theta}{2Br_0^3} & \frac{ml_2^2 c \delta s \theta}{2Br_0^3} \\ 0 & 0 & 0 & 0 & 0 & 0 \\ \frac{ml_1^2 s \delta}{2Cr_0^3} & -\frac{ml_1^2 s \delta}{2Cr_0^3} & \frac{ml_2^2 s \delta}{2Cr_0^3} & -\frac{ml_2^2 s \delta}{2Cr_0^3} & 0 & 0 \end{bmatrix} \quad (4.5)$$

Design # 2  $G_2(t)$ :

$$\begin{bmatrix} 0 & 0 & 0 & 0 & 0 & 0 & 0 & 0 \\ 0 & 0 & -\frac{ml_2 s \delta}{M_1 r_0^3} & -\frac{ml_2 s \delta}{M_1 r_0^3} & 0 & 0 & -\frac{ml_{c2} s \delta}{M_1 r_0^3} & -\frac{ml_{c2} s \delta}{M_1 r_0^3} \\ 0 & 0 & 0 & 0 & 0 & 0 & 0 & 0 \\ \frac{ml_1 s \delta}{M_1 r_0^3} & \frac{ml_1 s \delta}{M_1 r_0^3} & 0 & 0 & \frac{ml_{c1} s \delta}{M_1 r_0^3} & \frac{ml_{c1} s \delta}{M_1 r_0^3} & 0 & 0 \\ 0 & 0 & 0 & 0 & 0 & 0 & 0 & 0 \\ \frac{ml_1 c \delta s \theta}{M_1 r_0^3} & \frac{ml_1 c \delta s \theta}{M_1 r_0^3} & -\frac{2ml_2 c \delta c \theta}{M_1 r_0^3} & -\frac{2ml_2 c \delta c \theta}{M_1 r_0^3} & \frac{ml_{c1} c \delta s \theta}{M_1 r_0^3} & \frac{ml_{c1} c \delta s \theta}{M_1 r_0^3} & -\frac{2ml_{c2} c \delta c \theta}{M_1 r_0^3} & -\frac{2ml_{c2} c \delta c \theta}{M_1 r_0^3} \\ 0 & 0 & 0 & 0 & 0 & 0 & 0 & 0 \\ 0 & 0 & -\frac{ml_2^2 c \delta c \theta}{Ar_0^3} & \frac{ml_2^2 c \delta c \theta}{Ar_0^3} & -\frac{ml_1 l_{c1} s \delta}{Ar_0^3} & \frac{ml_1 l_{c1} s \delta}{Ar_0^3} & 0 & 0 \\ 0 & 0 & 0 & 0 & 0 & 0 & 0 & 0 \\ -\frac{ml_1^2 c \delta s \theta}{2Br_0^3} & \frac{ml_1^2 c \delta s \theta}{2Br_0^3} & 0 & 0 & 0 & 0 & -\frac{ml_1 l_{c2} s \delta}{Br_0^3} & \frac{ml_1 l_{c2} s \delta}{Br_0^3} \\ 0 & 0 & 0 & 0 & 0 & 0 & 0 & 0 \\ \frac{ml_1^2 s \delta}{2Cr_0^3} & -\frac{ml_1^2 s \delta}{2Cr_0^3} & \frac{ml_2^2 s \delta}{2Cr_0^3} & -\frac{ml_2^2 s \delta}{2Cr_0^3} & 0 & 0 & 0 & 0 \end{bmatrix} \quad (4.6)$$

where the abbreviations  $c \equiv \cos$ ,  $s \equiv \sin$ , and  $\theta \equiv (u - \theta_s - \lambda)$  have been used for brevity.

The controllability of these conductor-only designs in non-equatorial orbits is not mathematically investigated in this thesis. However, we expect that the designs have controllability characteristics similar to those possessed in equatorial orbits for orbital inclinations *other than*  $11.5^\circ$  which are *less than*  $78.5^\circ$ . In appendix A we find that at certain times (once per sidereal day) the in-plane component ( $\underline{B}_\parallel = B_1 \hat{c}_1 + B_2 \hat{c}_2$ ) of  $\underline{B}$  approaches zero as the orbital inclination approaches  $11.5^\circ$ . At  $i = 11.5^\circ$ ,  $\underline{B}_\parallel$  disappears entirely once per sidereal day. Thus in an  $11.5^\circ$  inclination orbit all the control terms involving  $\alpha$  and  $\beta$  in the equations of motion will disappear once per sidereal day.  $11.5^\circ$  is the approximate angle between the magnetic poles and the corresponding geographic poles. Also in appendix A we find that the out-of-plane component ( $\underline{B}_\perp$ ) of  $\underline{B}$  is zero once per sidereal day at orbital inclinations greater than  $78.5^\circ$ . Thus all control terms involving  $\gamma$  in the equations of motion will disappear once per sidereal day at inclinations greater than  $78.5^\circ$ . Later we find that some of the restrictions mentioned in this paragraph disappear when a pair of electromagnetic thrusters is added.

Because both of these designs are periodic in nature, we do not have to assess the equatorial-orbit controllability of the designs at every time instant in order to prove controllability for all time. Instead we evaluate the rank of the controllability matrix  $M_c$  for both designs for the cases:

- $\theta = (u - \theta_g - \lambda) = 2k(90^\circ), k = 0, 1, 2, \dots \Rightarrow \sin \theta$  terms in  $G(t)$  go to zero
- $\theta = (u - \theta_g - \lambda) = (2k + 1)(90^\circ), k = 0, 1, 2, \dots \Rightarrow \cos \theta$  terms in  $G(t)$  go to zero
- $\theta = (u - \theta_g - \lambda) = \text{all other values} \Rightarrow \cos \theta, \sin \theta$  terms in  $G(t)$  are non-zero

Evaluating the equatorial-orbit controllability for these three cases is equivalent to investigating the controllability for all time instants. We want a design which proves to be totally controllable for all values of  $(u - \theta_g - \lambda)$ . We use the CONTROLLER.M program to evaluate controllability by determining the rank of the controllability matrix  $M_c$ . Design # 1 becomes *uncontrollable* when  $(u - \theta_g - \lambda)$  is an odd multiple of  $90^\circ$ . Design # 2 is *completely controllable* for all values of  $(u - \theta_g - \lambda)$ . This is an important result. We foresaw a result like this in chapter three when we noted that the  $\psi_1, \psi_2$  equations for Design # 1 (eqs. 3.15 and 3.16) did not include any "constant" control terms. Therefore all further discussion will be limited to Design # 2. Although we have only proved Design # 2 controllability for an equatorial orbit, we expect this result applies to other low-inclination orbits as well.

Surprisingly, Design # 2 turns out to be completely controllable at all points in an equatorial orbit *even when some conductors are removed* (columns of  $G$  eliminated). We believe that any three conductors can be removed while maintaining complete controllability. This conclusion arises from much experimentation with the CONTROLLER.M program. This redundancy can increase reliability and free conductor towers for other uses. There are practical constraints on which conductors could be removed. For instance, use of out-of-plane cross conductors for gross translation is not recommended due to structural design limitations.

#### 4.2 Controller Design and Performance

In this section we use the gain-scheduling concept to design a control system that applies to a particular instant in time. A series of such time-specific controllers designed

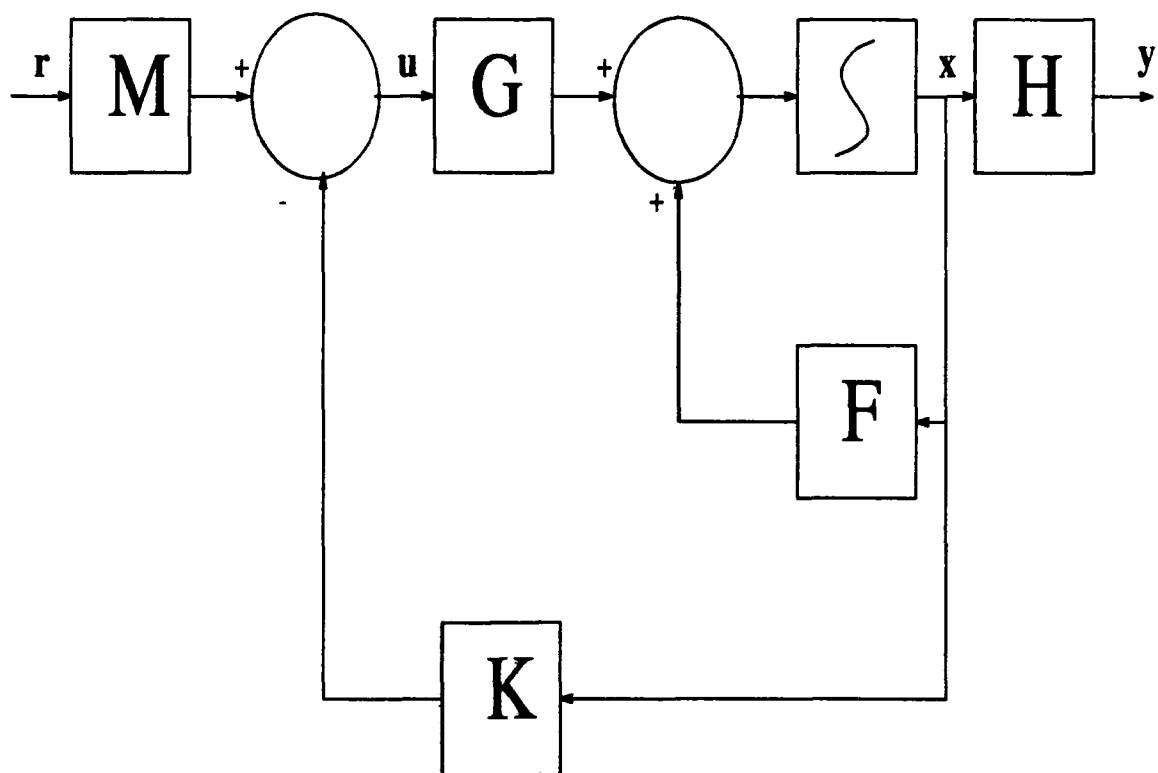


Figure 4.1. Closed-Loop System Block Diagram

over the time span of one sidereal day could be combined to form a full-blown time-varying control system.

The control system should allow the tracking vehicle to stay a fixed distance away from and maintain a constant attitude with respect to the target vehicle.

This goal is stated in control terminology as: the tracking vehicle must *track* a constant *reference command*. We use the words “tracking” and “command-following” interchangeably. The reference command consists of the variables we want to track: 3 relative positions and three relative attitude angles:

$$\underline{r} = \begin{bmatrix} x_{des} & y_{des} & z_{des} & \psi_{1des} & \psi_{2des} & \psi_{3des} \end{bmatrix}^T$$

The reference command vector  $\underline{r}$  defined here should not be confused with the POTV inertial position vector  $\underline{r}$  defined in chapter two. The controller should ensure system stability and be robust with respect to modeling error and noise. Figure 4.1 shows the

block diagram of the closed-loop control system proposed to accomplish these goals. Note that all states are assumed to be available for feedback. If this were not the case, a Kalman filter (11:224) could be used to obtain an estimate of the state. The feedback controller  $K$  is chosen to provide robust closed-loop stability. The pre-filter  $M$  is designed for good reference command tracking. The dimensions of all vectors and matrices in figure 4.1 are as follows:

$\underline{r}^{6 \times 1}$	$\equiv$	reference command vector
$\underline{u}^{8 \times 1}$	$\equiv$	control vector
$\underline{x}^{12 \times 1}$	$\equiv$	system state vector
$\underline{y}^{6 \times 1}$	$\equiv$	output vector
$F^{12 \times 12}$	$\equiv$	system matrix
$G^{12 \times 8}$	$\equiv$	input matrix
$H^{6 \times 12}$	$\equiv$	output matrix
$M^{8 \times 6}$	$\equiv$	pre-filter matrix
$K^{8 \times 12}$	$\equiv$	controller gain matrix

There are many methods of feedback controller design. We choose the Linear Quadratic Regulator (LQR) method because this method guarantees closed-loop stability and provides good stability margins (11:223,227-229). The LQR controller is the controller  $K$  that minimizes the performance index:

$$J = \int_0^{\infty} (\underline{x}^T Q \underline{x} + \underline{u}^T R \underline{u}) dt$$

subject to the constraint:

$$\dot{\underline{x}} = F \underline{x} + G \underline{u}$$

where  $Q$  is the state-weighting matrix and  $R$  is the control-weighting matrix. These matrices are of the form  $\rho U$ , where  $U$  is the identity matrix.  $\rho_x$  is the weighting on the  $Q$  matrix.  $\rho_u$  is the weighting on the  $R$  matrix. These weightings are chosen by the designer.



Usually one of the weightings is fixed at unity while the other is varied. Then the resulting output response and corresponding control behavior are studied. The methodology behind the derivation of the controller  $K$  that minimizes the performance index  $J$  is described by Maciejowski (11:222-227) and will not be gone into here. The resulting  $K$  is a constant gain matrix. In practice, the MATLAB command "LQR(F,G,Q,R)" is used to derive the gain matrix  $K$ .

After the controller  $K$  is designed, we derive the pre-filter  $M$ .  $M$  should be designed with optimal command-following in mind. We assume that  $M$ , like  $K$ , is a constant gain matrix. After studying the interconnections of the system blocks in figure 4.1 we write:

$$\begin{aligned}\dot{\underline{x}} &= F\underline{x} + G\underline{u} \\ &= F\underline{x} + G(M\underline{r} - K\underline{x}) \\ &= (F - GK)\underline{x} + GM\underline{r} \\ \underline{y} &= H\underline{x}\end{aligned}$$

$\dot{\underline{x}}$  should be zero in the steady-state as a consequence of good tracking of the constant reference command. Then the state equations become:

$$\begin{aligned}\dot{\underline{x}} = 0 &= (F - GK)\underline{x}_{ss} + GM\underline{r} \\ \underline{y}_{ss} &= H\underline{x}_{ss}\end{aligned}$$

These equations combine to yield:

$$\underline{y}_{ss} = -H(F - GK)^{-1}GM\underline{r} \quad (4.7)$$

But since the output  $\underline{y}_{ss}$  should track the reference command  $\underline{r}$ , the pre-filter  $M$  must be chosen to satisfy:

$$-H(F - GK)^{-1}GM = U \quad (4.8)$$

where  $U$  is the identity matrix. We note that  $M$  is non-square. Solving this equation for  $M$  we arrive at:

$$M = -(H(F - GK)^{-1}G)^{\dagger} \quad (4.9)$$

where the  $\dagger$  symbol denotes the pseudo-inverse operation.

**4.2.1 Stability Robustness** Uncertainty in the plant model can lead to closed-loop system instability. The quality of a system that makes it stable in the face of uncertainty is called stability robustness. There is a major source of uncertainty in the POTV plant model. This is the magnetic field magnitude error inherent in the use of the simple dipole model of the geomagnetic field. This error may be up to 30% at the earth's surface and decreases as orbital altitude increases. In control terminology this error is termed a "multiplicative perturbation at the plant input". Fortunately the LQR design method guarantees a gain margin of 6 dB when the weighting matrices used are of the form  $\rho U$  (11:229). This is more than enough margin to guarantee POTV closed loop stability in the face of magnetic field modeling error. This margin also helps overcome model linearization error.

**4.2.2 Steady-State Controllability** The most surprising result from experimentation with the CONTROLLER.M program is that even though the system is completely controllable, it does not appear to be *steady-state controllable* (a term coined for this thesis by Dr. B. Liebst). In other words, the POTV can reach any position state but can't remain at that state unless it happens to be an equilibrium state. No controller can be designed that acceptably tracks a reference command consisting of three relative positions and three attitude angles for a POTV using *only* electrical conductors for thrust. All attitude angles are tracked but no position components are tracked accurately. The designed controller for the conductor-only POTV works acceptably only when the CONTROLLER.M program is modified to include only *two* of the position components plus the three attitude angles in the reference command vector. The position component that was not included in the reference command then behaves in an unpredictable manner. The problem arises from the rank deficiency of the  $G$  input matrix as shown below. Remember we have shown already that its rank can never exceed five because rows two, four, and six are linearly dependent. The rank deficiency arises from the "translational part" of the input matrix. To understand more about why  $G$  should have rank six for steady-state controllability, we return to equations 4.7 and 4.8:

$$\begin{aligned}\underline{y}_{ss} &= -H(F - GK)^{-1}GM\underline{r} \\ -H(F - GK)^{-1}GM &= U\end{aligned}$$

Recall that the second equation is the necessary condition for the steady-state output  $\underline{y}_{ss}$  to track the six-component reference command  $\underline{r}$ . The  $6 \times 6$  identity matrix  $U$  obviously has rank six. According to Strang (20:201), the rank of the expression  $-H(F - GK)^{-1}GM$  must be less than or equal to the smallest matrix rank found in the expression. We have already shown that the rank of  $G$  is always less than or equal to five. Thus the expression  $-H(F - GK)^{-1}GM$  can never have rank six and thus can never equal the identity matrix. The steady-state output  $\underline{y}_{ss}$  can only track five of the components of the six-component reference command  $\underline{r}$ .

The seeming solution to the steady-state position controllability problem is to somehow increase the rank of  $G$  to six. We introduced conductors to the design at many different locations and orientations in an attempt to accomplish this desirable result. The new conductors added columns to the  $G$  matrix but unfortunately  $G$  still lost rank in the old, familiar fashion:

$$\frac{-2\alpha}{\gamma}(\text{Row}_2) + \frac{\beta}{\gamma}(\text{Row}_4) + \text{Row}_6 = \underline{0}$$

We also deleted conductors to make the design unsymmetrical with similar lack of success.

Steady-state controllability can also be interpreted as the ability of the control system to exert thrust in any direction at any time. Clearly this is not the case with the POTV. The cross-product nature of the electrodynamic force tells us that a force can not be exerted in the direction of the instantaneous  $\underline{B}$  vector:

$$\underline{F}_B = I \underline{L} \times \underline{B} \quad (4.10)$$

We thus make the important conclusion that no conductor-only design configuration leads to steady-state position controllability. Thus while the system is completely controllable using only electrodynamic forces (any state can be reached in a finite amount of time), it cannot maintain any state continuously other than equilibrium states.

One method of improving the rank of the  $G$  matrix is to introduce force-producing devices which do not rely upon the electrodynamic effect. We introduce a pair of electromagnetic thrusters to produce out-of-plane thrust. They are attached to the centers of the out-of-plane crosses and produce thrust in the "north" or "south" out-of-plane directions. Only one thruster operates at a time. The modified control vector  $\underline{u}$  is:

$$\underline{u} = \begin{bmatrix} I_{1_n} & I_{1_s} & I_{2_n} & I_{2_s} & I_{1_n} & I_{1_s} & I_{2_n} & I_{2_s} & T \end{bmatrix}^T$$

for a total of nine controls. Positive  $T$  means that the southern cross thruster is firing and negative  $T$  means the northern cross thruster is firing. The modified  $12 \times 9 G(t)$  matrix is:

$$\begin{bmatrix} 0 & 0 & 0 & 0 & 0 & 0 & 0 & 0 & 0 \\ 0 & 0 & -\frac{m\gamma l_2}{M_t r_0^3} & -\frac{m\gamma l_2}{M_t r_0^3} & 0 & 0 & -\frac{m\gamma l_{c2}}{M_t r_0^3} & -\frac{m\gamma l_{c2}}{M_t r_0^3} & 0 \\ 0 & 0 & 0 & 0 & 0 & 0 & 0 & 0 & 0 \\ \frac{m\gamma l_1}{M_t r_0^3} & \frac{m\gamma l_1}{M_t r_0^3} & 0 & 0 & \frac{m\gamma l_{c1}}{M_t r_0^3} & \frac{m\gamma l_{c1}}{M_t r_0^3} & 0 & 0 & 0 \\ 0 & 0 & 0 & 0 & 0 & 0 & 0 & 0 & 0 \\ -\frac{m\beta l_1}{M_t r_0^3} & -\frac{m\beta l_1}{M_t r_0^3} & -\frac{2m\alpha l_2}{M_t r_0^3} & -\frac{2m\alpha l_2}{M_t r_0^3} & -\frac{m\beta l_{c1}}{M_t r_0^3} & -\frac{m\beta l_{c1}}{M_t r_0^3} & -\frac{2m\alpha l_{c2}}{M_t r_0^3} & -\frac{2m\alpha l_{c2}}{M_t r_0^3} & \frac{1}{M_t} \\ 0 & 0 & 0 & 0 & 0 & 0 & 0 & 0 & 0 \\ 0 & 0 & -\frac{m\alpha l_2^2}{Ar_0^3} & \frac{m\alpha l_2^2}{Ar_0^3} & -\frac{m\gamma l_1 l_{c1}}{Ar_0^3} & \frac{m\gamma l_1 l_{c1}}{Ar_0^3} & 0 & 0 & 0 \\ 0 & 0 & 0 & 0 & 0 & 0 & 0 & 0 & 0 \\ \frac{m\beta l_1^2}{2Br_0^3} & -\frac{m\beta l_1^2}{2Br_0^3} & 0 & 0 & 0 & 0 & -\frac{m\gamma l_1 l_{c2}}{Br_0^3} & \frac{m\gamma l_1 l_{c2}}{Br_0^3} & 0 \\ 0 & 0 & 0 & 0 & 0 & 0 & 0 & 0 & 0 \\ \frac{m\gamma l_1^2}{2Cr_0^3} & -\frac{m\gamma l_1^2}{2Cr_0^3} & \frac{m\gamma l_2^2}{2Cr_0^3} & -\frac{m\gamma l_2^2}{2Cr_0^3} & 0 & 0 & 0 & 0 & 0 \end{bmatrix} \quad (4.11)$$

which has a rank of six. The addition of electromagnetic thrusters makes the POTV *completely steady-state controllable*. In addition to this desirable result, the addition of the thrusters has another benefit: from experimentation with the CONTROLLER.M program we expect that the POTV becomes completely controllable at all points in an  $11.5^\circ$  orbit (the conductor-only design was already completely controllable for other low-inclination orbits). This was not the case for a conductor-only design. Unfortunately, we do not believe that the thrusters make the POTV completely controllable at all points in orbits with inclinations of greater than  $78.5^\circ$  (as was also the case with the conductor-only design). The Design #1 configuration may be a more appropriate design for high-inclination orbits. This possibility is not investigated.

## V. Steady-State Tracking and Docking Performance

In the previous chapter we discussed the design of a controller that enables the POTV to track a target vehicle. In this chapter we discuss POTV conductor sizing, steady-state tracking performance, and docking performance. General features of tracking/docking performance are related to controller design parameters. One steady-state tracking example and two docking examples are shown and results described.

### 5.1 Vertical In-Plane Conductor Sizing for Orbit Transfer

In this section we size the vertical ( $x$ ) in-plane conductors for an orbital transfer requirement. The horizontal ( $y$ ) in-plane conductors are discussed in the docking section of this chapter. The out-of-plane cross conductors and their non-conducting support towers are not explicitly sized. We assume that the cross conductors are much smaller than the in-plane conductors because we expect they will be used primarily for attitude control.

A practical method to move a low thrust vehicle like the POTV from a low prograde orbit to a higher altitude prograde orbit is to exert a small constant thrust along the orbital velocity vector (eastward). Thrust in the westward direction would cause the orbit to degrade. The trajectory resulting from a small constant eastward thrust is a gentle spiral outward from the lower orbit to the higher orbit assuming the lower orbit was circular. Wiesel (24:89-90) derives the time-of-flight equation for this method of orbital transfer:

$$t - t_0 = \frac{M_t \sqrt{GM_\oplus}}{F} \left( \frac{1}{\sqrt{r_l}} - \frac{1}{\sqrt{r_u}} \right) \quad (5.1)$$

where  $F$  is the applied thrust,  $M_t$  is the total system mass,  $r_l$  is the lower orbital radius, and  $r_u$  is the upper orbital radius. We use this equation to determine the thrust required to move the POTV from one circular orbit to another for a given transfer time and vehicle mass.

The ASSET version of the POTV spacecraft is required to move aluminum salvaged from space shuttle external fuel tanks from an orbital altitude of approximately 300 km to an altitude of 460 km. Here we assume that the space shuttle can deliver its external

tank to 300 km (4). The proposed maximum altitude of the space station Freedom is 460 km (13). The space station travels in an almost circular orbit ( $e \equiv 0.009$ ). We assume for ease of derivation that the POTV is traveling in circular orbit when it finishes scavenging a shuttle external tank for aluminum. Now we can determine the amount of thrust required to move a 50,000 kg POTV from 300 km to 460 km in thirty days. We have chosen 50,000 kg as the maximum allowed value of the total system mass. This figure includes a fixed 31,300 kg central mass and the total mass of the conductor towers, which has not been determined yet. Evaluating equation 5.1 we find the required force (thrust) is approximately 1.75 newtons. Now we will "size" the two vertical in-plane conductors (one "up" and one "down") required to produce this thrust assuming a certain current level can be sustained. Penzo and Ammann (15:129) discuss a proposed electrodynamic tether system capable of handling 125 amps of current. We take this to be a reasonable sustainable current limit. Then the familiar Lorentz equation (eq. 1.1) is used to make an engineering estimate of the total conductor length required:

$$\underline{F}_B = I \underline{L} \times \underline{B}$$

We assume that the needed force (1.75 newtons) is produced by the interaction of the two vertical in-plane conductors with the out-of-plane component of the geomagnetic field ( $B_{\perp}$ ). At the space station inclination of  $28.5^{\circ}$  (13),  $B_{\perp}$  consists of a large constant component and a smaller sinusoidal component (see appendix A for a plot of  $B_{\perp}$  ( $B_3$ ) at  $i = 28.5^{\circ}$ ). Over the altitude range of 300-460 km,  $B_{\perp}$  varies from a low of approximately  $1.94 \cdot 10^{-5}$  tesla to a high of  $2.60 \cdot 10^{-5}$  tesla. For calculation purposes we take  $B_{\perp}$  to be approximately a constant  $2.26 \cdot 10^{-5}$  tesla over the orbital transfer. Solving the Lorentz equation for  $L$ , we find that the two vertical in-plane conductors must have a combined length of approximately 620 meters for the mission parameters we have outlined.

We would like to minimize the amount of thrust needed for planar orbital radial change because this minimizes the product of current and conductor length. Since power is proportional to current squared, current is a variable worth minimizing. There are several ways to accomplish this:

- Minimize the amount of radial distance to be traversed.
- Increase the amount of time allowed for the maneuver.
- Decrease the system mass by minimizing the central mass and by minimizing the linear mass density of the conductor towers.

We can also minimize the amount of current needed for a given thrust level by making the conductors as long as possible. Unfortunately this conflicts with the goal of minimizing total system mass.

What size power plant would be needed for the particular orbital transfer example (ASSET POTV) we have described? We use the approximate induced voltage equation (eq. C.1) for low-inclination orbits, and the power equation (eq. C.2) derived in appendix C to derive the necessary power supply power:

$$\begin{aligned} V_{ind} &= \left( \sqrt{\frac{GM_{\oplus}}{r}} - \omega_{\oplus} r \right) B(L) \\ &\simeq 101 \text{ volts} \end{aligned}$$

where we have used  $r = 300$  km to be conservative in our calculation of  $V_{ind}$  because the induced voltage is greatest at the lower orbital radius. Then we derive the needed power:

$$P_{ps} = IV_{ind} + I^2 R_{tot}$$

where:

$$R_{tot} = R_c + R_{ion} + R_{load}$$

If we assume that all power is being used for thrust,  $R_{load}$  is zero. From chapter one we know  $R_{ion}$  varies from approximately one ohm to twenty ohms. The conductor resistance  $R_c$  is equal to the conductor resistance per unit length multiplied by the total conductor length. The 125 amp example electrodynamic tether discussed by Penzo and Ammann has a resistance per length of approximately  $7.7 \cdot 10^{-5}$  ohms per meter (15:129). Using this value, the conductor resistance is 0.05 ohms. So most of the resistance arises in the ionospheric current path. The total power  $P_{ps}$  for this example for a current of 125 amps



and the worst case ionospheric resistance of twenty ohms is calculated to be about 325,000 watts, with most of the power being dissipated in the ionosphere resistance. If we use the best case one ohm value for the ionospheric resistance, the total power is approximately 44,000 watts. These figures have a great deal of built-in uncertainty because the resistance of the ionosphere is not well understood. To minimize power requirements a practical vehicle must be designed to minimize all sources of resistance. More importantly, conductor lengths should be maximized to reduce the amount of current needed for a given thrust level since power is proportional to the current squared. A possible option to maximize conductor length would be to deploy retractable, low-mass, flexible tethers at the end of the rigid conductors. These flexible tethers would be suitable for the orbital transfer task since precision position control is not required.

Would the magnetic field generated by a 125 amp current in the vertical in-plane conductors interfere with the currents flowing through other conductors? If we assume a minimum distance between conductors, we can answer this question. Let's assume a minimum separation distance of 5 meters. Then equation 1.2 is used to estimate the magnetic field generated by a 125 amp current at a 5 meter radial distance. The answer is  $5 \cdot 10^{-5}$  tesla. This is approximately one-fourth of the geomagnetic strength at the altitudes at which we expect to use the ASSET POTV. A robust control system should be able to handle this "disturbance".

## *5.2 Steady-State Tracking Performance*

The controller design program CONTROLLER.M is a MATLAB program written for this study which lets the user enter various parameters which describe the POTV system, enter the initial standoff position and relative attitude (initial state), enter the desired standoff position and relative attitude (reference command), enter the LQR design weightings  $\rho_x$  and  $\rho_u$ , and evaluate the resulting transient and steady-state response of the outputs and controls. See appendices E and F for three sample runs, corresponding plots, and a complete program listing. All conclusions reached about steady-state and non-steady-state tracking performance in this and following sections are the result of experimentation with this program. The input matrix  $G(t)$  in the program includes the pair

of electromagnetic plasma thrusters added at the end of chapter four as well as the Design # 2 conductor configuration. We evaluate the tracking performance of the controller for two general cases:

- **Steady-State Tracking:**  $\underline{r} = \underline{x}(t_0)$  The reference command is equal to the initial state of the system. The POTV is being directed to stay at its initial position and attitude relative to the target vehicle.
- **Non-Steady-State Tracking:**  $\underline{r} \neq \underline{x}(t_0)$  The reference command is not equal to the initial state of the system. The system is being commanded to a new relative position and/or relative attitude. This is the case when the POTV is commanded to dock with a target vehicle. We show two docking examples.

In this section we discuss the steady-state tracking case. The docking cases are discussed in the next section.

A steady-state tracking example is the first of three examples shown in appendix E. A sample run at the beginning of the appendix shows the data the user enters to describe the POTV configuration, design weightings, and tracking requirements. Plots are made of: position states, attitude states, forces, moments, and conductor currents. For the first example we choose an  $l_2$  length of 310 meters to provide the required large steady-state force in the  $x$  direction. This is also the length derived in the previous section for the orbital transfer requirement. We have assumed here without proof that the POTV can rotate 90 degrees about its  $z$  axis when it transitions from orbital transfer mode to steady-state tracking mode. From section 2.2.1.2 we know that no steady-state force will be required in the  $y$  direction. Thus,  $l_1$  can be chosen to be "short". We assume here that most of the generated forces are the result of current interactions with the large out-of-plane component of  $\underline{B}$  present in low-inclination orbits. We choose an  $l_1$  length of 50 meters because this is a convenient length if the vertical in-plane towers are also used for docking purposes. The non-conducting out-of-plane towers are chosen to be 50 meters long and all the conductor lengths in the out-of-plane crosses are chosen to be 20 meters long. The out-of-plane crosses are designed with attitude control in mind. We do not want large currents to be generated in the crosses because the resulting large forces might cause the

non-conducting support towers to fail structurally. All of the conductor length information presented here and other information about the specific vehicle used in the examples is tabulated in appendix D. The same vehicle configuration is used for all three examples.

The LQR controller design methodology we have used appears to be well-suited to the steady-state tracking example. The plots in appendix section E.1 backup the following observations: No transient position output behavior is observed. The position outputs are always constant and equal to their initial values  $\underline{x}(t_0)$  regardless of state and control weighting. The attitude outputs each exhibit a decaying oscillatory sort of behavior which settles down to a constant steady-state value. The observed sign and magnitude of the steady-state forces and moments are the same as those predicted in sections 2.2.1.2 and 2.2.2.2. If we increase the state-weighting  $\rho_x$ , the amplitude of oscillation of the attitude outputs decreases and settling times decrease. We believe that the extremely small non-constant force observed in the  $y$  direction arises from moment required for attitude control. We think that other small non-constant forces required for attitude control do not appear on the plots of forces in the  $x$  and  $z$  directions because the constant forces needed for steady-state position standoff are many orders of magnitude greater than the non-constant forces required for attitude control.

### 5.3 General Non-Steady-State Tracking Performance

The findings in this section apply to both of the docking examples that follow. Unlike steady-state tracking, transient output behavior is observed for position as well as attitude outputs. All outputs exhibit the "decaying oscillation to a constant steady-state value" type behavior. As in steady-state tracking, the amplitude of oscillation and the settling time decrease as the state-weighting  $\rho_x$  is increased. Unfortunately as  $\rho_x$  is increased, the transient initial control requirement increases. We also observe that as the difference between the initial state vector and the reference command vector increases, the transient initial control requirement increases. Also for a fixed state-weighting, as the difference increases, the amplitude of the initial oscillation of the outputs increases.

Heavy state-weighting is wanted for desirable transient response behavior. Light state-weighting is desired to minimize the transient initial control effort required. This is

a good example of the conflicting requirements commonly found in engineering problems. One solution is to make the state-weighting  $\rho_x$  large enough to satisfy the speed of response requirements of a particular problem. Then the initial reference command is made equal to the initial state. Then the reference command is moved away from the initial state toward the desired final state by small enough increments such that the initial control requirement is brought below an acceptable level. We refer to this process as "stepping" the reference command. Another possible solution to this problem which is applicable to R-BAR docking is presented in the R-BAR docking subsection.

#### 5.4 Docking Examples

In the docking examples in this section we assume that the POTV has been moved close enough to the target vehicle for the linearized relative positional and rotational equations of motion to be valid. Examples are shown in appendix E for two different in-plane docking approaches. The vehicle lengths used for the steady-state tracking example are used here. An out-of-plane docking approach (Z-BAR) is discussed.

**5.4.1 R-BAR** An R-BAR approach assumes that both of the vehicles are in the same orbital plane. The POTV approaches the target vehicle by moving along the radius vector connecting the center of the earth and the target vehicle. Forces in the  $x$  and  $y$  direction are exerted to move the POTV downward/upward along the radius vector and to keep the POTV from moving east or west as it moves along the radius vector. A specific example is shown in appendix section E.2.

R-BAR position standoff in the  $x$  direction is the most energy-expensive type of standoff. Standoff in the  $z$  direction requires three times less control effort. Standoff in the  $y$  direction requires no control effort. We have repeated these conclusions here from section 2.2.1.2 for convenience. Long horizontal in-plane conductors are required to produce the necessary force in the  $x$  direction. We can in fact make an engineering approximation to the length of the horizontal in-plane conductors ( $l_2$ ) needed for a given vehicle mass, maximum current, and R-BAR standoff distance ( $x$ -direction). The following derivation

makes use of equations 1.1 and 2.17.

$$\begin{aligned} F_{x,,} &= 3n^2 M_t x_{,,} \\ I_2(2l_2)B_{\perp} &= 3n^2(M_{cyl} + 2\rho(l_1 + l_2 + l_t + l_{c_1} + l_{c_2}))x_{,,} \end{aligned}$$

which can be solved for  $l_2$  to yield:

$$l_2 = \frac{M_{cyl} + 2\rho(l_1 + l_t + l_{c_1} + l_{c_2})}{2I_2 B_{\perp} / 3n^2 x_{,,} - 2\rho} \quad (5.2)$$

We note that  $l_2$  is extremely sensitive to the denominator expression  $2I_2 B_{\perp} / 3n^2 x_{,,} - 2\rho$ . Any parameter in this expression that varies will significantly affect the sizing of  $l_2$ . We repeat some of the example vehicle descriptive information from appendix D here for the calculation of  $l_2$ . Using  $M_{cyl} = 31300$  kg,  $\rho = 7.3$  kg/m,  $l_1 = 50$  m,  $l_t = 50$  m,  $l_{c_1} = l_{c_2} = 20$  m,  $I_2 = 125$  amperes,  $B_{\perp} \simeq 2.6 \cdot 10^{-5}$  tesla,  $n^2 = 1.28 \cdot 10^{-6}$  rad<sup>2</sup>/sec<sup>2</sup>, and  $x_{,,} = 100$  m:

$$l_2 \simeq 14000 \text{ m}$$

which is clearly an excessive length for "rigid" conductor towers. If we recalculate  $l_2$  using an  $x$  standoff distance of 50 m, the required  $l_2$  length is approximately 1700 m. One way the problem of long  $l_2$  conductors can be remedied is by allowing more current. This could be done by "bundling" several conductors together in a single structural tower, splitting the required current among several conductors.

**5.4.2 V-BAR** When the POTV and the target vehicle are in the same orbit, one way the POTV can approach the target is by moving in the  $y$  direction along the orbit. This is known as a V-BAR docking approach. Forces in the  $x$  and the  $y$  direction are exerted to move the POTV eastward/westward in the orbit and to keep the POTV from moving up or down in the orbital plane. A specific example of V-BAR docking is shown in appendix section E.3.

5.4.3 *Z-BAR* The Z-BAR approach starts with the POTV and target vehicle not in the same orbital plane. The POTV approaches the target vehicle along the normal to the target orbit. An example for this approach is not shown in this thesis because when we ran a Z-BAR approach with CONTROLLER.M, no currents were used for position control. The only "controls" that were used for position change were the electromagnetic plasma thrusters. The conductor currents were very small and appeared to be used only for attitude control.

## VI. Conclusions and Recommendations

In this final chapter we summarize the major results of the thesis work and make recommendations for further research.

While the derivation of the linearized relative position equations of motion (Clohessy-Wiltshire equations) has been "done", we are not aware of others performing our particular derivation of the small-angle relative rotational equations of motion. These equations are the rotational equivalent of the Clohessy-Wiltshire equations. From these two sets of equations we derived the steady-state forces and moments required to maintain a continuous standoff in position and attitude. These steady-state predictions were confirmed in the example force and moment plots contained in appendix E. Further research should be done to determine at what point the linearization assumptions (used extensively in the derivation of the equations of motion) start to break down.

The derivation of the geomagnetic field in spacecraft coordinates was the most important early result in the thesis research. Without this knowledge the derivation of the full equations of motion including magnetic forces and moments would have been impossible. The behavior of the in-plane and out-of-plane  $\underline{B}$  components over the orbital period and over the period of a day was unexpected. Further research should employ a better model of the geomagnetic field than the simple dipole model to determine if the in-plane components of  $\underline{B}$  really do "disappear" at one-day intervals in an  $11.5^\circ$  inclination orbit. A similar analysis could be done for the out-of-plane component of  $\underline{B}$  in the  $78.5^\circ$  inclination orbit. The error arising from our use of the simple dipole model was compensated for by the design of a robust control system. NASA software (15:168) exists that more accurately models the geomagnetic field in geocentric coordinates. This software could be modified to translate between geocentric coordinates and spacecraft coordinates if this has not been done already.

The derivation of  $\underline{B}$  in spacecraft coordinates enabled us to derive the full equations of motion including the effects of magnetic force as well as gravitational force. While aerodynamic and oblateness effects were described in appendix B, they were not considered

in the controller design. These forces are significant in low earth orbit and are deserving of further study. The air drag especially needs to be quantified.

After deriving the full equations of motion we used a state space model to represent the system. This sort of representation was convenient in addressing the issues of controllability, steady-state controllability, and controller design. We found that all conductor designs were not equal. Design # 1 lost control authority in equatorial orbits at points where Design # 2 did not. Future researchers could investigate whether Design #1 is a better design than Design #2 for high-inclination orbits. We suspect that this is the case. We also found that some of the conductors were redundant. Further work should address the design of a minimal conductor configuration with one or more redundant conductors for docking purposes.

One of the most significant findings of the thesis was the seeming impossibility of building an electrical conductor-only design that was *steady-state controllable*. This was clearly a disappointing result. We had hoped to build a conductor-only design. The addition of a pair of electromagnetic plasma thrusters allowed the POTV to track all components of position as well as attitude.

An important accomplishment of this work was the successful design of a closed-loop controller using the LQR method. This was not a "given" at the beginning of the research because the open-loop state responses of the system to the control currents appeared to be hopelessly coupled. In other words, a control action giving a desired change in one state would produce simultaneous undesired changes in other states.

The LQR design method had one major shortcoming: no bounds could be placed on the amount of control energy the controller could "ask for." Future researchers could conceivably use a design methodology other than LQR that would allow the designer to place bounds upon the allowable control energy. Also, the possibility of the design of a reduced state controller should be investigated.

We felt that the gain-scheduling concept was an adequate way to use time-invariant control techniques to analyze a time-varying system. Future researchers could modify the CONTROLLER.M program to produce a controller  $K$ /pre-filter  $M$  combination for many



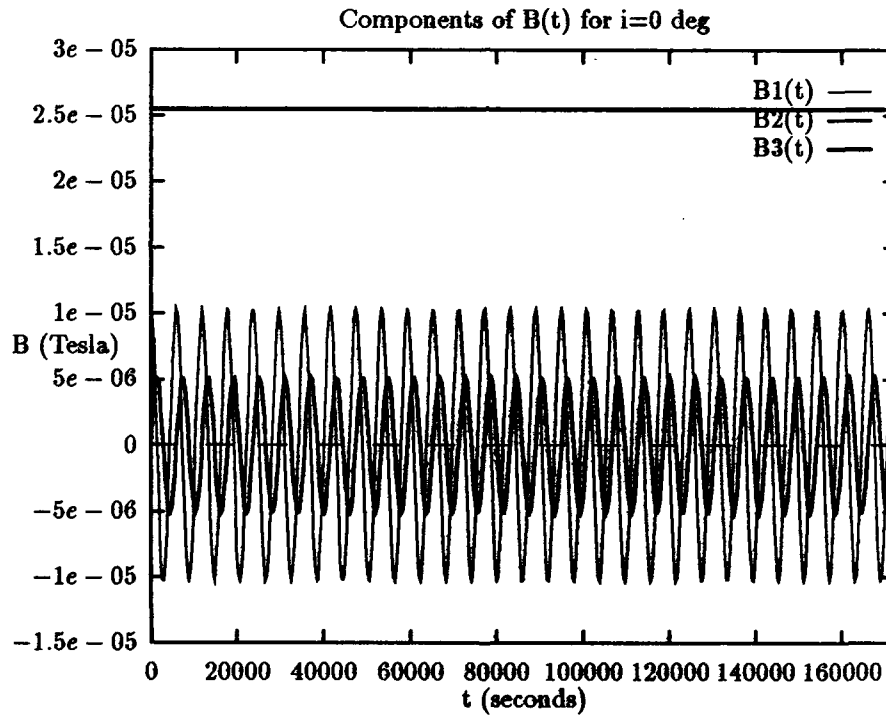
"steps" (times) in the POTV orbit over the period of a sidereal day. Then each component of the gain matrix  $K$  could be plotted versus time to deduce the characteristics of the time-varying controller. We predict that the components of the time-varying gain matrix  $K(t)$  will consist of constants and sinusoidal terms.

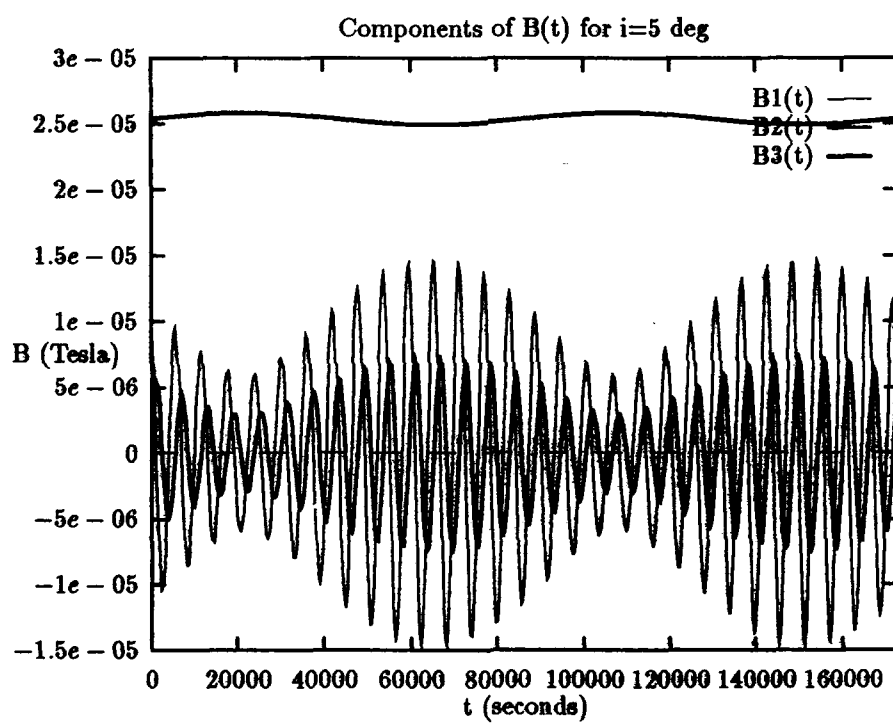
An important result of this research was the finding that large tracking vehicles require large currents for steady-state position standoff in any direction other than along the orbital velocity vector. Perhaps this problem could be handled by "bundling" several conductors together in a single structural tower, splitting the required current among several conductors. This idea may not be technically feasible. The currents generated by the PMGs associated with each conductor might interfere with each other. This idea is a good candidate for further research.

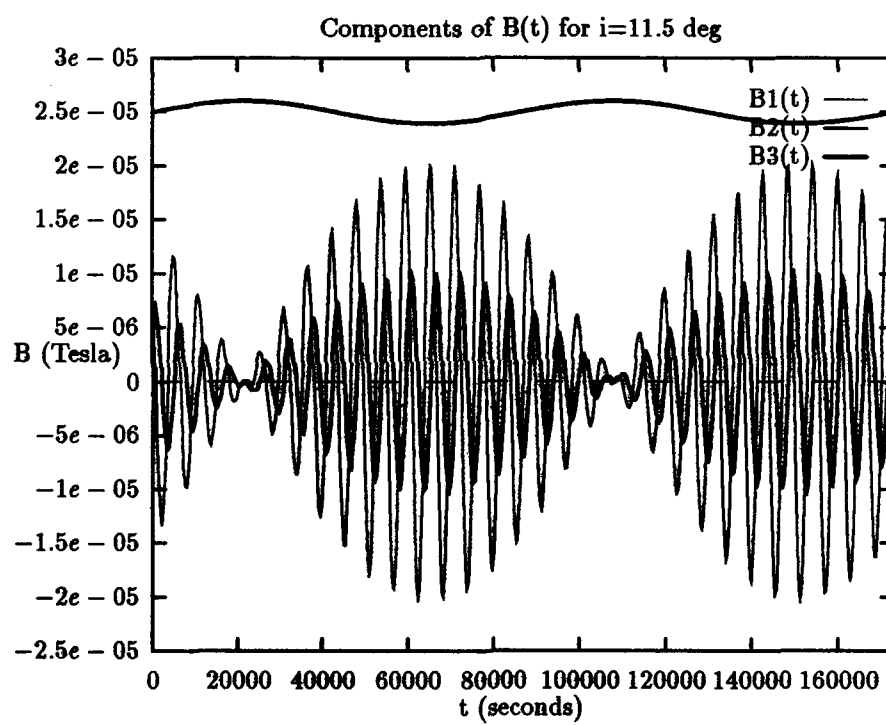
We addressed the problem of orbital radial change in the sizing of the vertical in-plane conductors. The most important type of orbital maneuver for the POTV after radial change is that of inclination change. Penzo and Ammann claim that an electrodynamic tether can be used to alter all six orbital elements (15:168-169). Their ideas should be applicable to the POTV. The amount of current needed for maneuvers decreases with increasing magnetic field strength. A Jupiter Inner Magnetosphere Maneuvering Vehicle (15:66-67) has been proposed to explore the Jovian system, where the field strength is approximately twenty times that of the earth. Another more near term application is that of pure attitude control. We do not know of any research being performed in the area of attitude control using *multiple, external* conductors. A POTV-like vehicle could theoretically be used anywhere a strong magnetic field and plasma exist. We believe an exciting application would be to use POTV technology to design a vehicle to explore the magnetosphere of the sun. On that futuristic note we end the thesis.

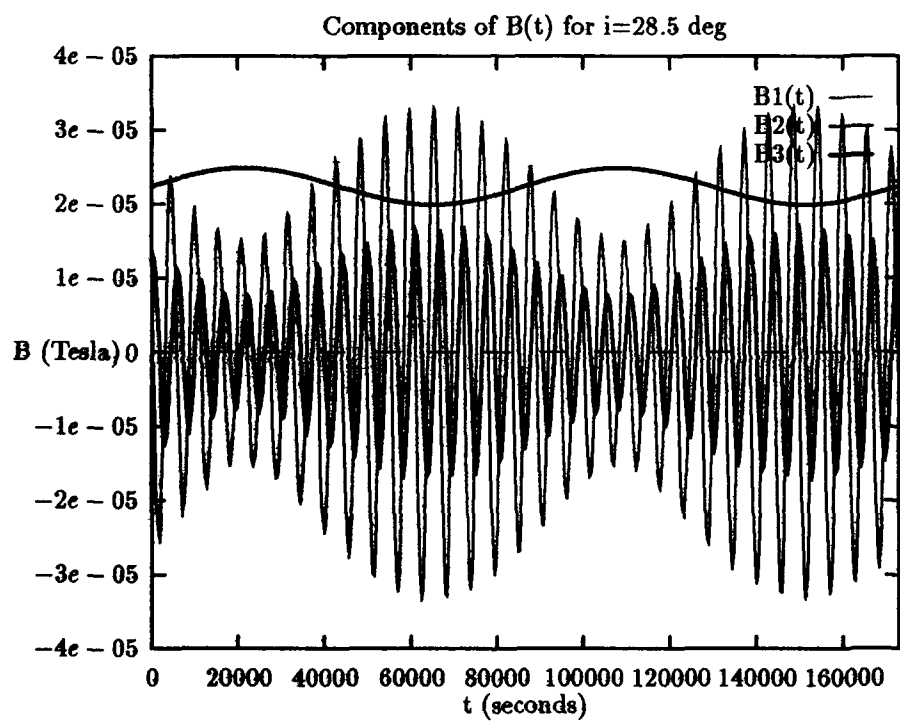
## Appendix A. *Plots of the Geomagnetic Field in the Orbital Reference Frame*

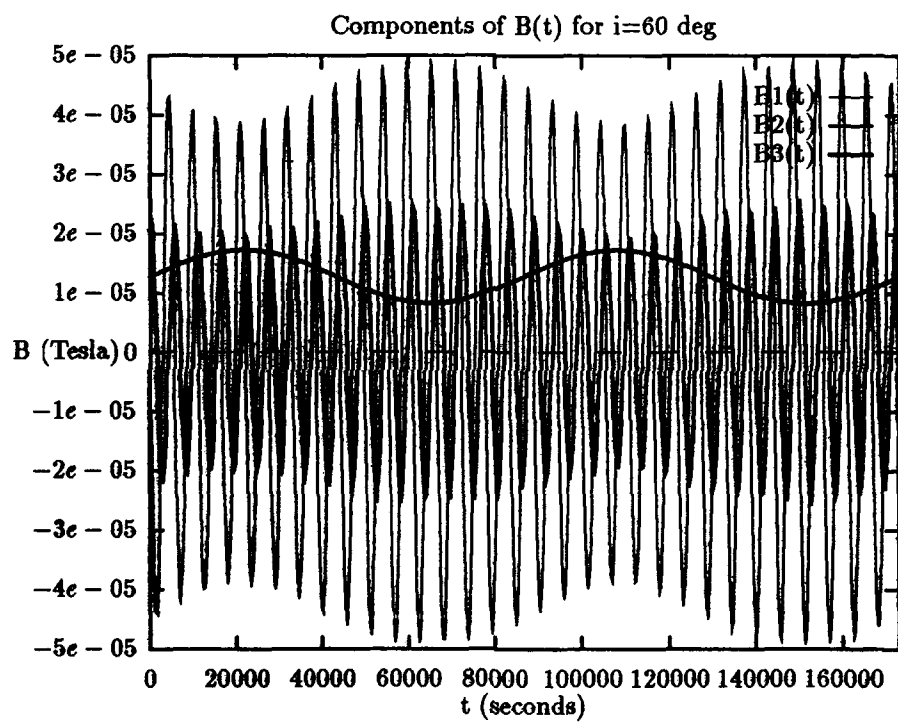
These plots of magnetic field strength in  $\hat{c}$  frame coordinates assume a circular orbit of 400 km altitude. The orbital period at this altitude is approximately 5500 seconds. The time duration of the plots is two siderial days (172328 mean solar seconds). Plots are generated for orbital inclinations of  $0^\circ$ ,  $5^\circ$ ,  $11.5^\circ$ ,  $28.5^\circ$ ,  $60^\circ$ ,  $78.5^\circ$ , and  $90^\circ$ . The inclinations of  $0^\circ$ ,  $11.5^\circ$ ,  $28.5^\circ$ , and  $78.5^\circ$  are especially important to the thesis development.  $B_1(t)$  and  $B_2(t)$  are the in-plane components of the magnetic field.  $B_3(t)$  is the out-of-plane component.

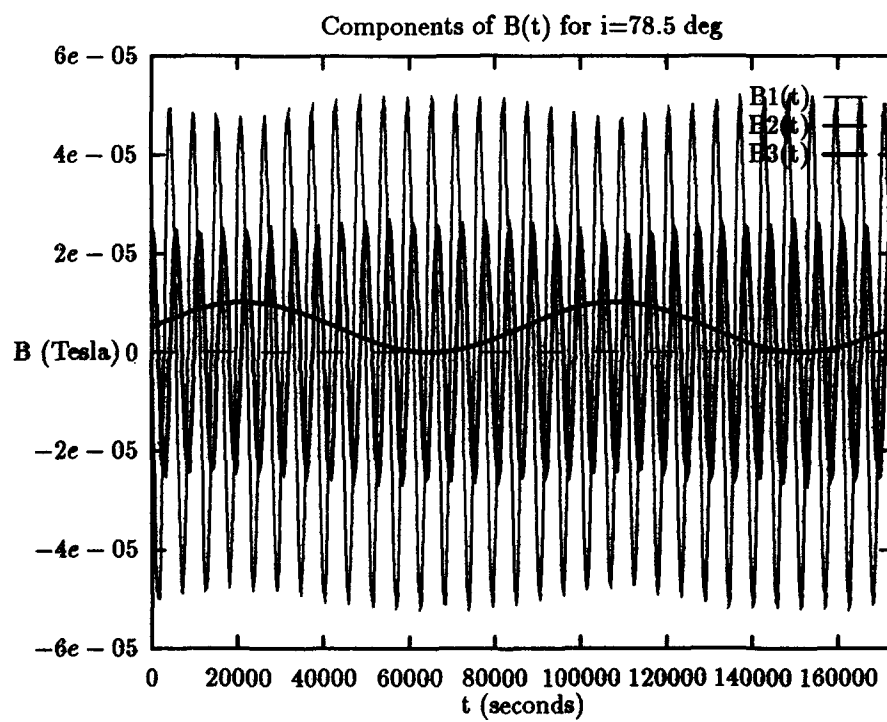


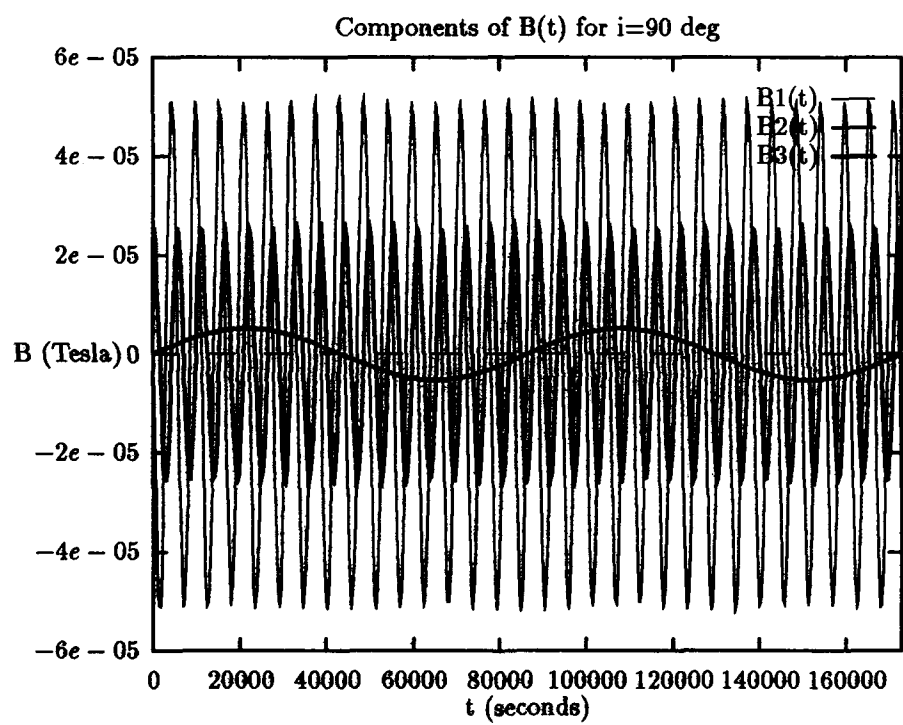














## Appendix B. *Aerodynamic and Earth Oblateness Effects in Low Earth Orbit*

In chapters two and three we quantified the gravitational and magnetic forces and torques acting on the tracking vehicle. These are the only forces/moments included in the POTV equations of motion. Other forces and torques include those caused by aerodynamic drag, the oblate shape of the earth, solar radiation pressure, solar and lunar gravity, dust impingement, etc. We believe the most significant perturbations in low earth orbit (LEO) are aerodynamic drag and earth oblateness.

The drag due to friction with the earth's atmosphere opposes the orbital motion of the POTV. The net effect of this force is to circularize an elliptical orbit and to decrease the orbital radius. Wiesel (24:83), and Penzo and Ammann (15:144), model the aerodynamic drag  $\underline{F}_d$  as:

$$\underline{F}_d = -\frac{1}{2}C_d A \rho v_{rel}^2 \hat{c}_2$$

where  $C_d$  is the drag coefficient,  $A$  is the presented area of the POTV,  $\rho$  is the atmospheric density, and  $v_{rel}$  is the velocity of the POTV relative to the air. At the orbital altitude range of the POTV (300-460 km), a simple exponential model of the atmospheric density  $\rho$  does not suffice. Penzo and Ammann give an empirical formula for the atmospheric density for altitudes greater than 200 km when the particle density is greater than  $10^{14}$  particles per cubic meter:

$$\rho = \frac{1.47 \cdot 10^{-16} T_{ex} (3000 - T_{ex})}{(1 + 2.9(\frac{Alt - 200}{T_{ex}}))^{10}}$$

where  $\rho$  is measured in kg/meter<sup>3</sup>,  $T$  is the atmospheric temperature in degrees Kelvin, and  $Alt$  is the orbital altitude in kilometers.

Aerodynamic drag is the major force to be countered for simple station-keeping in low earth orbit (LEO). No attempt is made here to determine the amount of vehicle thrust needed to counter the drag force. The calculation of the drag coefficient for the complex shape of the POTV is difficult. In practical tracking and docking applications the drag coefficient for both the tracker and target should be calculated.

The effects of the oblate shape of the earth must also be considered for a vehicle in LEO. The earth's equatorial bulge affects an elliptical orbit in two significant ways (24:86-87):

- Regression of the line of nodes.
- Rotation of the line of apsides (also known as the advance of the perigee).

The second of these effects does not apply to a circular orbit. We have always assumed that the POTV is traveling in circular orbit or tracking another vehicle in a circular orbit. The regression of the line of nodes is quantified:

$$\dot{\Omega} = -\frac{3nJ_2r_\oplus^2}{2a^2(1-e^2)^2} \cos i$$

which for a circular orbit simplifies to:

$$\dot{\Omega} = -\frac{3nJ_2r_\oplus^2}{2r^2} \cos i$$

where  $\dot{\Omega}$  is the time rate of change of the right ascension of the ascending node,  $n$  is the orbital angular velocity (or mean motion),  $J_2 = 0.001082$  is a number describing the oblate shape of the earth,  $r_\oplus$  is the radius of the earth,  $r$  is the POTV orbital radius, and  $i$  is the orbital inclination. The way this effect could be included in the POTV equations of motion would be to substitute the expression " $\Omega_0 + \dot{\Omega}t$ " wherever " $\Omega$ " appears in the equations.

### Appendix C. *Electrodynamic Propulsion Power Requirements*

What are the power requirements inherent in electrodynamic propulsion? The voltage induced across a conductor moving in a magnetic field is an important variable in power calculations. The voltage induced across a straight conductor moving through a uniform magnetic field is given by the relationship (15:119):

$$\begin{aligned} V_{ind} &= \underline{E}_{ind} \cdot \underline{L} \\ &= (\underline{v} \times \underline{B}) \cdot \underline{L} \end{aligned}$$

where  $\underline{E}_{ind}$  is the electrical field induced across the conductor and  $\underline{v}$  is the velocity of the conductor relative to the magnetic field. The velocity  $v$  of an earth orbiting conductor relative to the geomagnetic field is equal to its orbital velocity minus the velocity of the co-rotating magnetic field. For a circular, equatorial orbit, the relative velocity is written:

$$v = \sqrt{\frac{GM_{\oplus}}{r}} - \omega_{\oplus} r$$

where  $G$  is the gravitational constant,  $M_{\oplus}$  is the mass of the earth,  $r$  is the orbital radius, and  $\omega_{\oplus}$  is the earth's rotational angular velocity. This expression is approximately correct for low-inclination orbits. The first term in this equation is always greater than the second term for low earth orbit. We note that no voltage is induced if the conductor is oriented such that the induced electrical field  $\underline{E}_{ind} = \underline{v} \times \underline{B}$  is perpendicular to the length vector. When the induced electrical field is parallel to  $\underline{L}$ , the induced voltage is simply:

$$V_{ind} = \left( \sqrt{\frac{GM_{\oplus}}{r}} - \omega_{\oplus} r \right) BL \quad (C.1)$$

This approximate equation is used in chapter five to estimate the power requirements for a radial orbital change application.

Figure C.1 shows an electrical circuit model of a conductor (tether) operating as a thruster. The induced voltage is modeled as a voltage source with polarity opposite to that of the power supply voltage source. We note that the current would flow in the

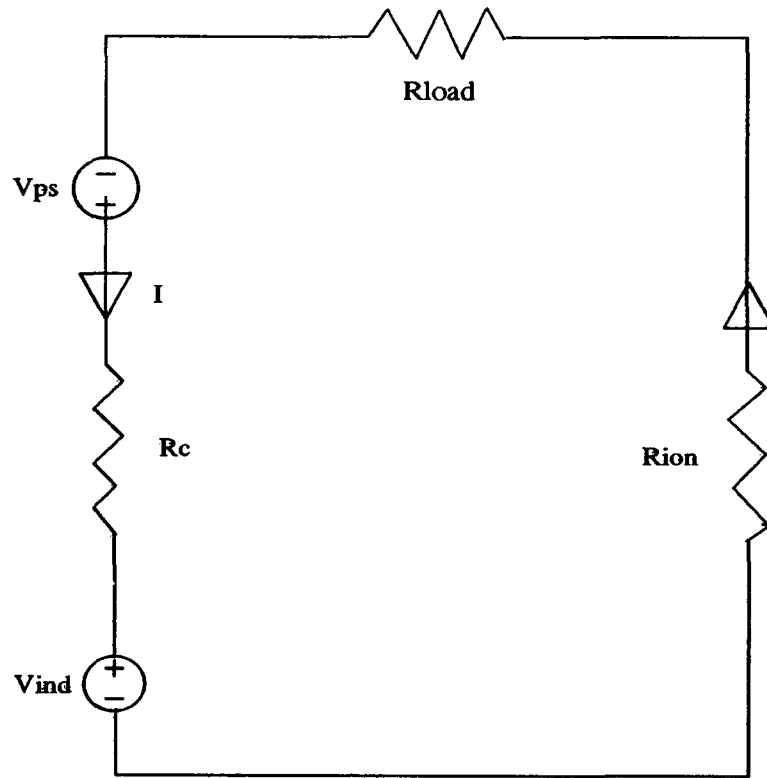


Figure C.1. Electrical Model of the Conductor in Thruster Mode

opposite direction of that shown if the power supply voltage was less than the induced voltage. This is in fact the case when a tether is used for power generation. Unfortunately, power generation is always accompanied by electrodynamic drag for a conductor in low earth orbit. We are interested in the power required to operate a conductor as a thruster. Regarding figure C.1 we use Kirchoff's voltage law to write:

$$V_{ps} = V_{ind} + IR_{tot}$$

where  $V_{ps}$  is the power supply voltage,  $V_{ind}$  is the induced voltage across the conductor,  $I$  is the current flowing through the conductor, and  $R_{tot}$  is the total electrical resistance.  $R_{tot}$  is the sum of the resistances:

$$R_{tot} = R_c + R_{ion} + R_{load}$$

where  $R_c$  is the conductor resistance,  $R_{ion}$  is the ionospheric resistance, and  $R_{load}$  is the load resistance. Penzo and Ammann state that the ionospheric resistance may be on the order of one to twenty ohms (15:125). Actual orbital tests are needed to verify this figure. The load resistance  $R_{load}$  is derived from POTV equipment other than the conductors that need electrical power. The conductor resistance  $R_c$  is equal to the product of the conductor length and resistance per unit length. The resistance per unit length is a function of the conductor material and conductor cross-section.

The power supply power is:

$$P_{ps} = IV_{ind} + I^2 R_{tot} \quad (C.2)$$

We use this equation in chapter five to characterize the power needed for an example application. Sources for the possibly large amount of vehicle power needed include solar photovoltaic arrays, nuclear reactors, and earth-based lasers.

#### Appendix D. *Approximate Mass and Moments of Inertia for the POTV*

The principal moments of inertia of a particular POTV design (ASSET) are calculated in this appendix. The resulting expressions are used in the MATLAB controller design and performance program CONTROLLER.M.

The ASSET POTV system with Design #2 conductor configuration consists of a modified shuttle external tank with attached rigid conductor towers. We model the system as a cylinder with attached thin rods. The rods are assumed to have constant linear mass density  $\rho$  (kg/m). The total system mass is then the simple expression:

$$M_t = M_{cyl} + 2\rho(l_1 + l_2 + l_t + l_{c_1} + l_{c_2}) \quad (D.1)$$

Where we have neglected the mass of the guidewire webbing, PMGs, power generation equipment, etc. From the ASSET study (4) we find that the mass of the central cylinder is approximately 31,300 kg (mass of an empty shuttle external fuel tank). By no means are the conductor towers required to all have the same linear mass density. Indeed, one or more conductor towers also serving as docking facilities could have larger linear mass densities than the other towers. Also, towers serving as structural "anchors" for the guidewire webbing could have large linear mass densities. Here we assume that all of the towers have the same linear mass density for ease of derivation.

The approximate moment of inertia matrix for the POTV about its center of mass is found by repeatedly applying the parallel-axis theorem to the moment of inertia matrices of the thin rods. The parallel-axis theorem is explained by Wiesel (24:106-107). The principal moments of inertia for a cylinder and a thin rod are found in the dynamics text by Likins (10:522-524). Let  $a$  be the cylinder radius and  $h$  be the length of the cylinder. After simple but extended calculation the moments of inertia of the POTV with the Design #2 conductor configuration are:

$$A = \frac{M_{cyl}a^2}{2} + 2\rho \left( \frac{l_2^3}{12} + l_2\left(\frac{l_2}{2} + a\right)^2 + \frac{l_t^3}{12} + l_t\left(\frac{l_t}{2} + a\right)^2 + l_{c_1}(l_t + a)^2 + \frac{l_{c_2}^3}{12} + l_{c_2}(l_t + a)^2 \right)$$

$$B = \frac{M_{cyl}(3a^2 + h^2)}{12} + 2\rho \left( \frac{l_1^3}{12} + l_1\left(\frac{l_1}{2} + \frac{h}{2}\right)^2 + \frac{l_t^3}{12} + l_t\left(\frac{l_t}{2} + a\right)^2 + \frac{l_{c_1}^3}{12} + l_{c_1}(l_t + a)^2 \right)$$

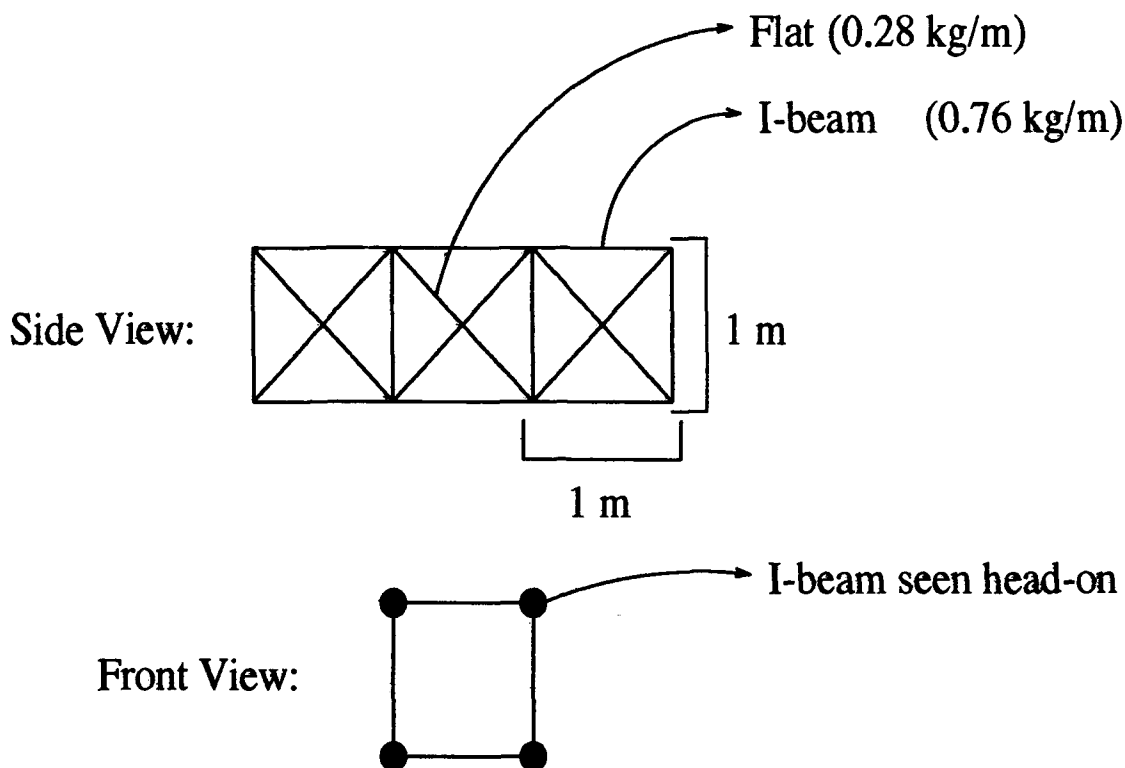


Figure D.1. Truss Assembly for Conductor Towers

$$C = \frac{M_{cyl}(3a^2 + h^2)}{12} + 2\rho \left( \frac{l_1^3}{12} + l_1 \left( \frac{l_1}{2} + \frac{h}{2} \right)^2 + \frac{l_2^3}{12} + l_2 \left( \frac{l_2}{2} + a \right)^2 + \frac{l_{c1}^3}{12} + \frac{l_{c2}^3}{12} \right) \quad (D.2)$$

End and side views of the proposed truss work for the conductor towers in shown in figure D.1. We assume that the cross-sectional area of each tower is a constant one meter<sup>2</sup>. Each tower section consists of four aluminum "I-beams" and twelve "flats". This material is readily available from a salvaged external tank (4). The linear mass density of a single I-beam is 0.76 kg/m. If we assume that the "strip" pieces mentioned in the ASSET report can be divided lengthwise into eight pieces, then the linear mass density of the resulting "flats" is 0.28 kg/m. With these assumptions we calculate the total linear mass density of the truss to be approximately 7.3 kg/m. This is the figure used in the CONTROLLER.M program listed in appendix F. A smaller total linear mass density could be realized if the tower cross-sectional area specification (1 meter<sup>2</sup>) was relaxed.

Here is the dimension data for the design used in the chapter five examples:

$$M_{cyl} = 31300 \text{ kg}$$

$$\rho = 7.3 \text{ kg/m}$$

$$l_1 = 310 \text{ m}$$

$$l_2 = 50 \text{ m}$$

$$l_t = 50 \text{ m}$$

$$l_{c_1} = 20 \text{ m}$$

$$l_{c_2} = 20 \text{ m}$$

The resulting total system mass and moments of inertia are:

$$M_t = 37870 \text{ kg}$$

$$A = 1.5374e + 08 \text{ kg} \cdot \text{m}^2$$

$$B = 1.0236e + 07 \text{ kg} \cdot \text{m}^2$$

$$C = 1.5872e + 08 \text{ kg} \cdot \text{m}^2$$

The added mass due to the conductor towers is 6570 kg.



## Appendix E. Controller Design Program Results

### E.1 Steady-State Tracking Example

>> cont

Welcome to the PGTV Controller Design and Performance Program.

Altitude of reference orbit (kilometers) ? 400

Trig angle (u-theta-g-lambda) to work with (degrees) ? 33

Mass of ASSET excluding towers (kg) ? 31300

Linear mass density of conductor towers (kg/m) ? 7.3

Length of vertical (x) in-plane conductors (meters) ? 50

Length of horizontal (y) in-plane conductors (meters) ? 310

Length of nonconducting cross support towers (meters) ? 50

Length of vertical (x) cross conductors (meters) ? 20

Length of horizontal (y) cross conductors (meters) ? 20

Orbital mean motion (rad/sec) =

1.1316e-03

Total system mass (kg) =

37870

Principle moment of inertia A (kg-m<sup>2</sup>) =

1.5374e+08

Principle moment of inertia B (kg-m<sup>2</sup>) =

1.0236e+07

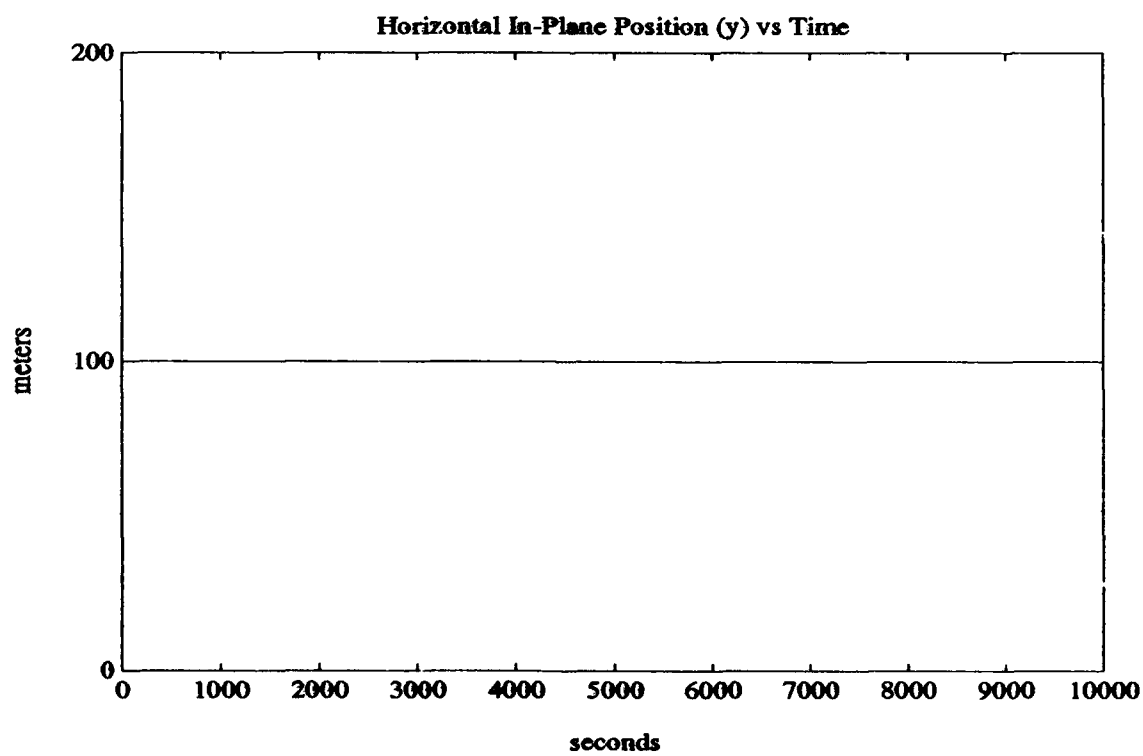
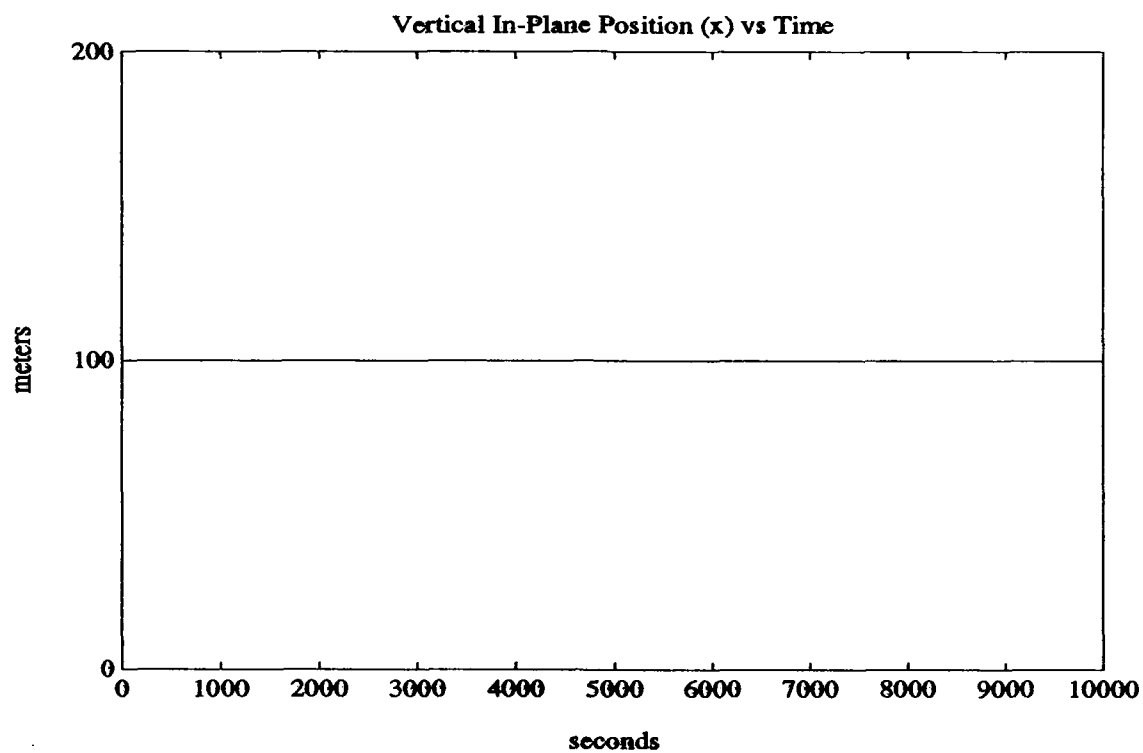
Principle moment of inertia C (kg-m<sup>2</sup>) =

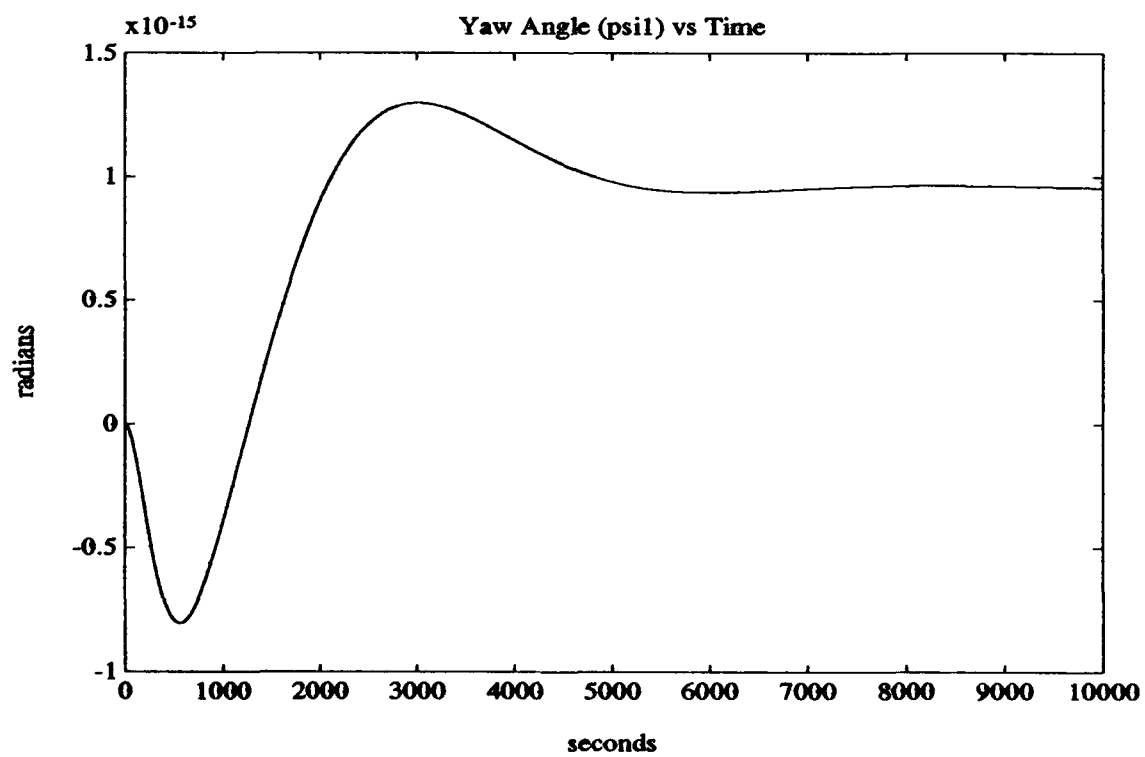
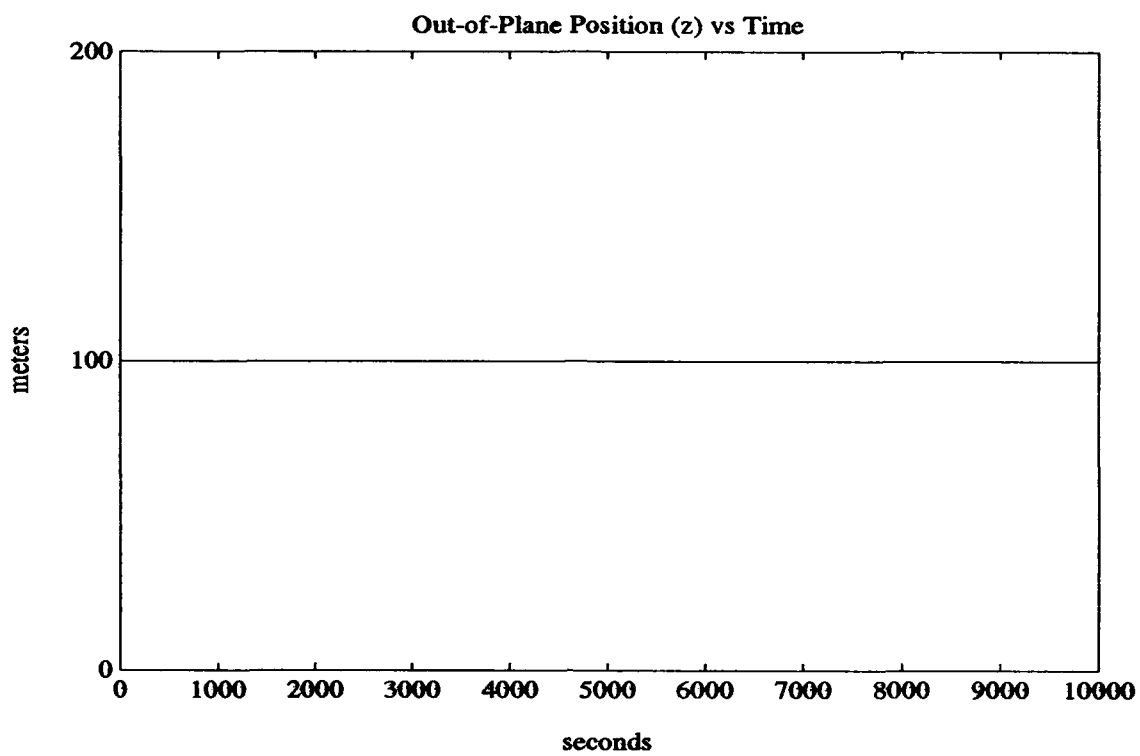
1.5872e+08

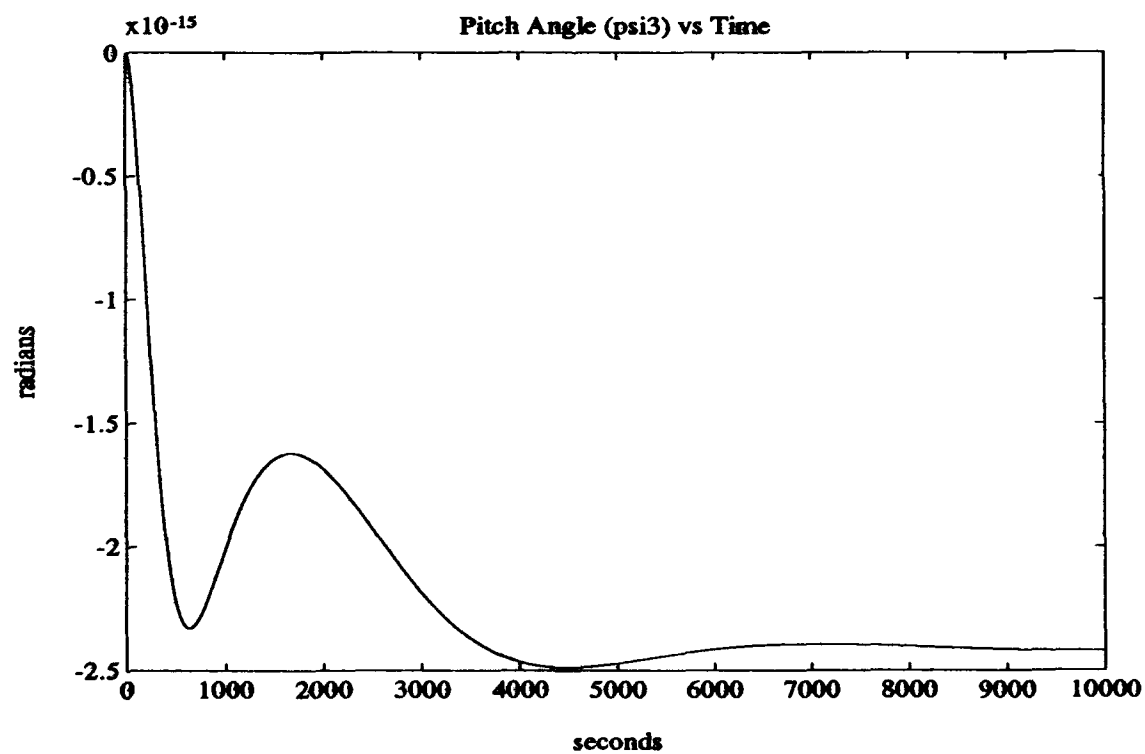
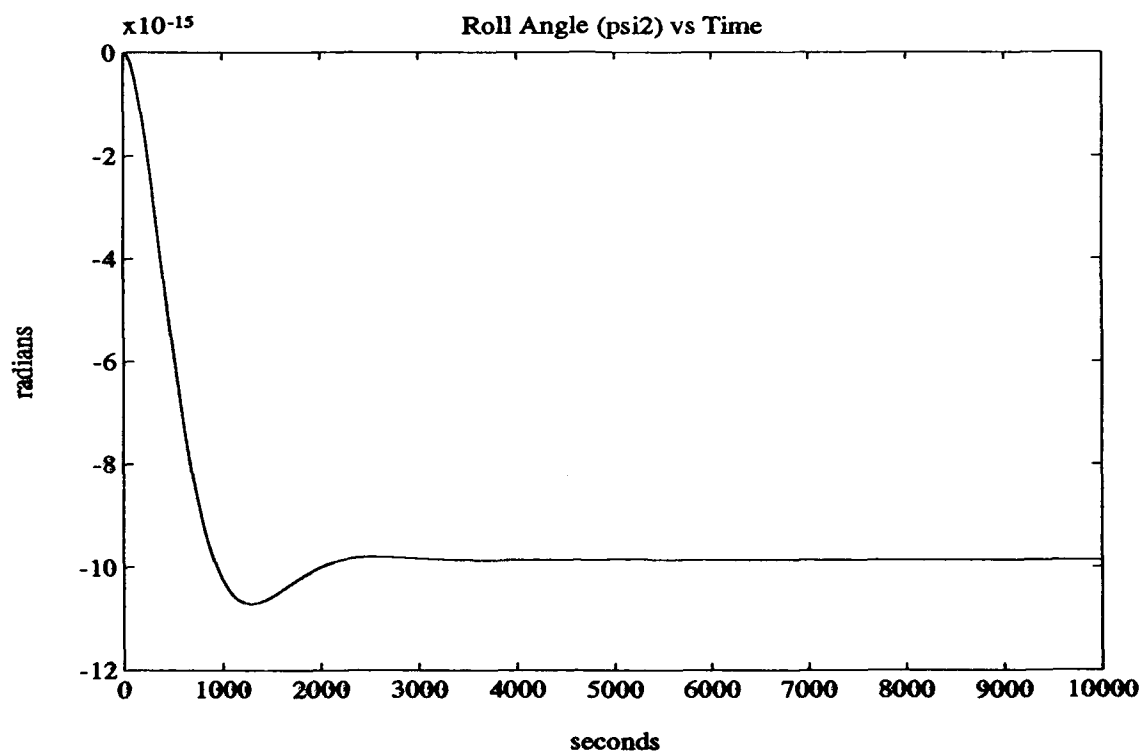
The (Fsys,Gsys) system is completely controllable.

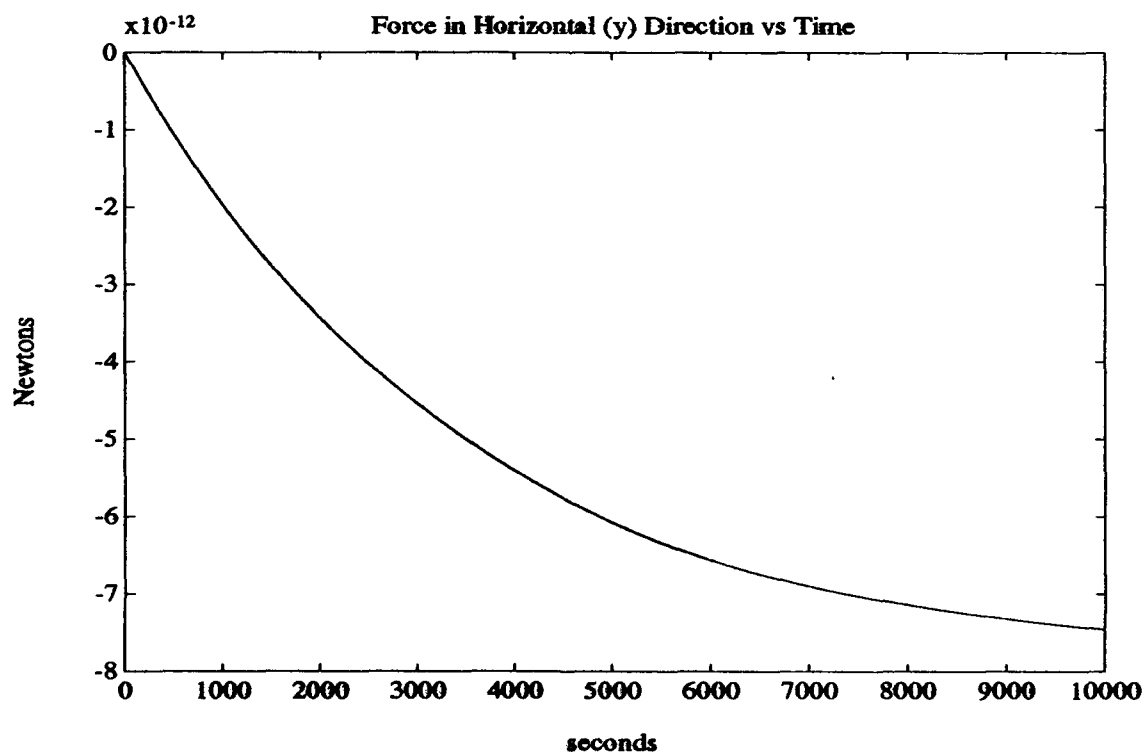
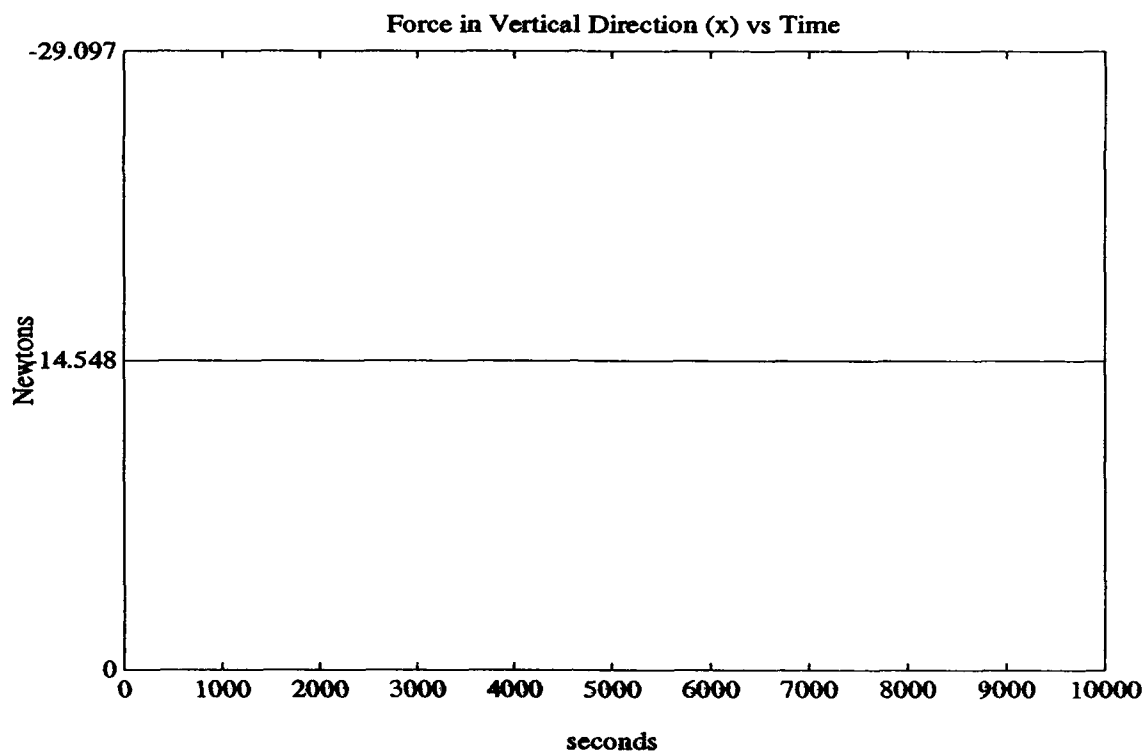
The (Fsys,Hsys) system is completely observable.

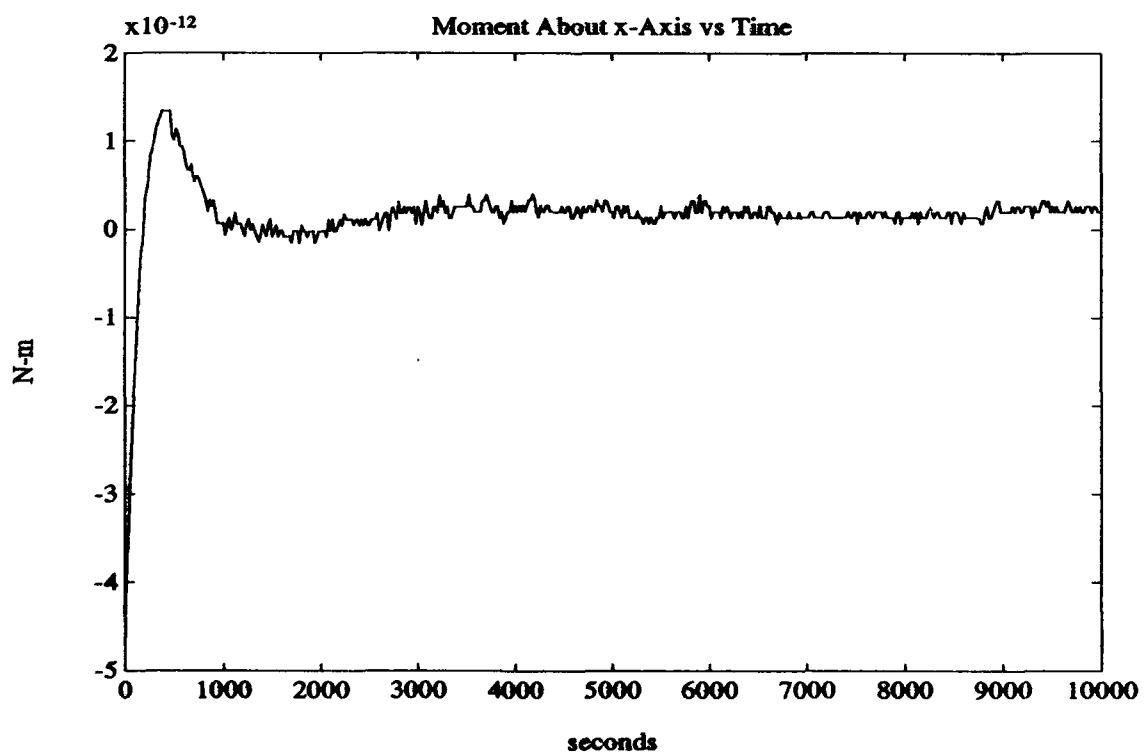
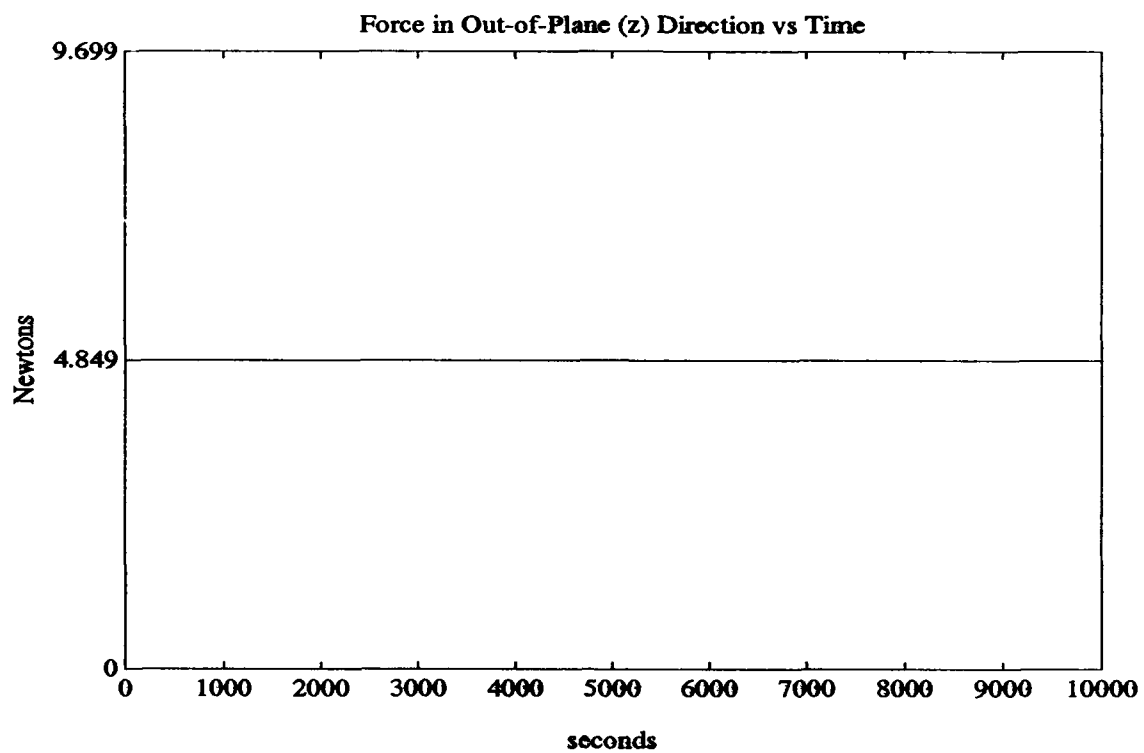
Weighting on the state weighting matrix Q ? 1  
Weighting on the control weighting matrix R ? 1  
What is the value of x to attain and track (m) ? 100  
What is the value of y to attain and track (m) ? 100  
What is the value of z to attain and track (m) ? 100  
What is the value of psi1 to attain and track (rad) ? 0  
What is the value of psi2 to attain and track (rad) ? 0  
What is the value of psi3 to attain and track (rad) ? 0  
What is the initial value of x (m) ? 100  
What is the initial value of y (m) ? 100  
What is the initial value of z (m) ? 100  
What is the initial value of psi1 (rad) ? 0  
What is the initial value of psi2 (rad) ? 0  
What is the initial value of psi3 (rad) ? 0  
How long of a time response to plot ? 10000  
Number of time increments (data points) ? 500

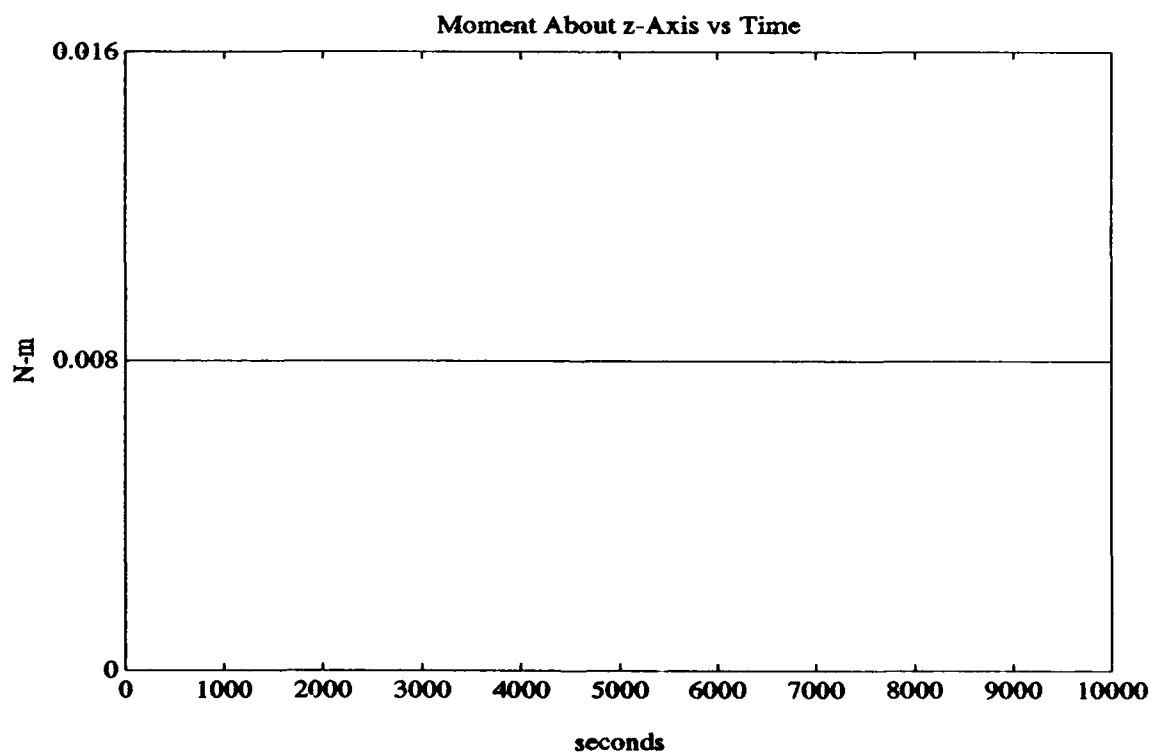
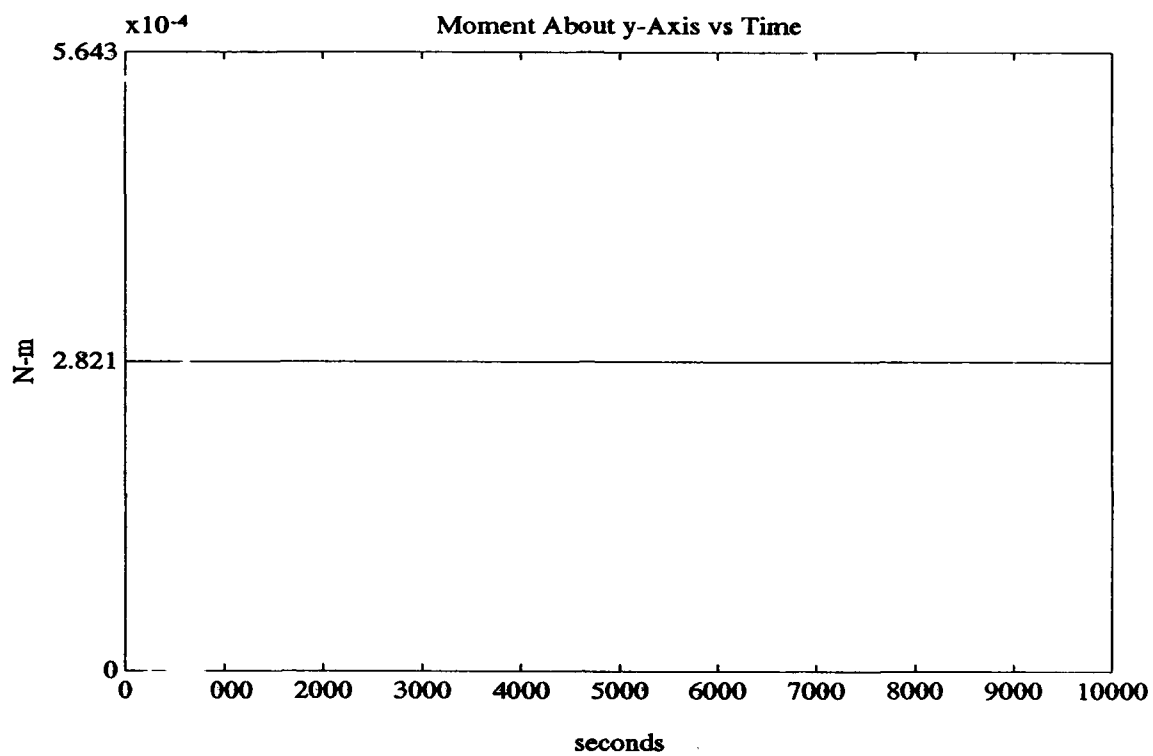




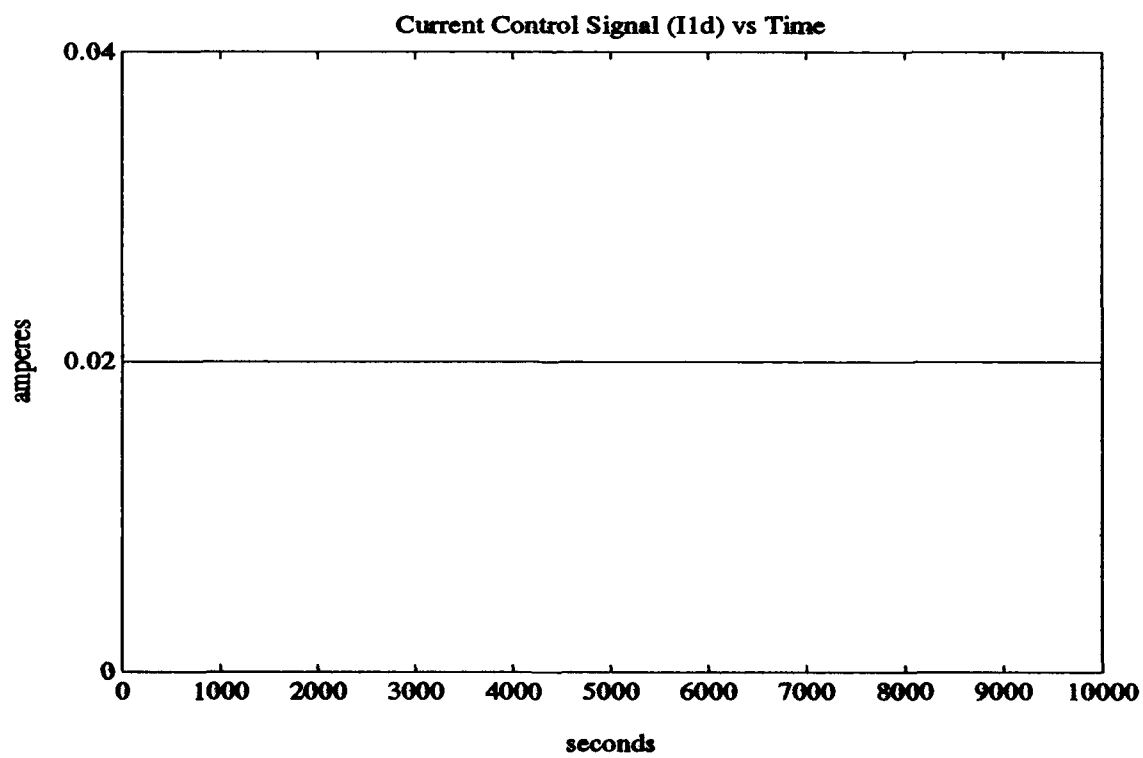
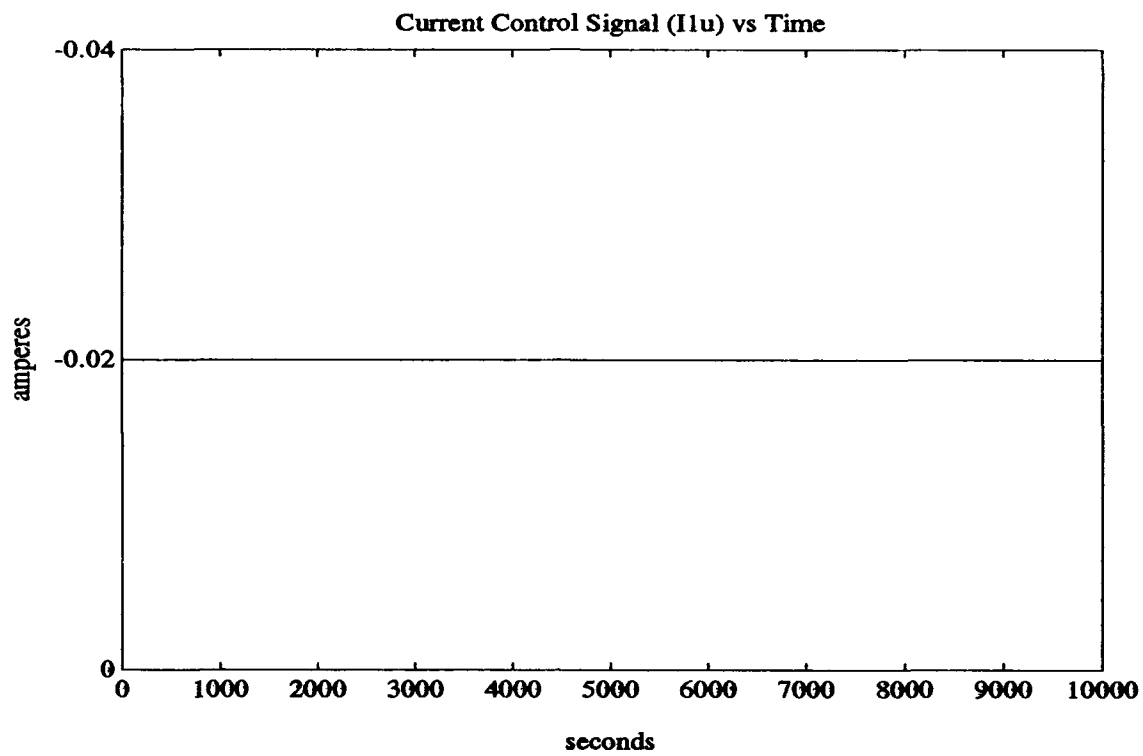


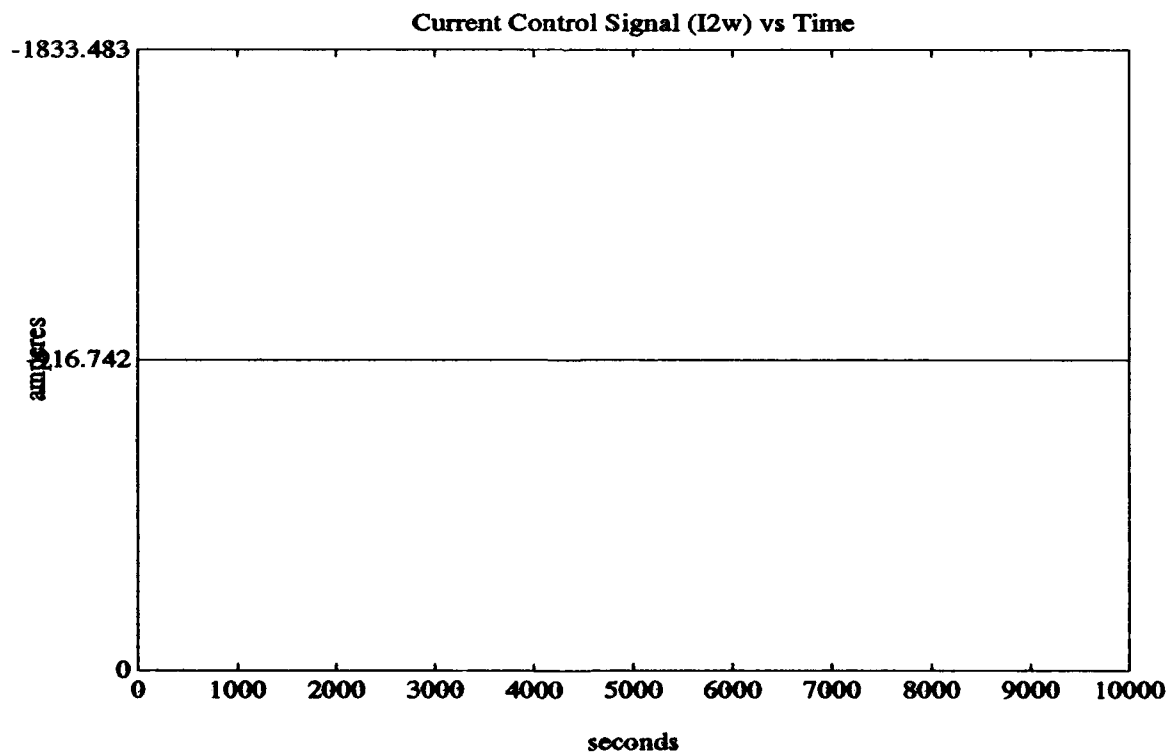
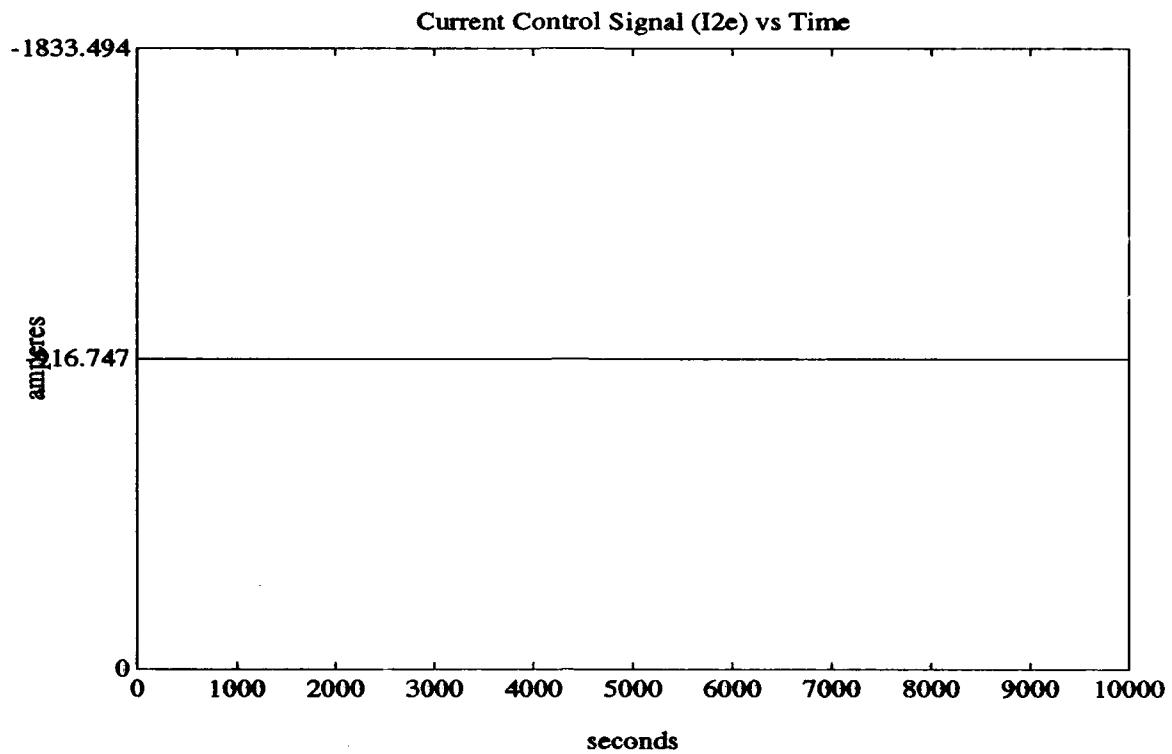


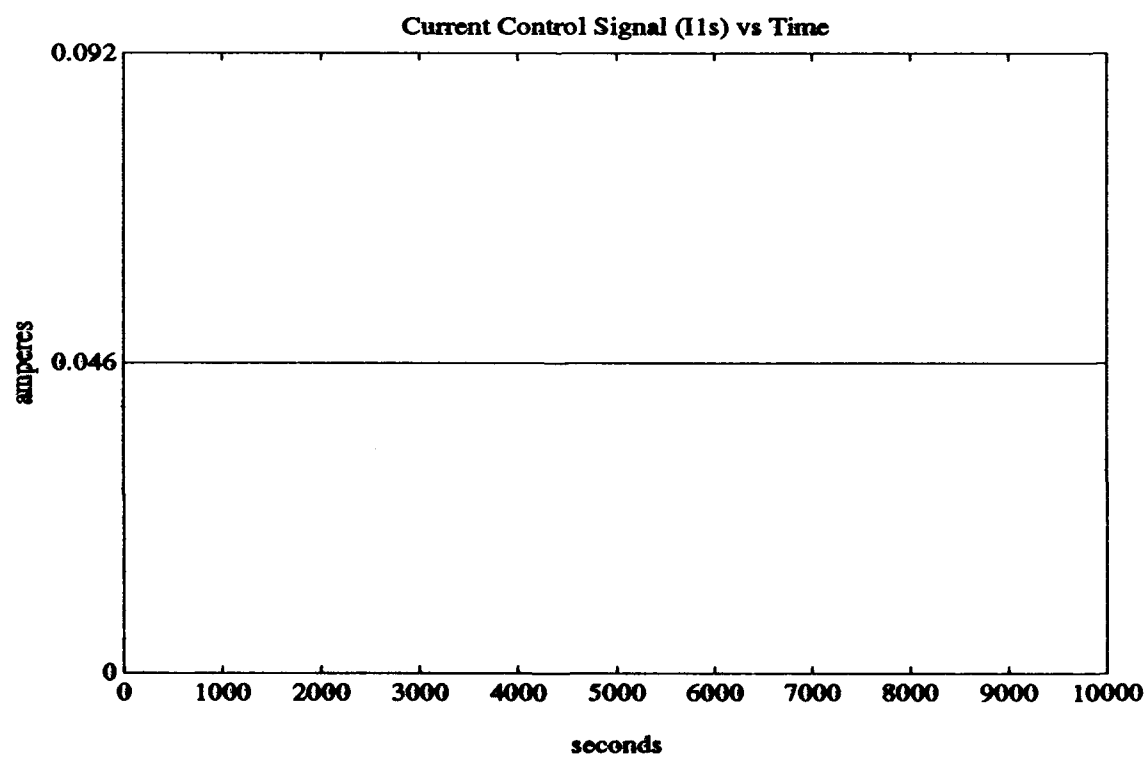
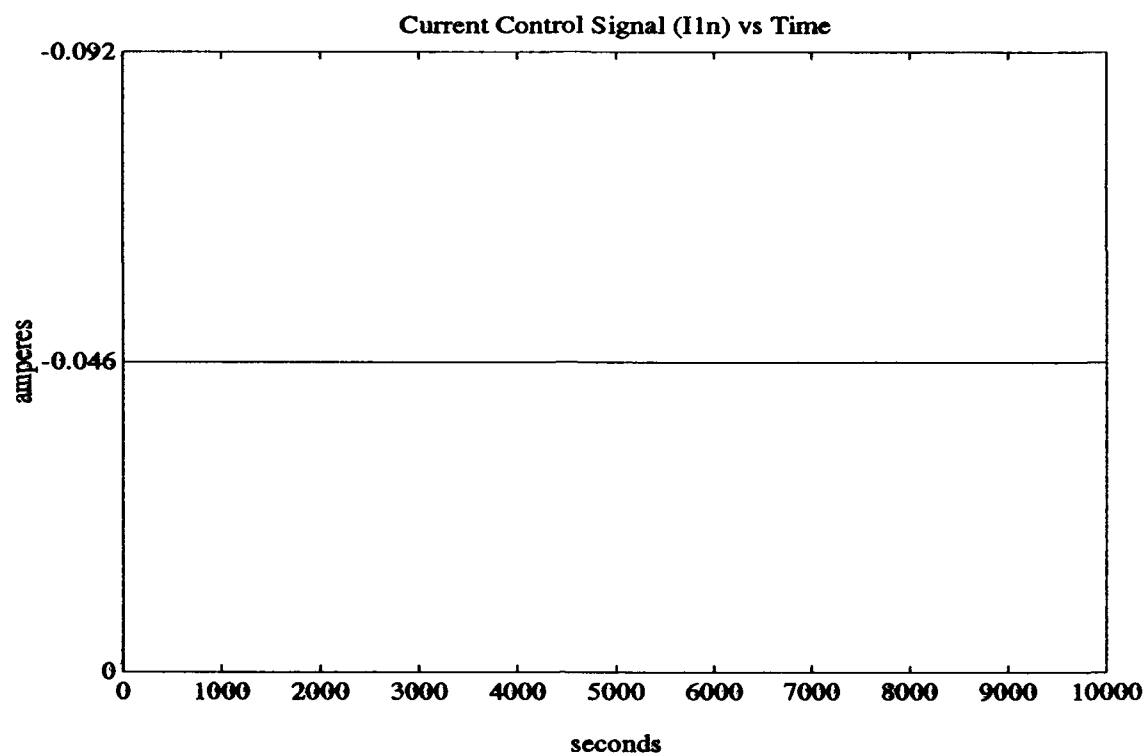


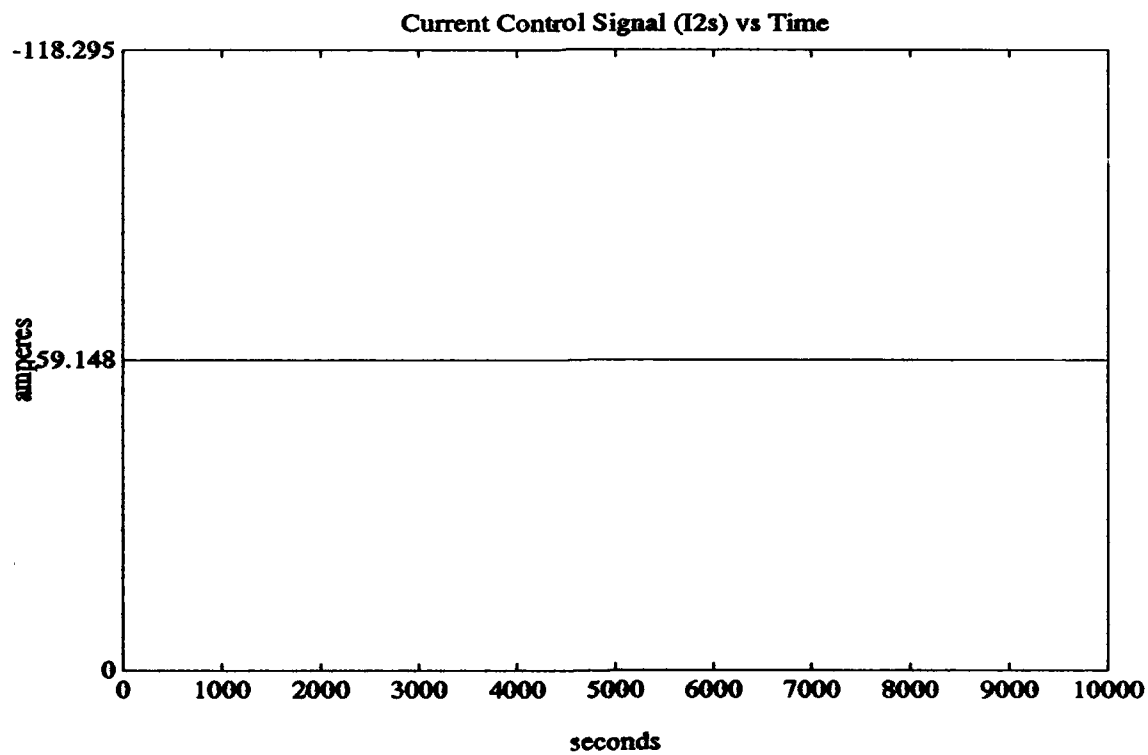
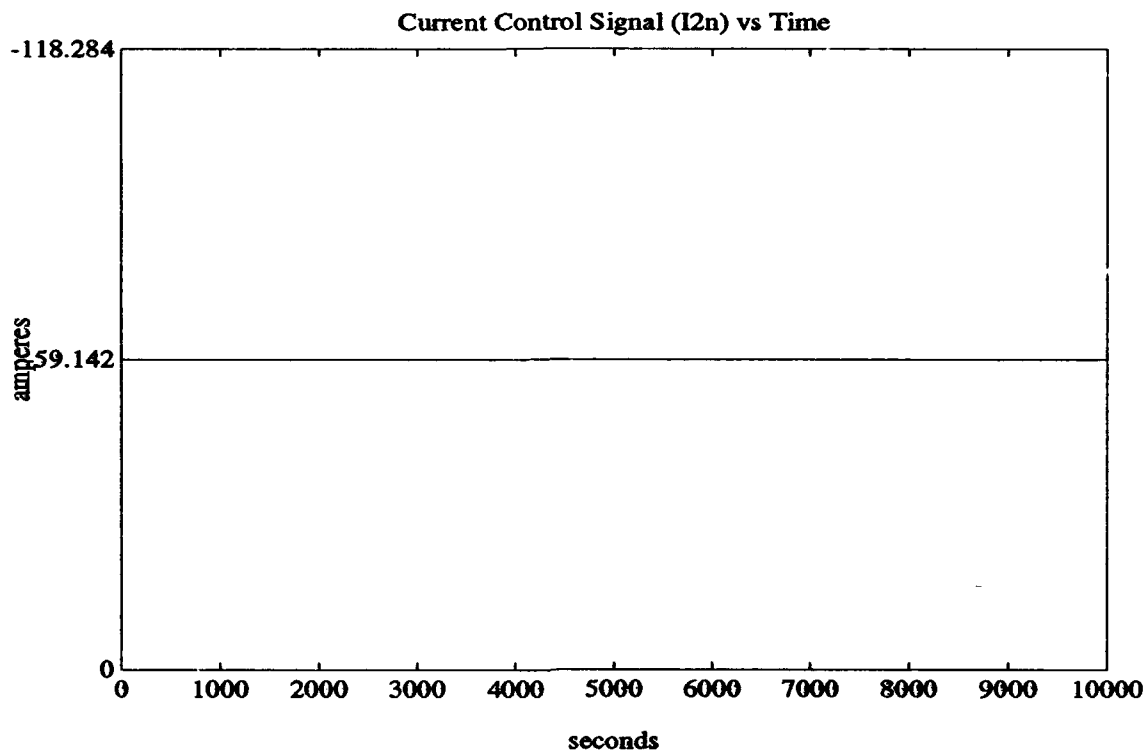


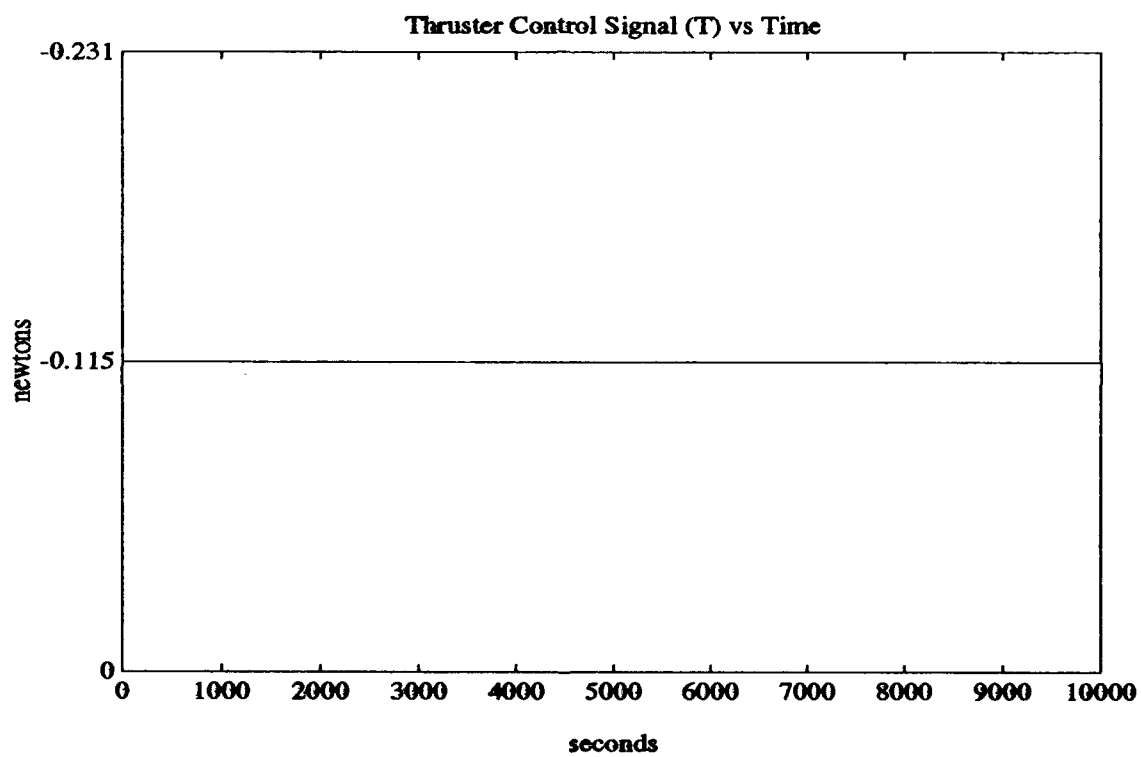












## E.2 R-BAR Docking Approach Example

>> cont

Welcome to the POTV Controller Design and Performance Program.

Altitude of reference orbit (kilometers) ? 400

Trig angle ( $u$ -thetag-lambda) to work with (degrees) ? 33

Mass of ASSET excluding towers (kg) ? 31300

Linear mass density of conductor towers (kg/m) ? 7.3

Length of vertical (x) in-plane conductors (meters) ? 50

Length of horizontal (y) in-plane conductors (meters) ? 310

Length of nonconducting cross support towers (meters) ? 50

Length of vertical (x) cross conductors (meters) ? 20

Length of horizontal (y) cross conductors (meters) ? 20

Orbital mean motion (rad/sec) =

1.1316e-03

Total system mass (kg) =

37870

Principle moment of inertia A ( $\text{kg-m}^2$ ) =

1.5374e+08

Principle moment of inertia B ( $\text{kg-m}^2$ ) =

1.0236e+07

Principle moment of inertia C ( $\text{kg-m}^2$ ) =

1.5872e+08

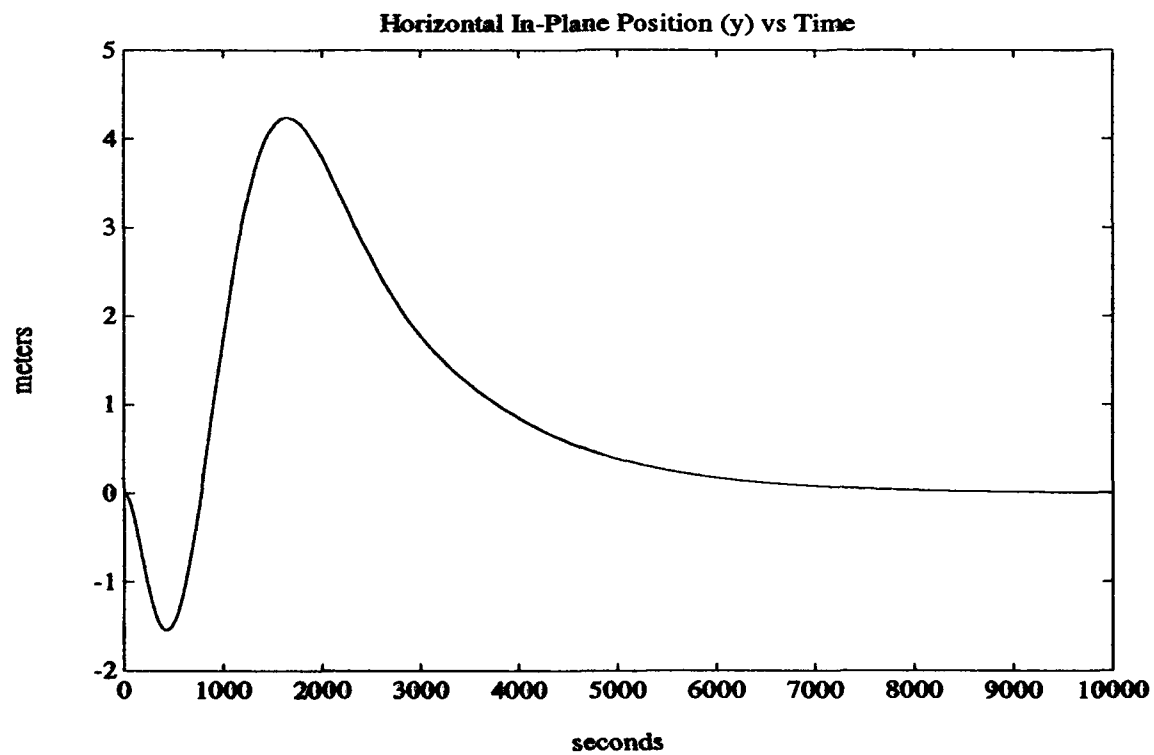
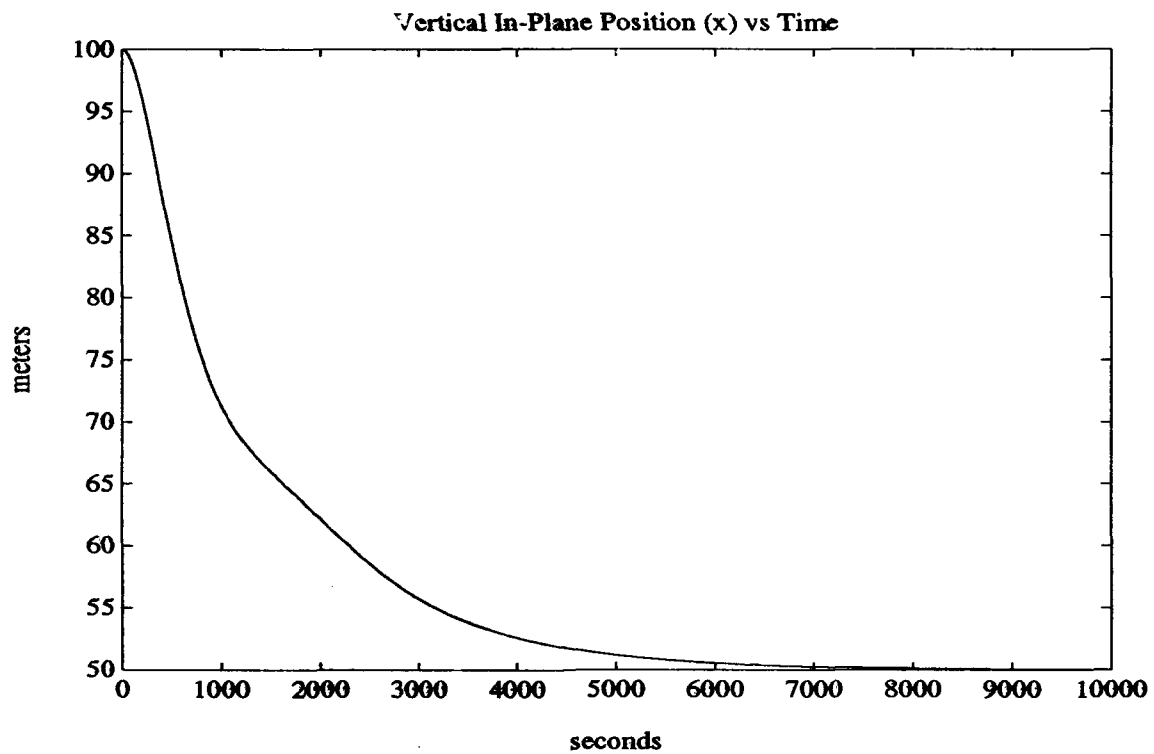
The (Fsys,Gsys) system is completely controllable.

The (Fsys,Hsys) system is completely observable.

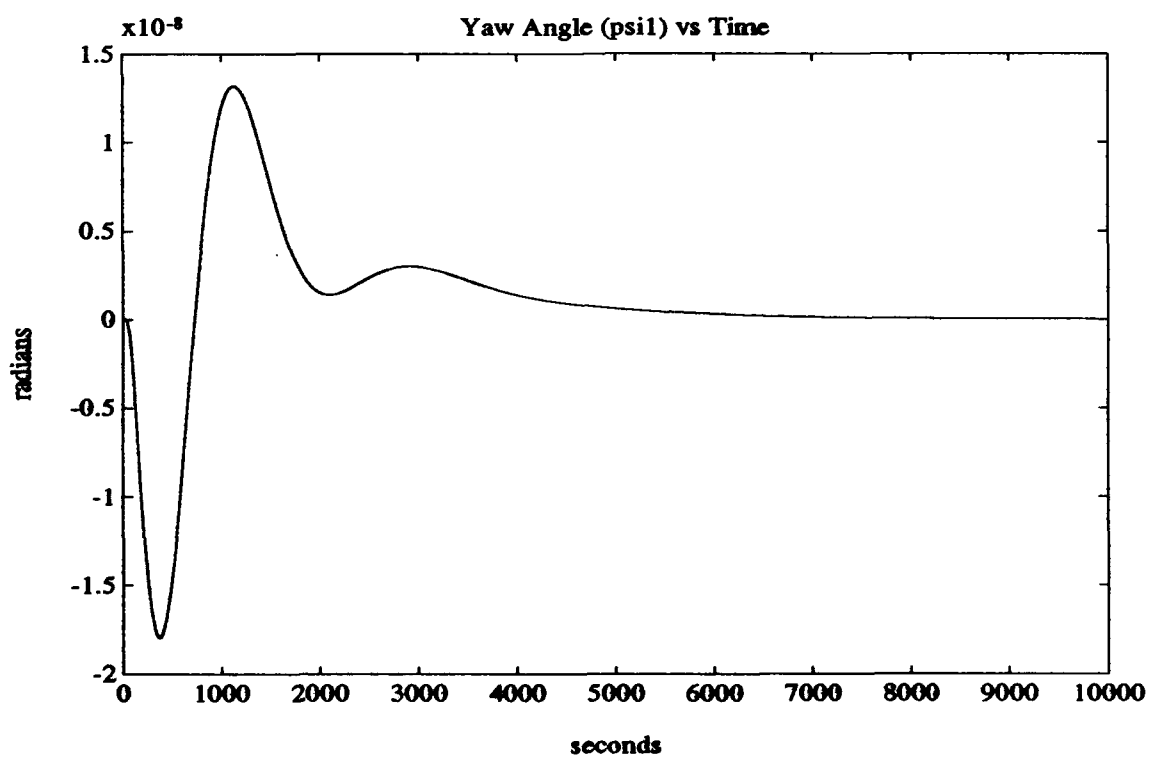
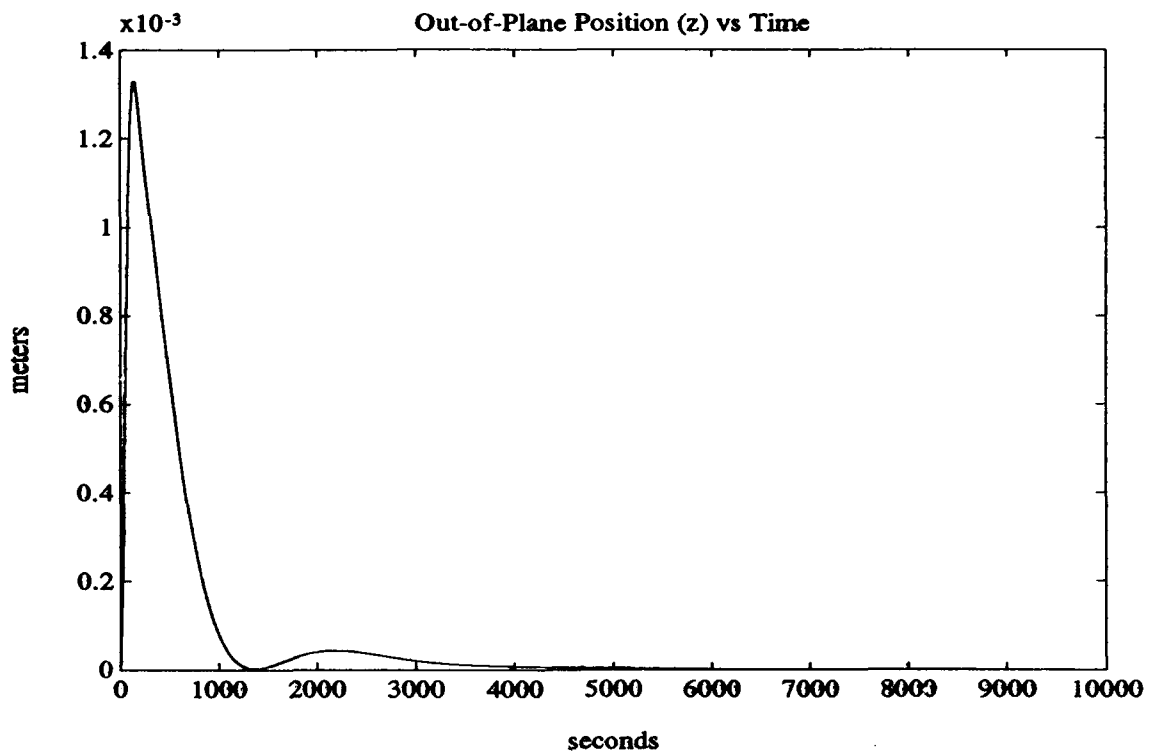
Weighting on the state weighting matrix Q ? 1000

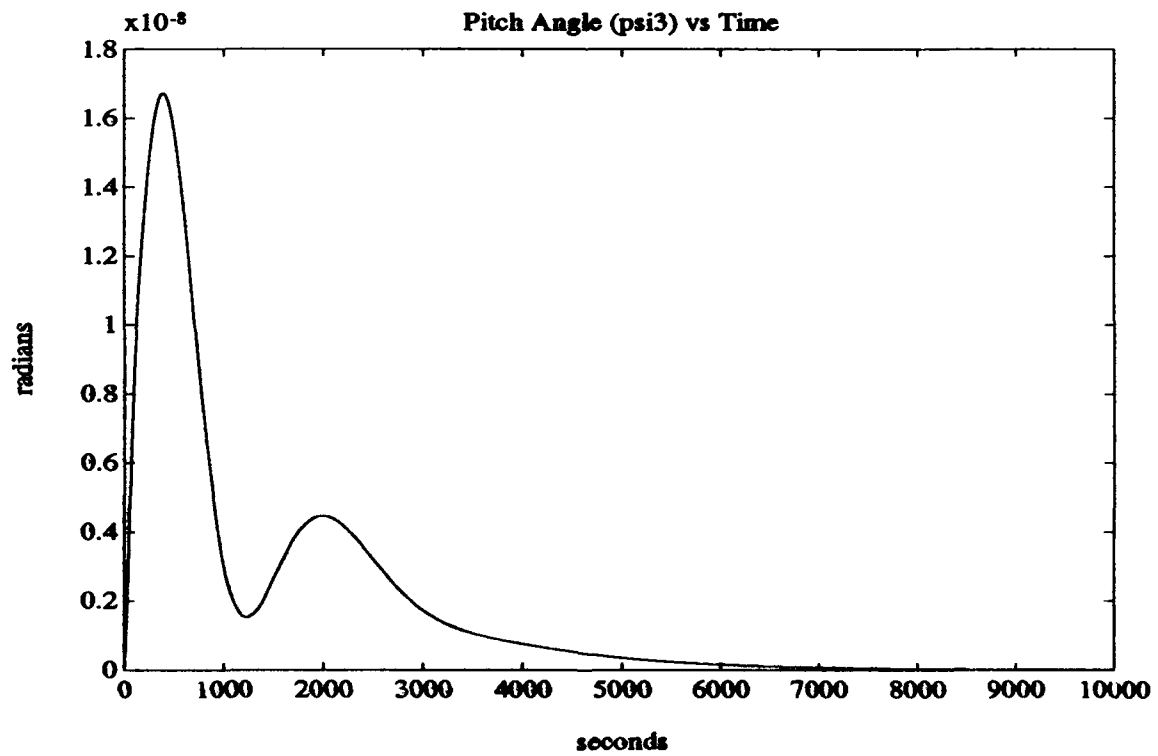
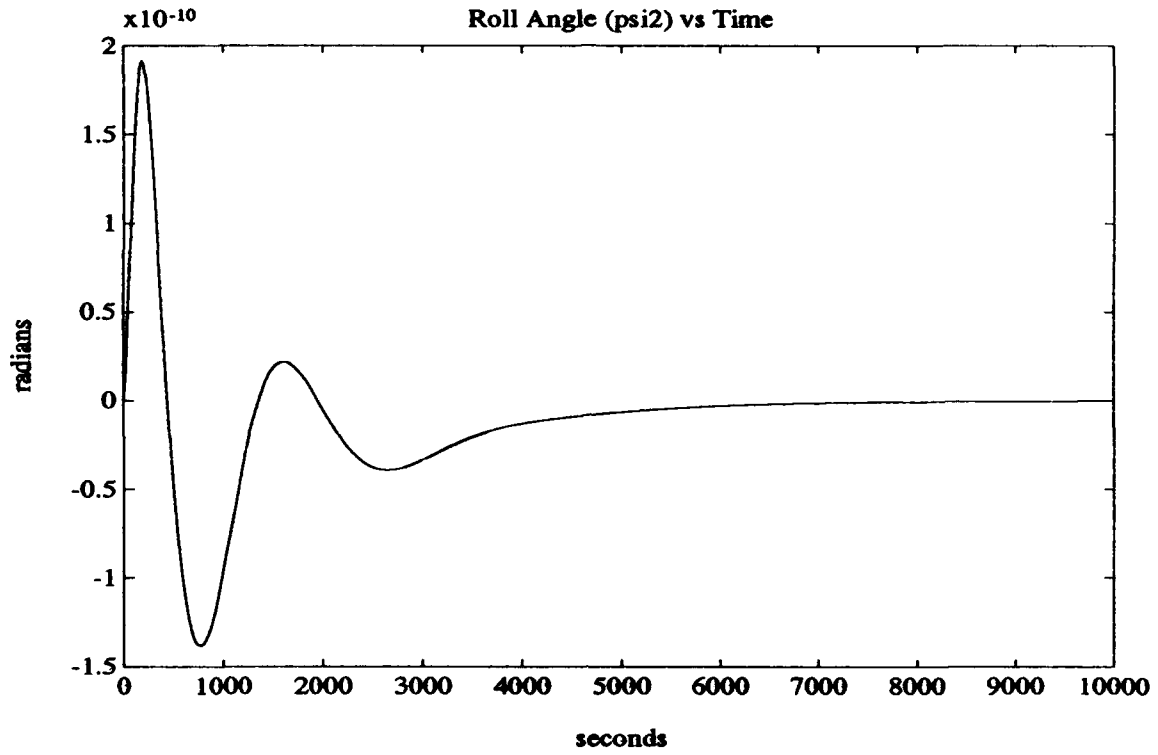
Weighting on the control weighting matrix R ? 1

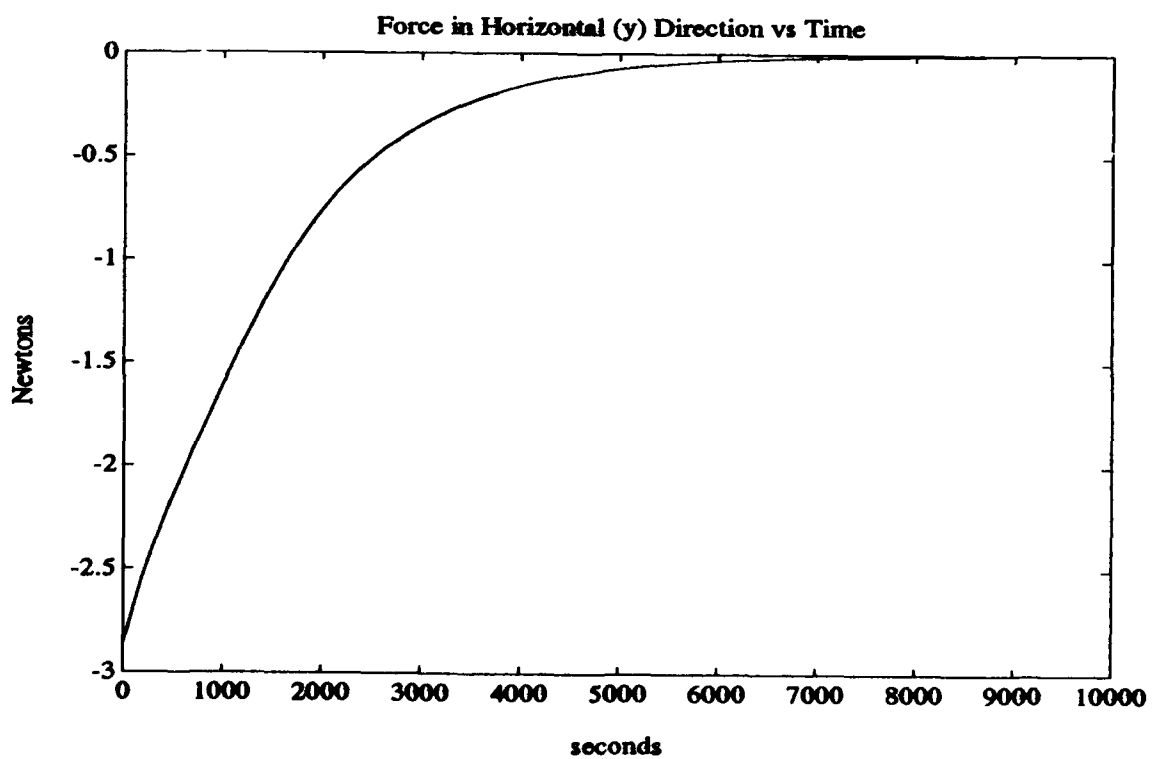
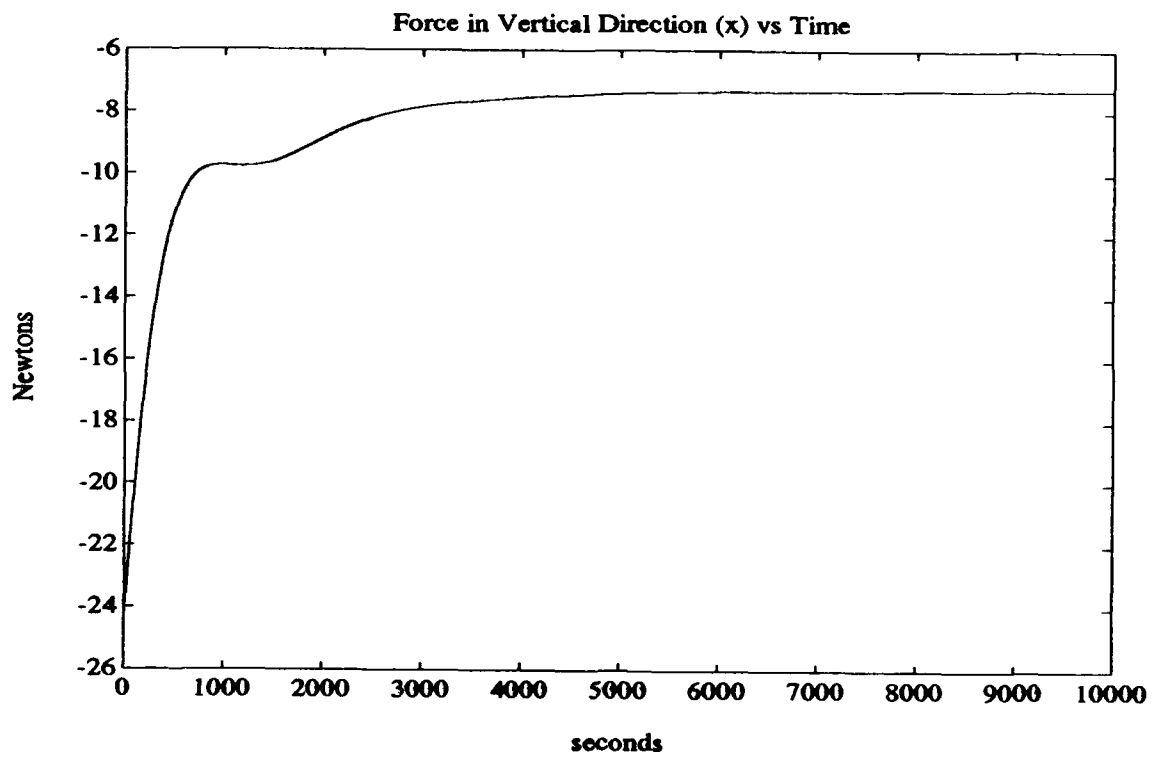
What is the value of  $x$  to attain and track (m) ? 50  
What is the value of  $y$  to attain and track (m) ? 0  
What is the value of  $z$  to attain and track (m) ? 0  
What is the value of  $\psi_1$  to attain and track (rad) ? 0  
What is the value of  $\psi_2$  to attain and track (rad) ? 0  
What is the value of  $\psi_3$  to attain and track (rad) ? 0  
What is the initial value of  $x$  (m) ? 100  
What is the initial value of  $y$  (m) ? 0  
What is the initial value of  $z$  (m) ? 0  
What is the initial value of  $\psi_1$  (rad) ? 0  
What is the initial value of  $\psi_2$  (rad) ? 0  
What is the initial value of  $\psi_3$  (rad) ? 0  
How long of a time response to plot ? 10000  
Number of time increments (data points) ? 500

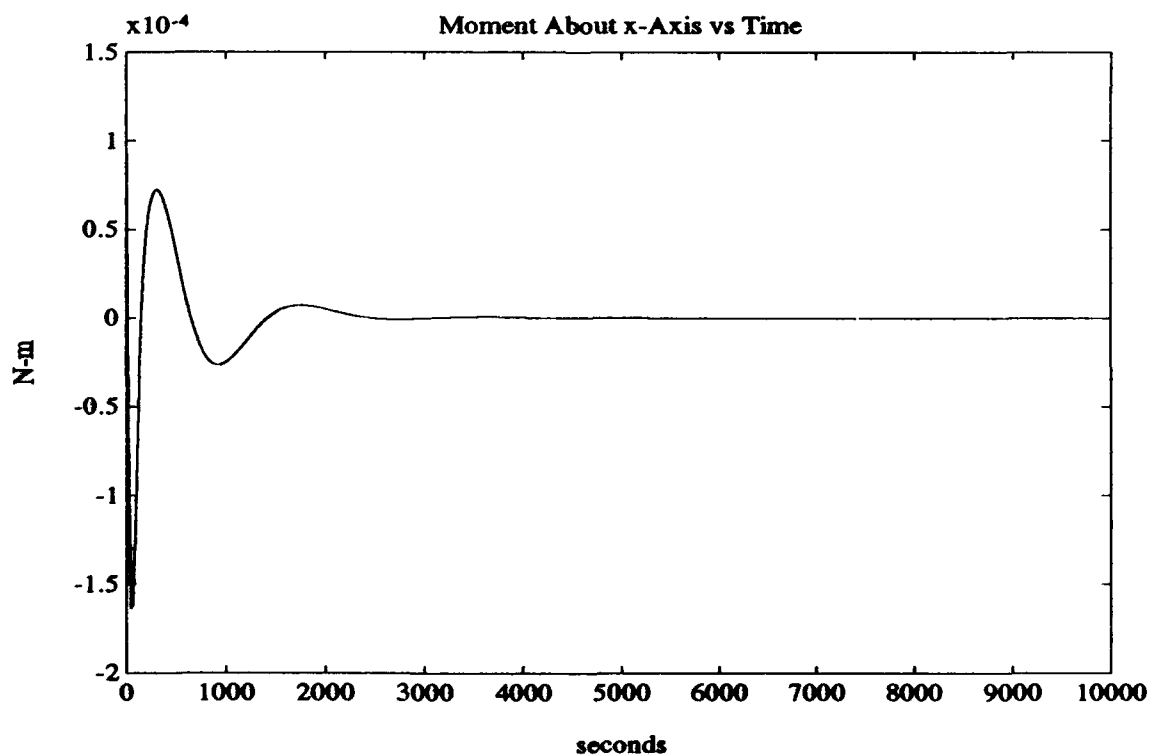
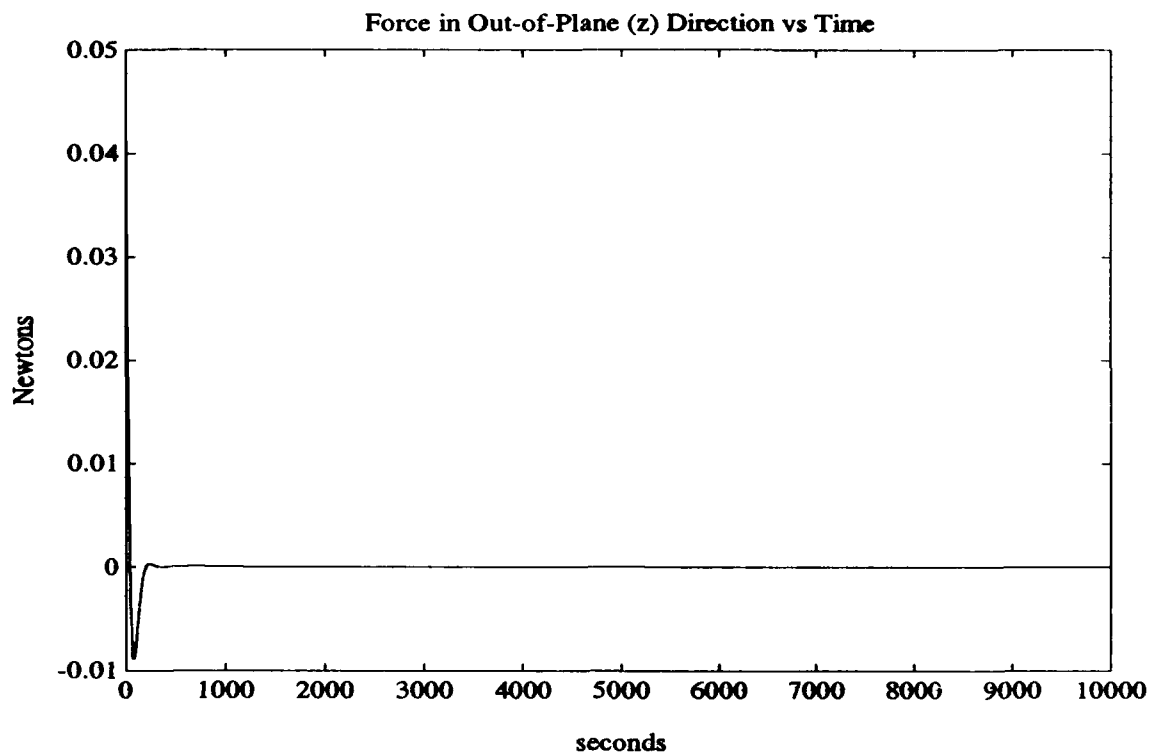


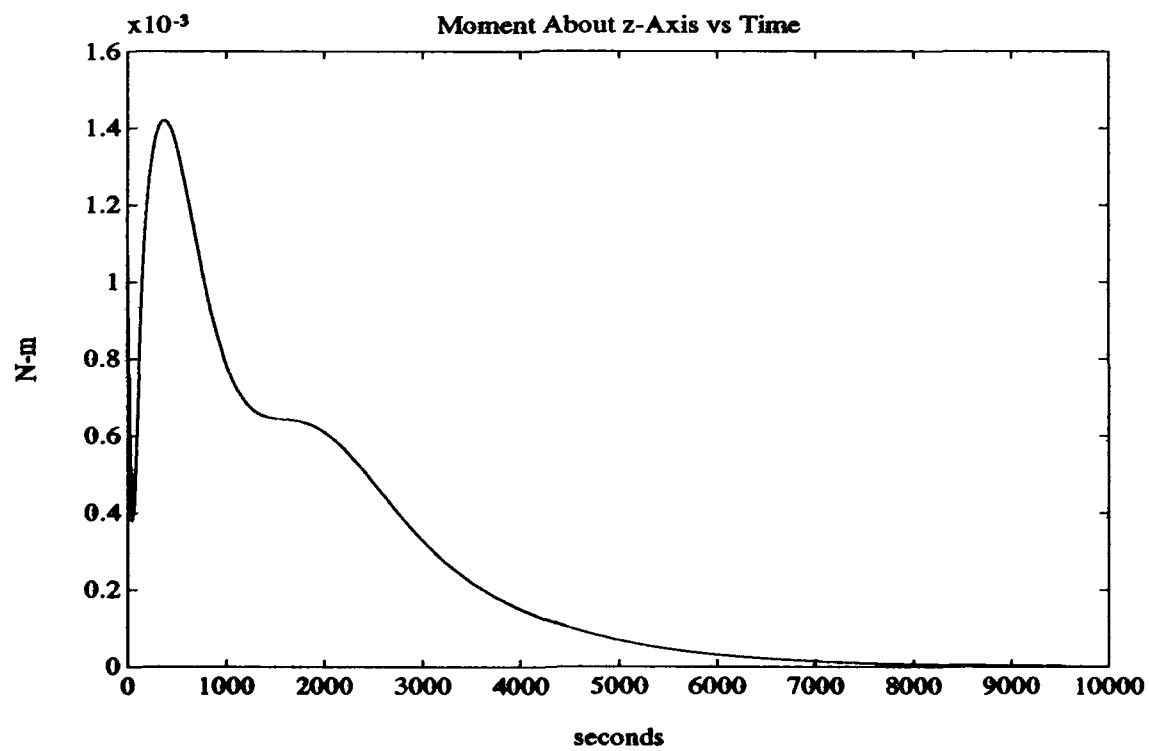
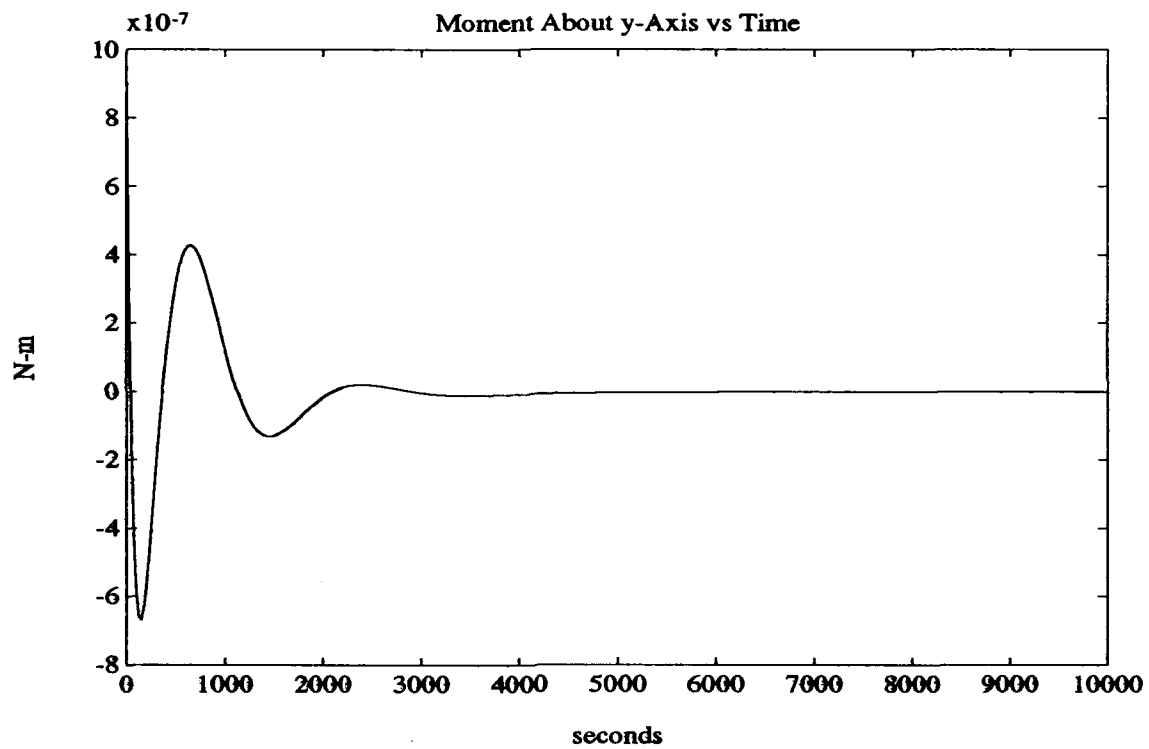


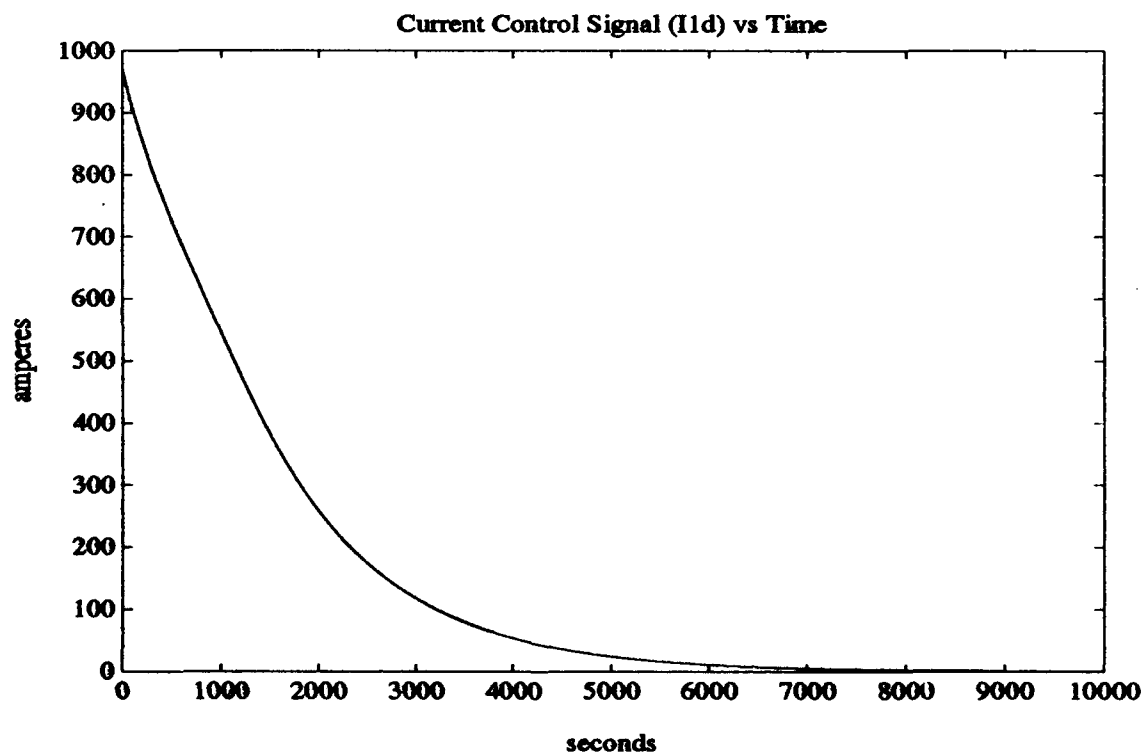
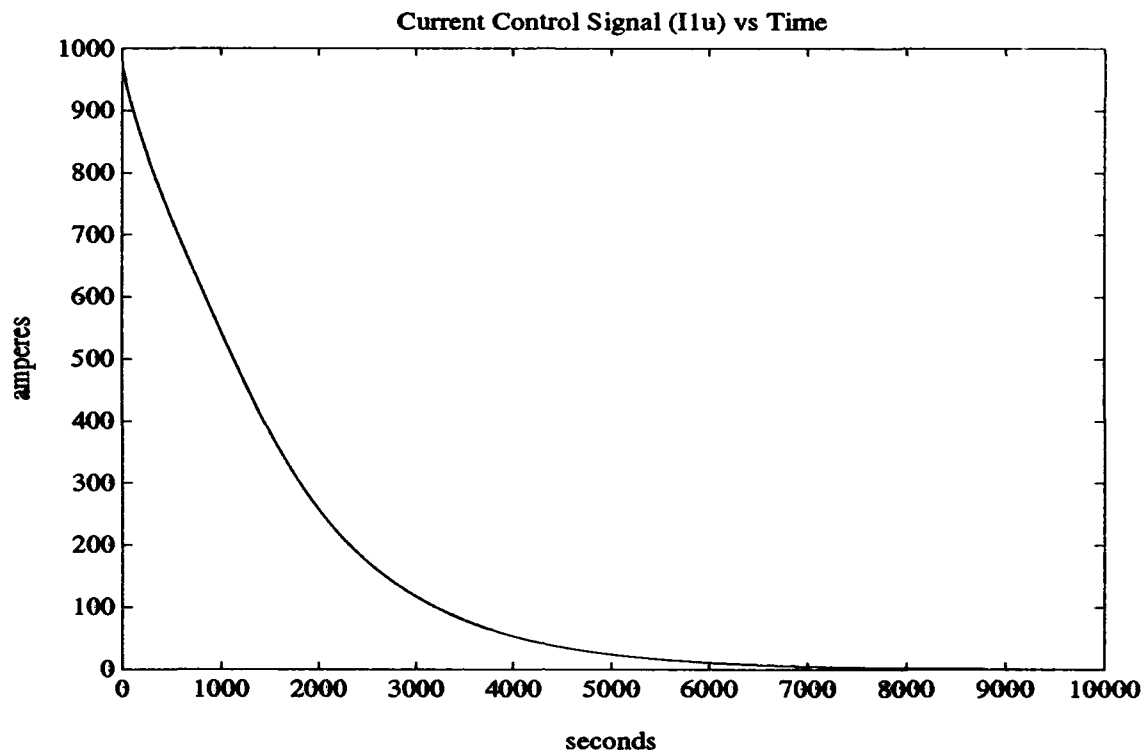


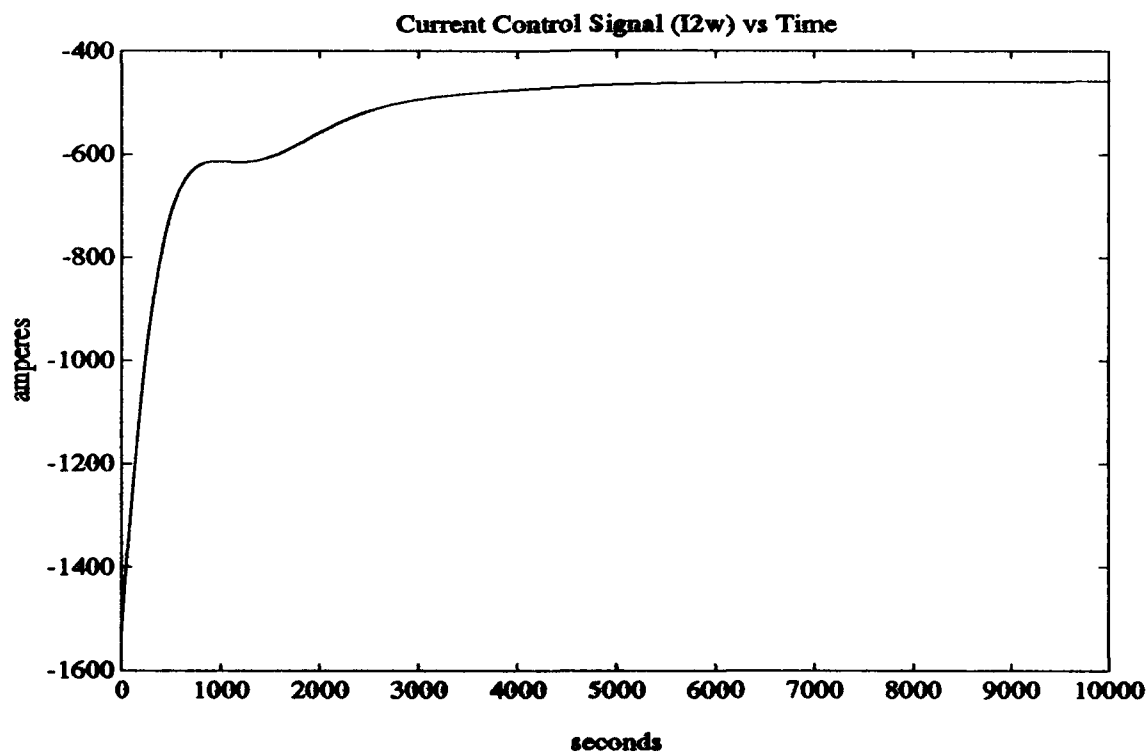
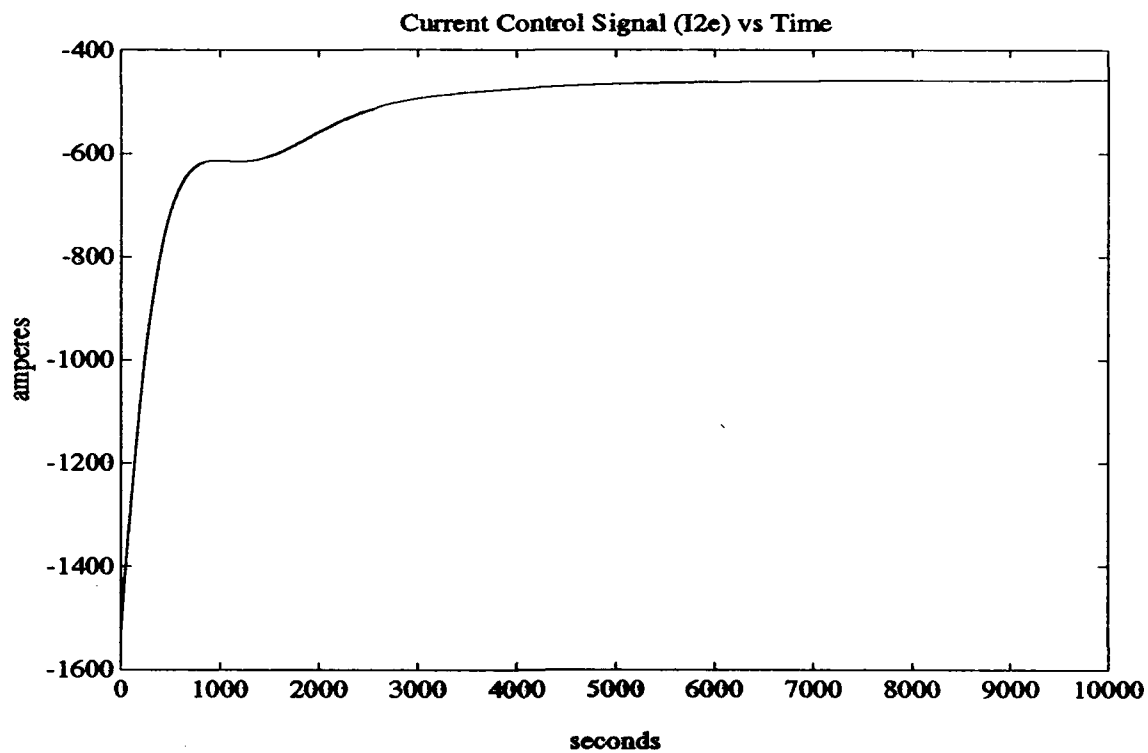


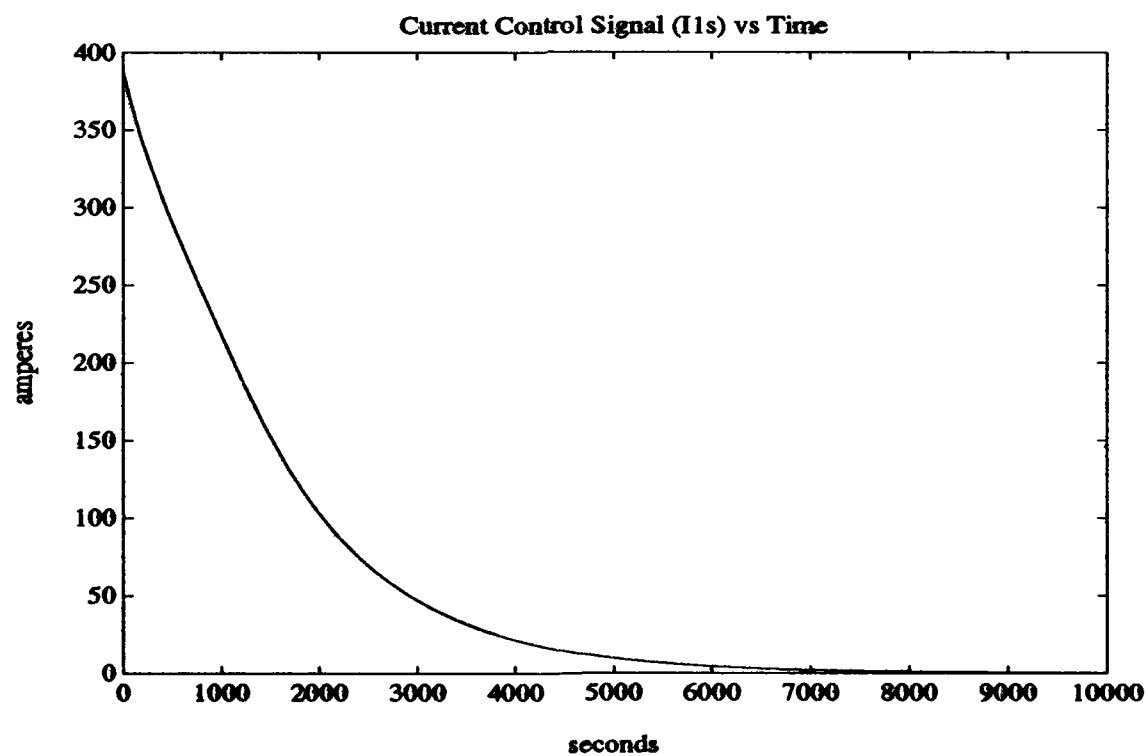
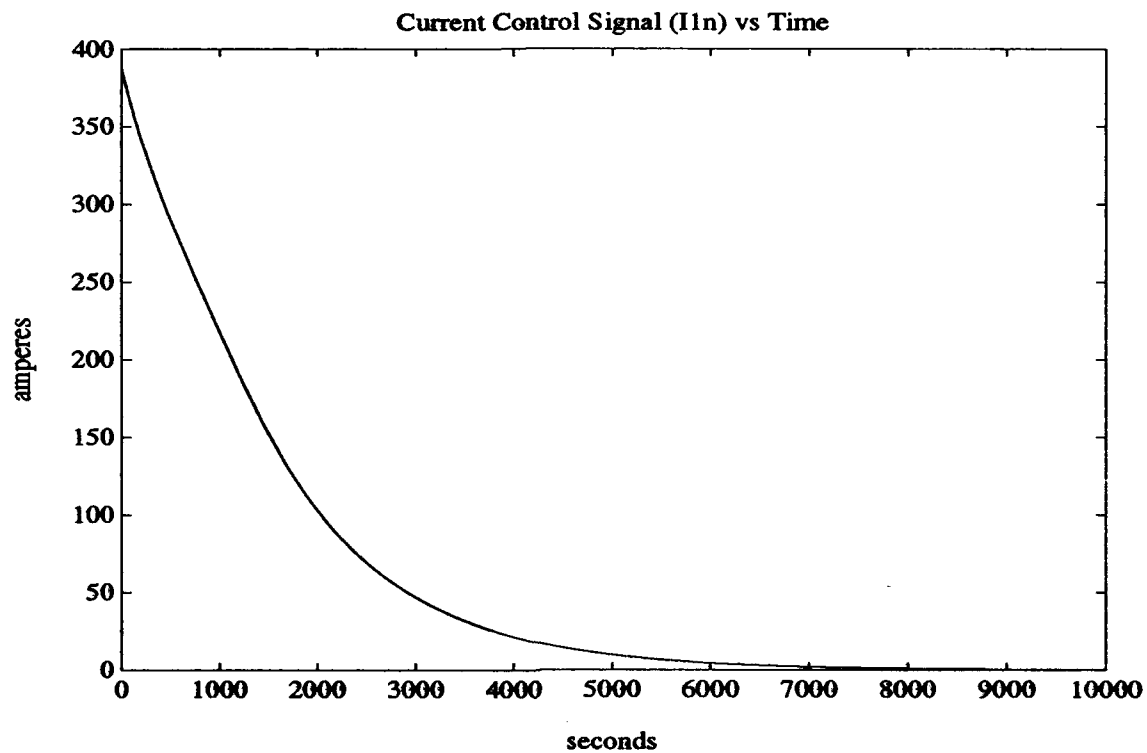




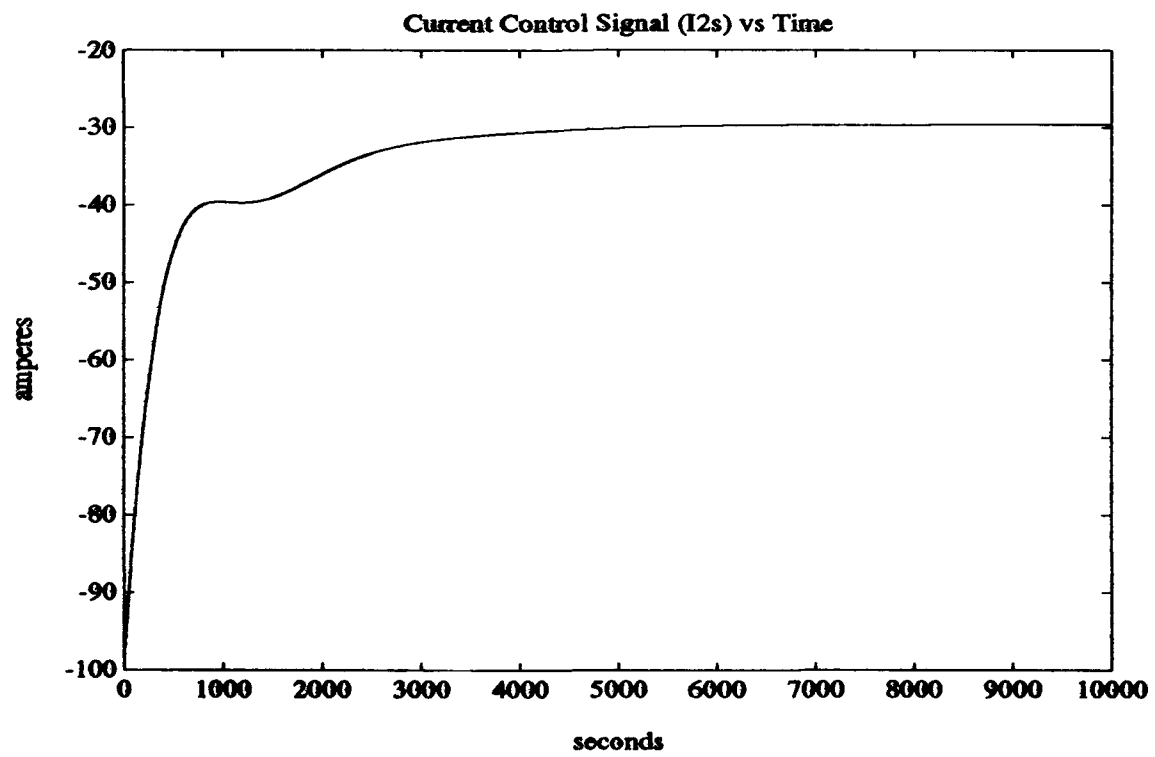
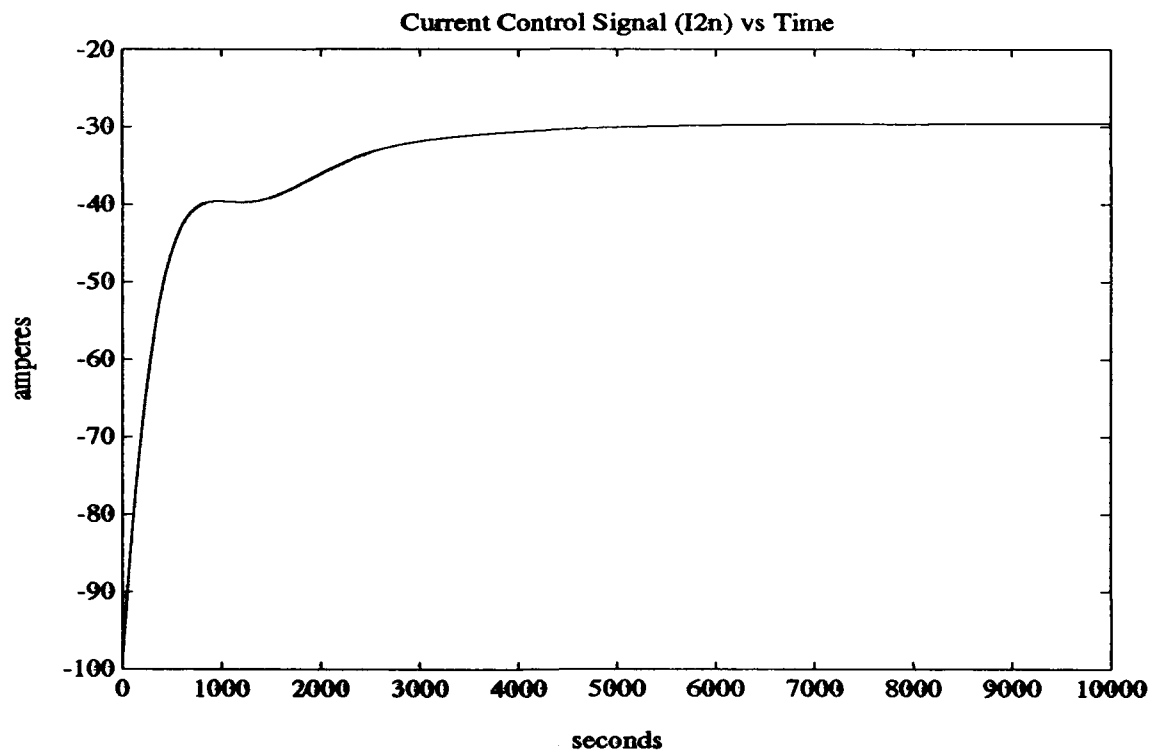












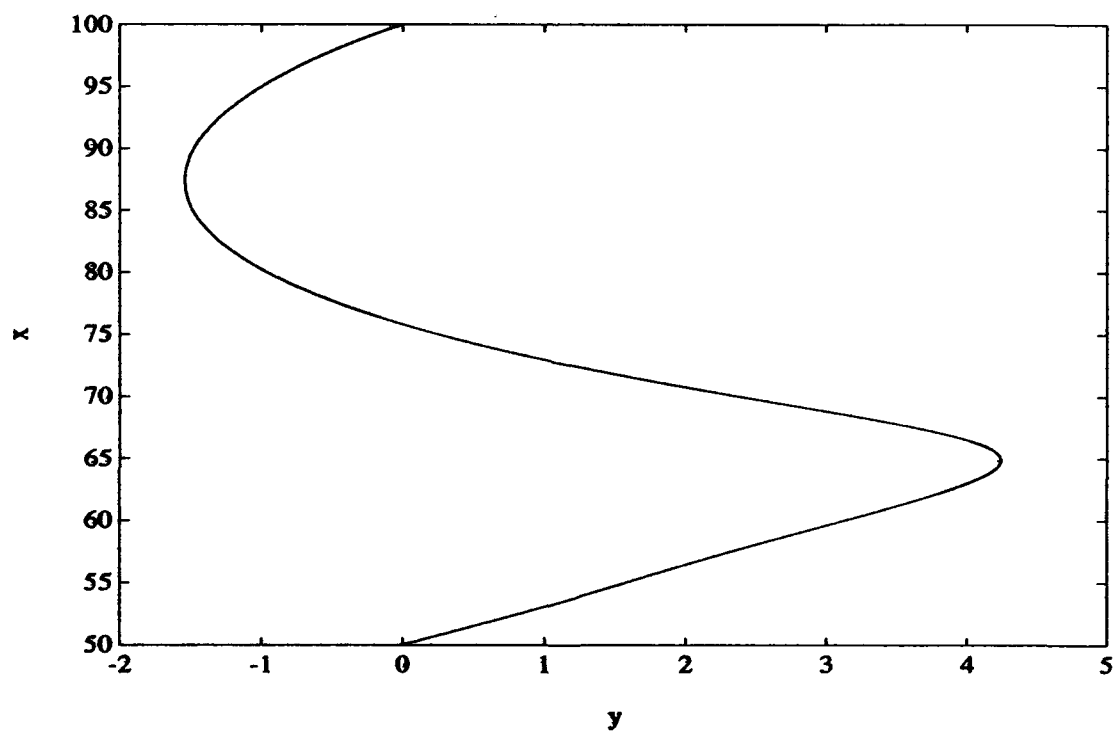
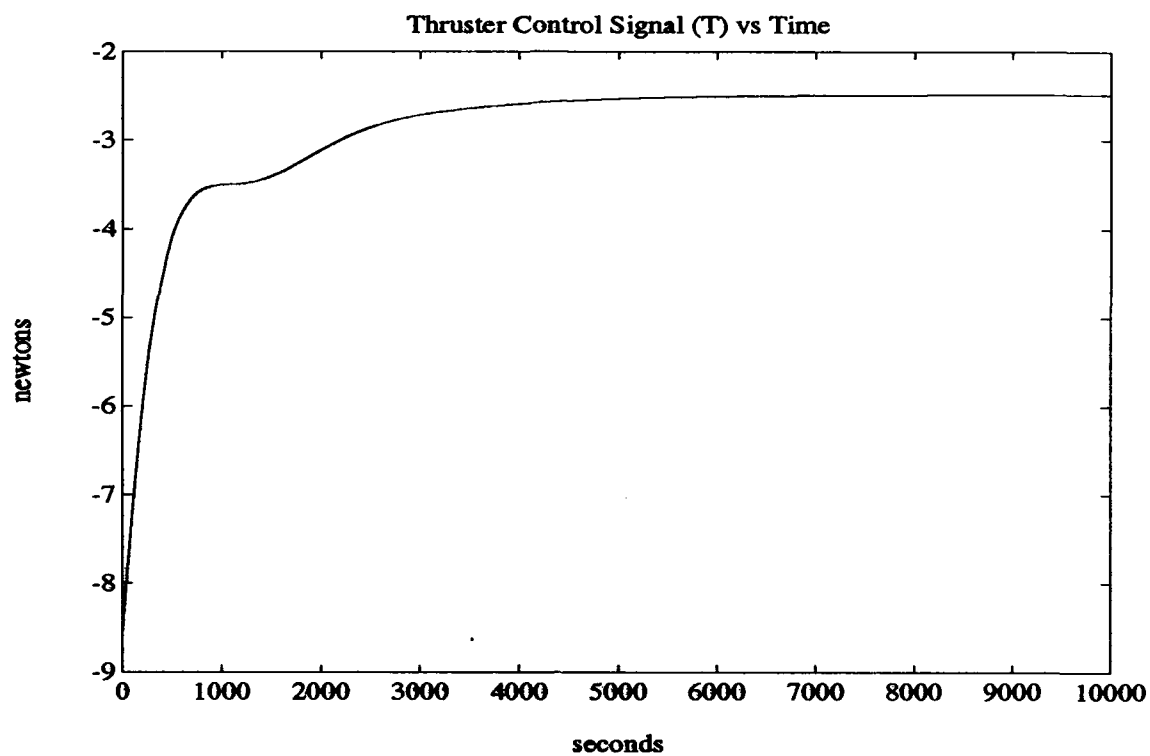


**Figure E.1. R-BAR Tracking Vehicle Trajectory in the X-Y Plane**

### E.3 V-BAR Docking Approach Example

>> cont

Welcome to the PDTV Controller Design and Performance Program.

Altitude of reference orbit (kilometers) ? 400

Trig angle (u-theta-g-lambda) to work with (degrees) ? 33

Mass of ASSET excluding towers (kg) ? 31300

Linear mass density of conductor towers (kg/m) ? 7.3

Length of vertical (x) in-plane conductors (meters) ? 310

Length of horizontal (y) in-plane conductors (meters) ? 50

Length of nonconducting cross support towers (meters) ? 50

Length of vertical (x) cross conductors (meters) ? 20

Length of horizontal (y) cross conductors (meters) ? 20

Orbital mean motion (rad/sec) =

1.1316e-03

Total system mass (kg) =

37870

Principle moment of inertia A (kg-m<sup>2</sup>) =

3.5521e+06

Principle moment of inertia B (kg-m<sup>2</sup>) =

1.8873e+08

Principle moment of inertia C (kg-m<sup>2</sup>) =

1.8702e+08

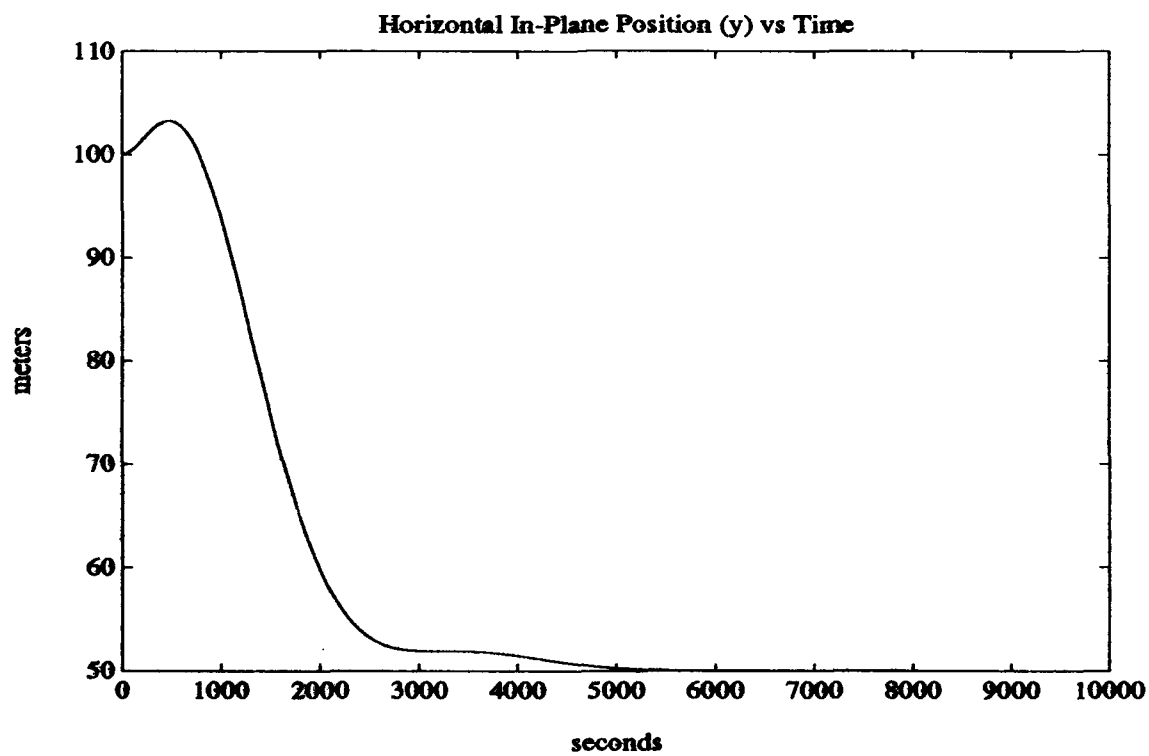
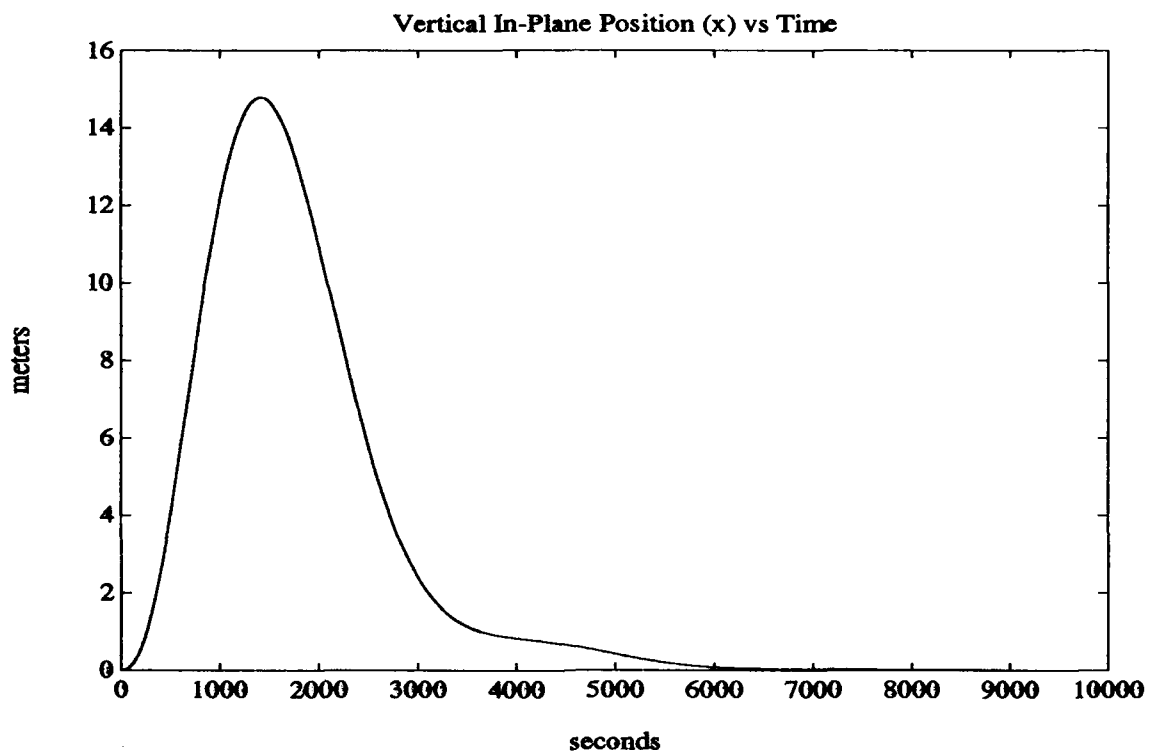
The (Fsys,Gsys) system is completely controllable.

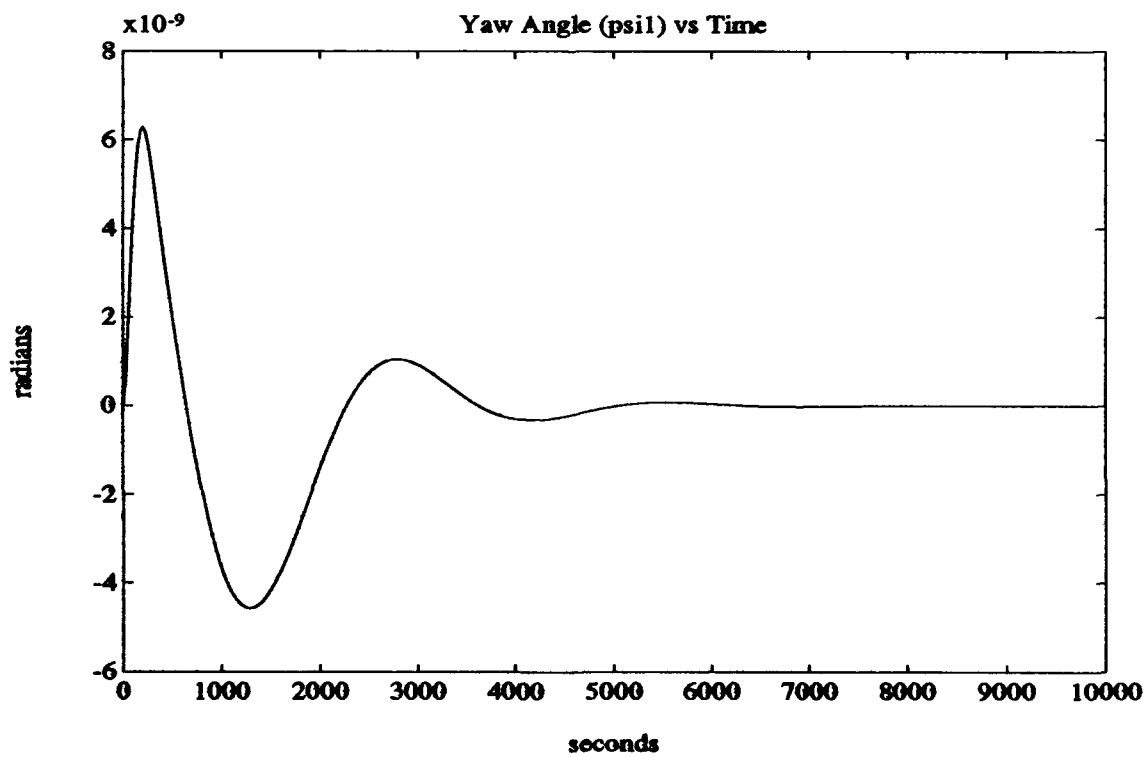
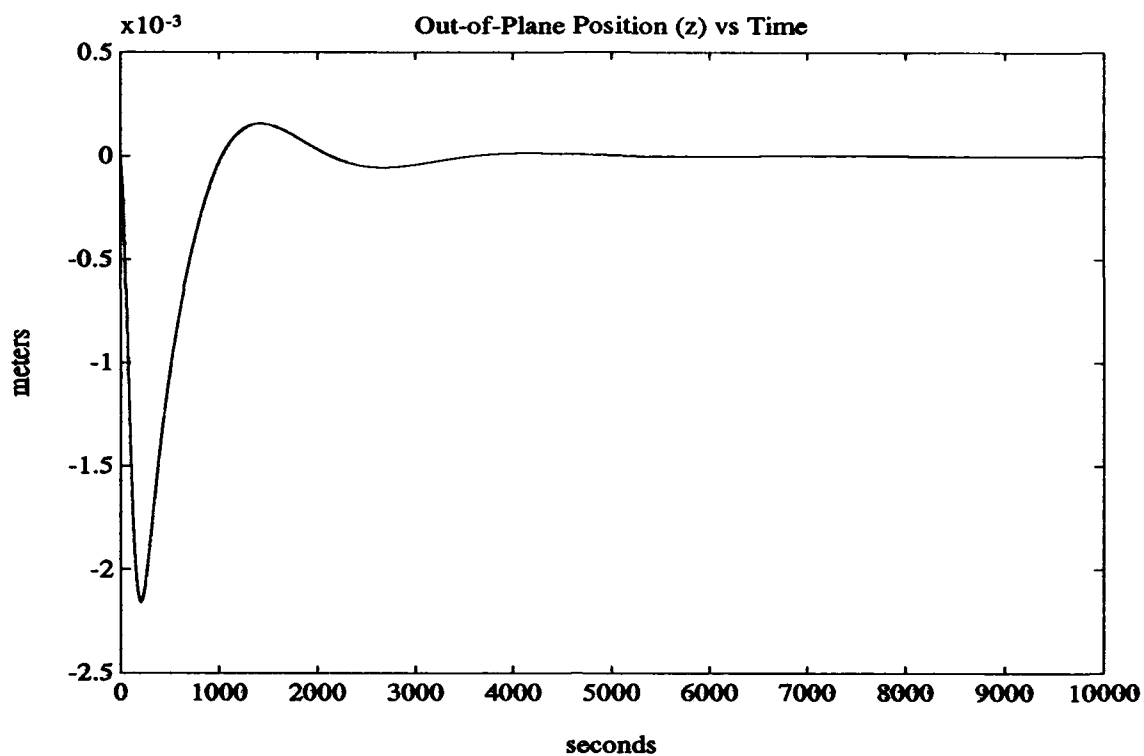
The (Fsys,Hsys) system is completely observable.

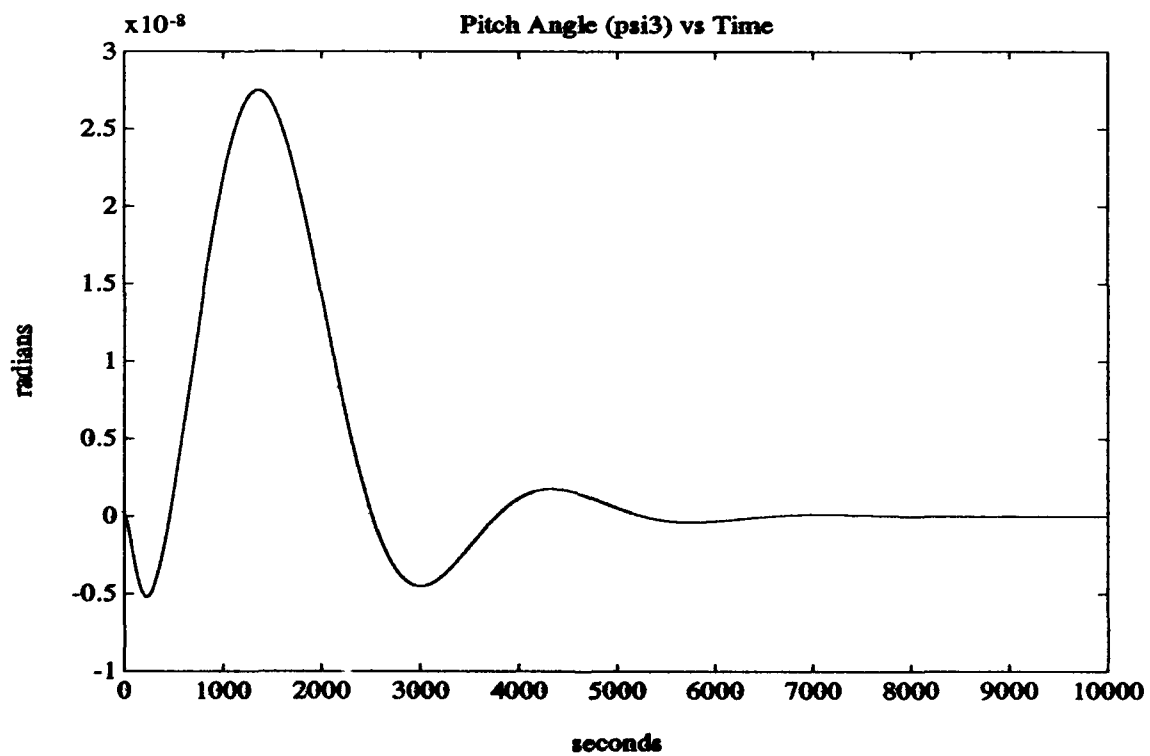
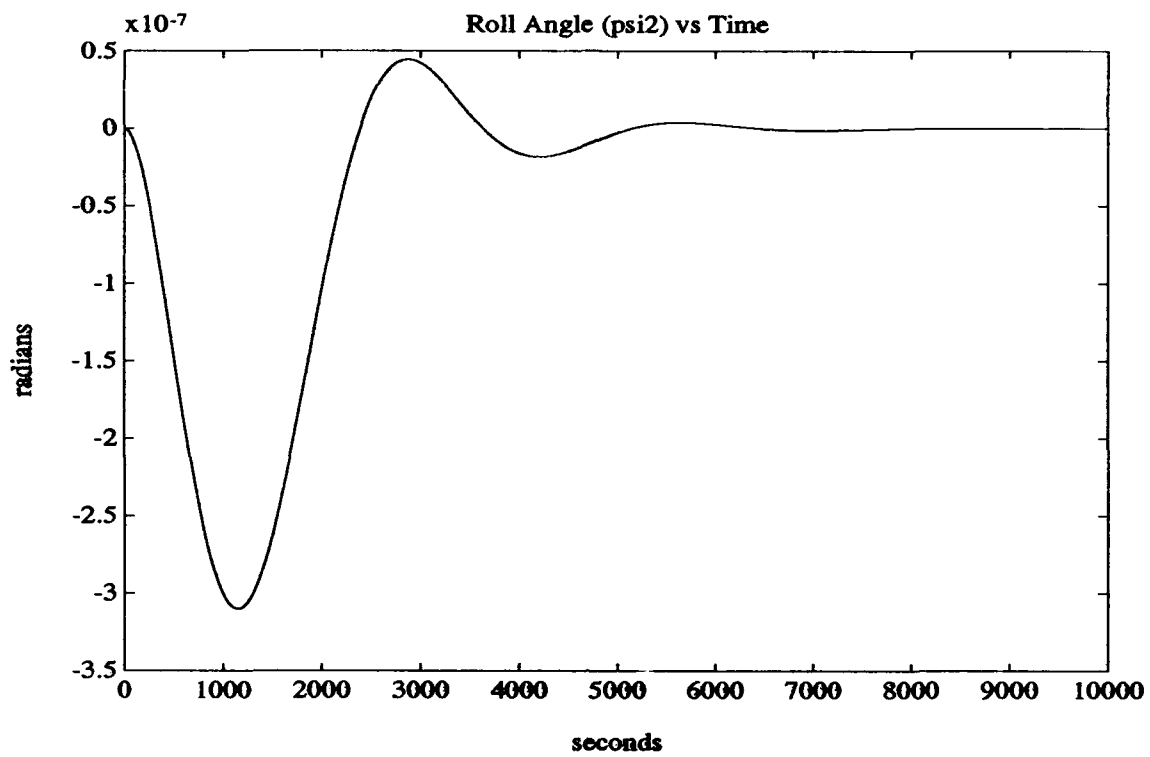
Weighting on the state weighting matrix Q ? 100

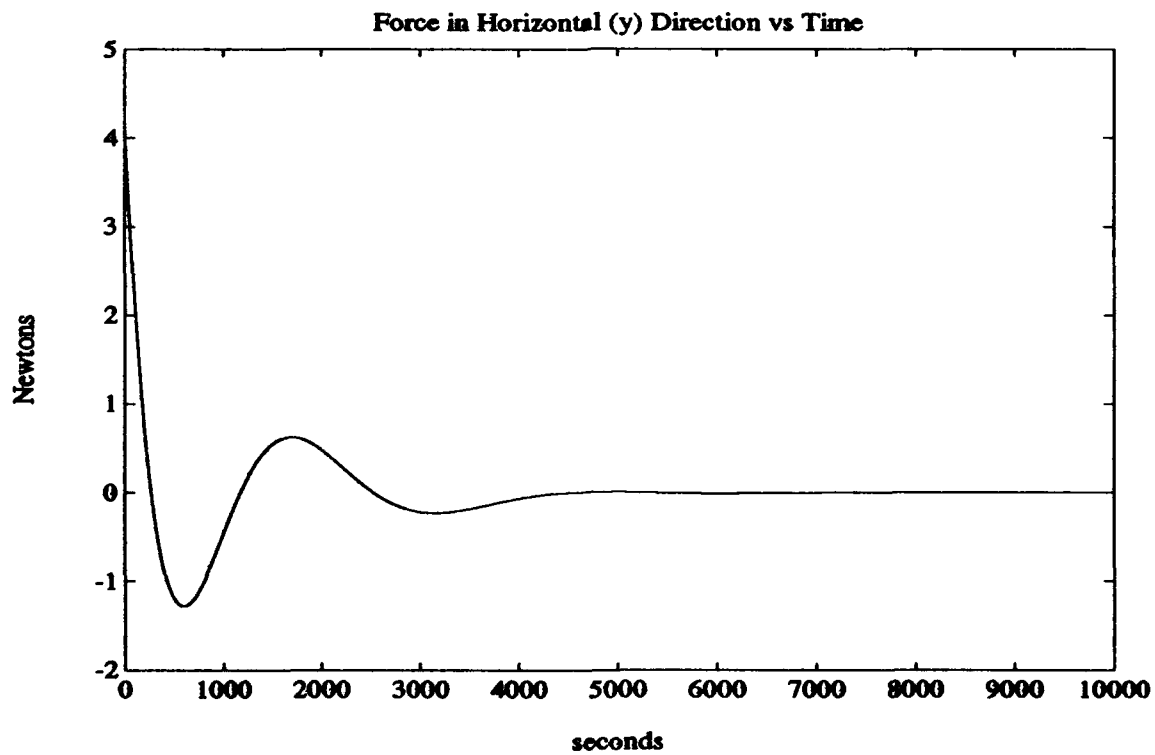
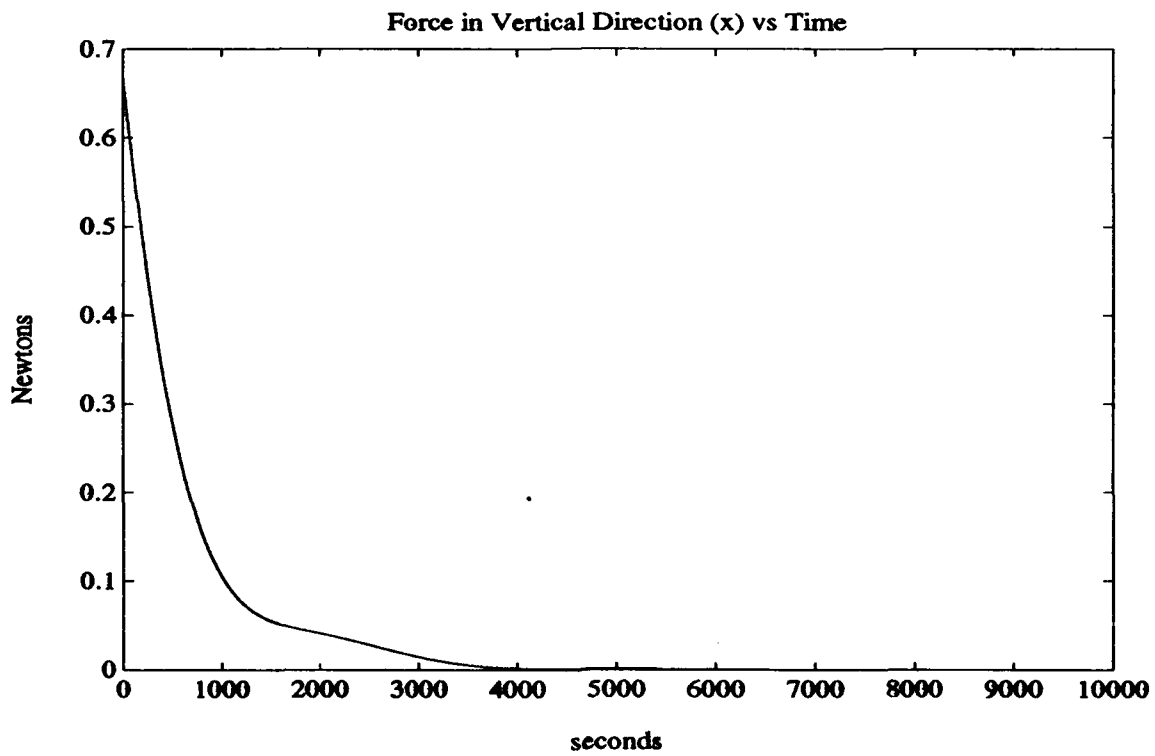
Weighting on the control weighting matrix R ? 1

What is the value of x to attain and track (m) ? 0  
What is the value of y to attain and track (m) ? 50  
What is the value of z to attain and track (m) ? 0  
What is the value of psi1 to attain and track (rad) ? 0  
What is the value of psi2 to attain and track (rad) ? 0  
What is the value of psi3 to attain and track (rad) ? 0  
What is the initial value of x (m) ? 0  
What is the initial value of y (m) ? 100  
What is the initial value of z (m) ? 0  
What is the initial value of psi1 (rad) ? 0  
What is the initial value of psi2 (rad) ? 0  
What is the initial value of psi3 (rad) ? 0  
How long of a time response to plot ? 10000  
Number of time increments (data points) ? 500

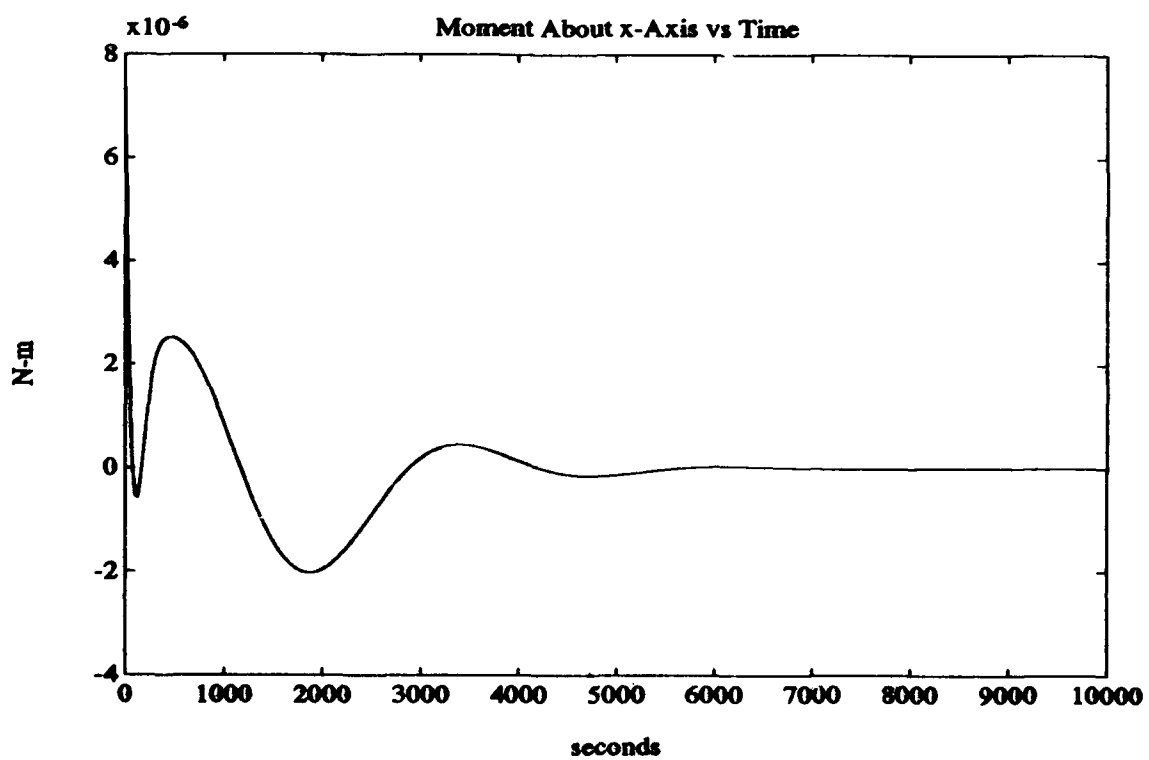
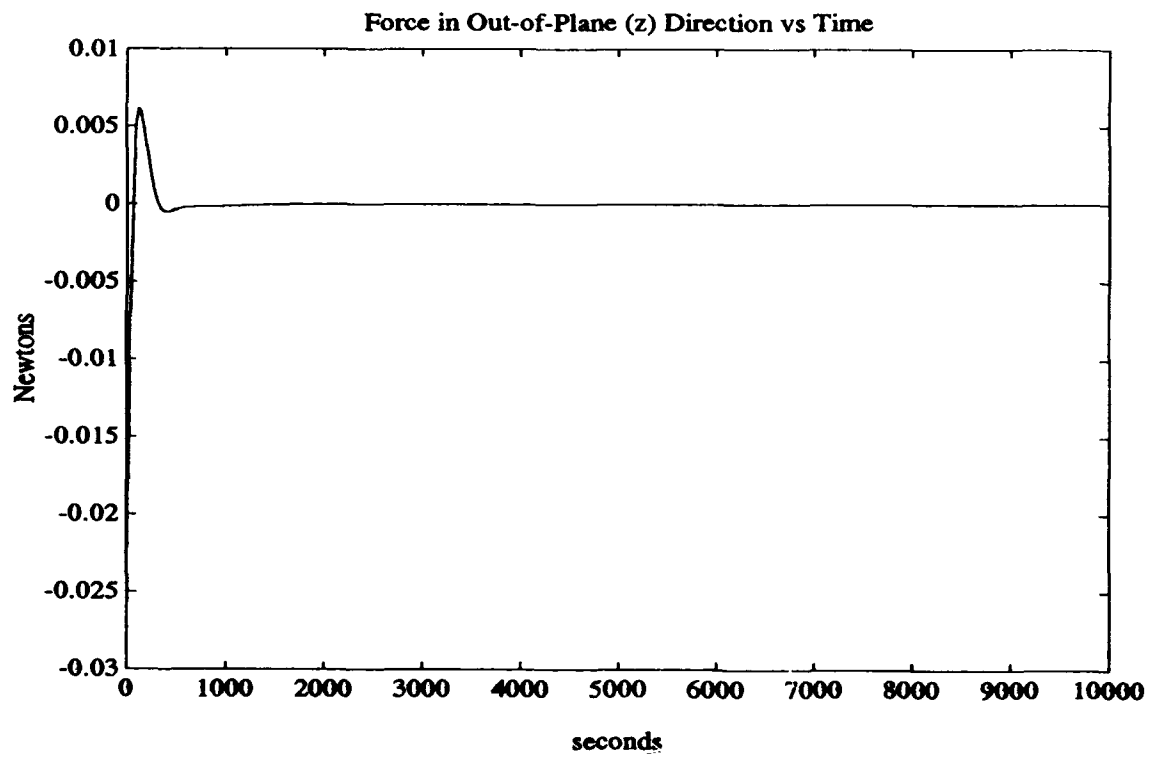


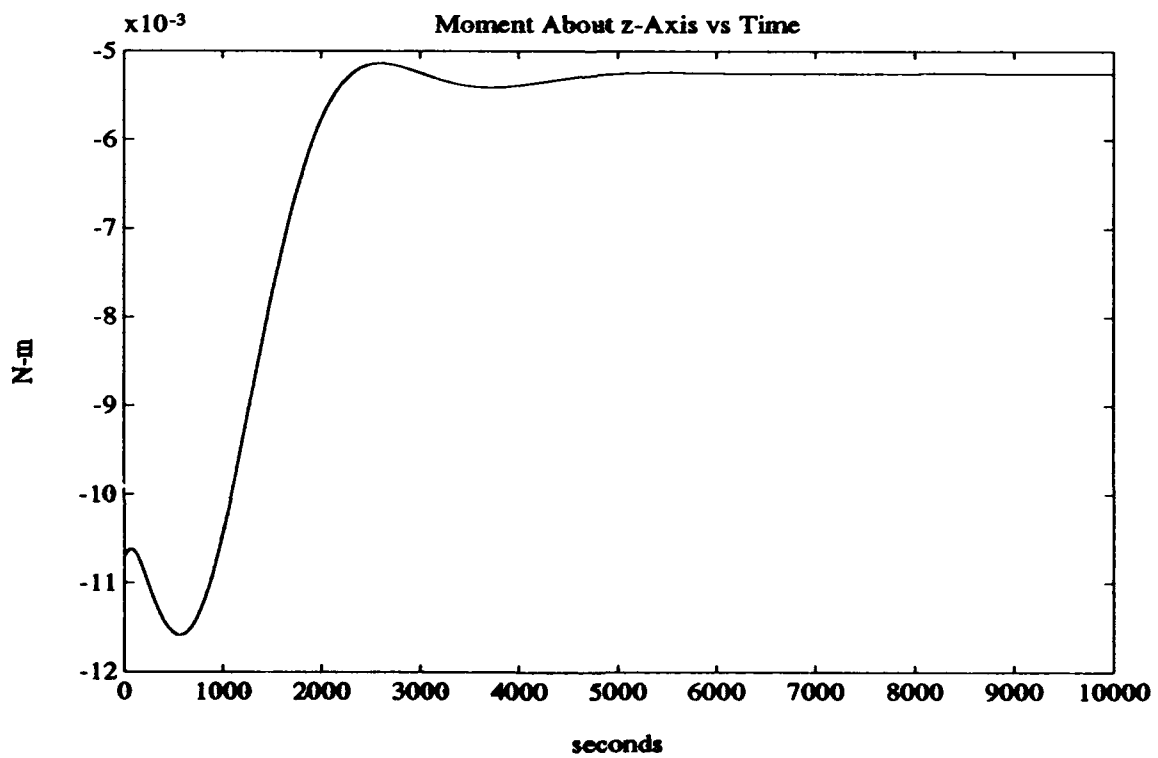
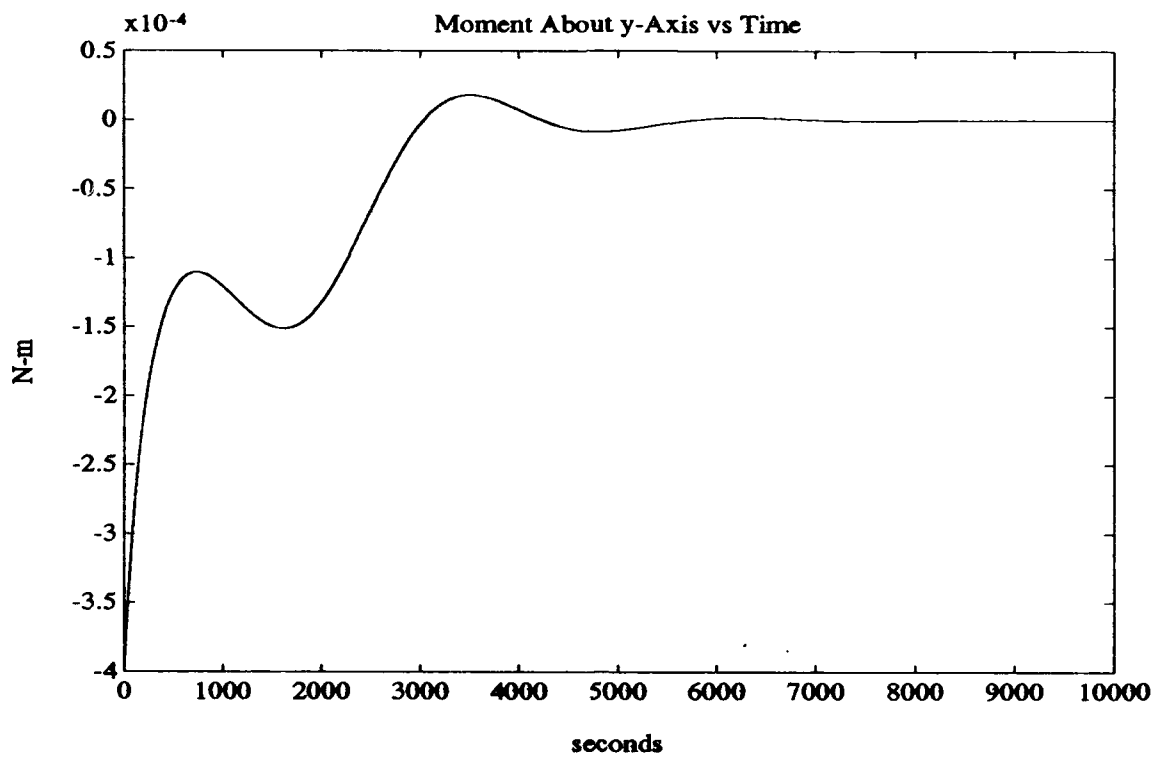




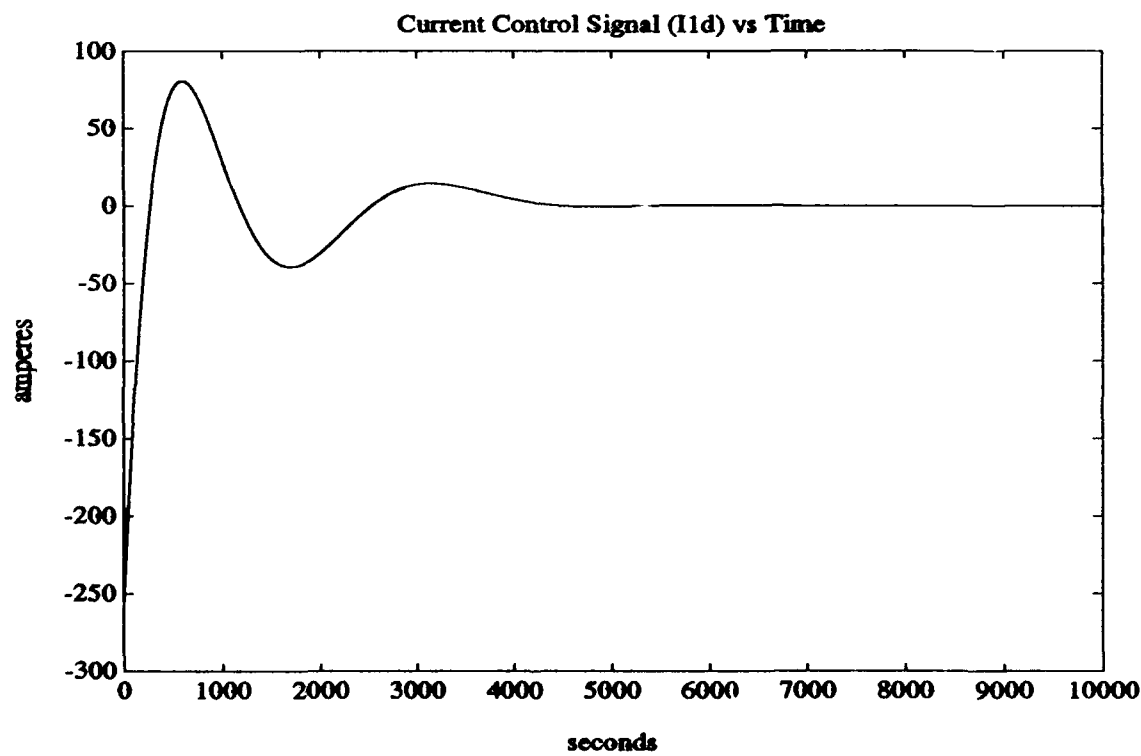
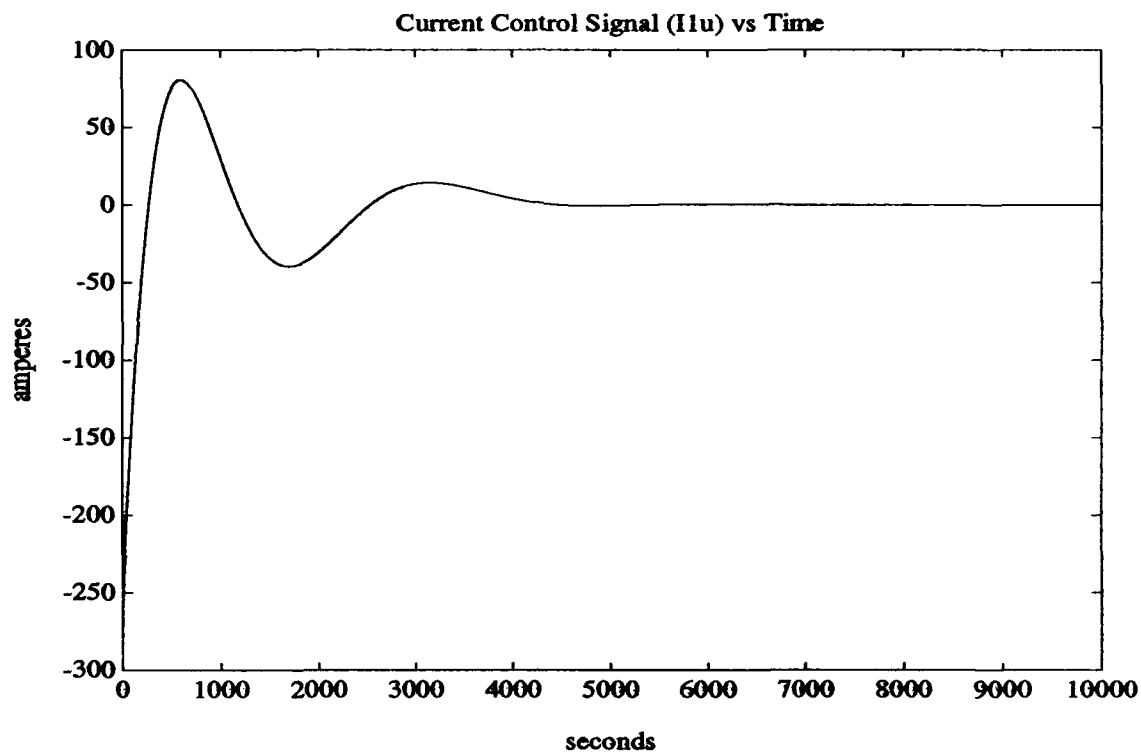


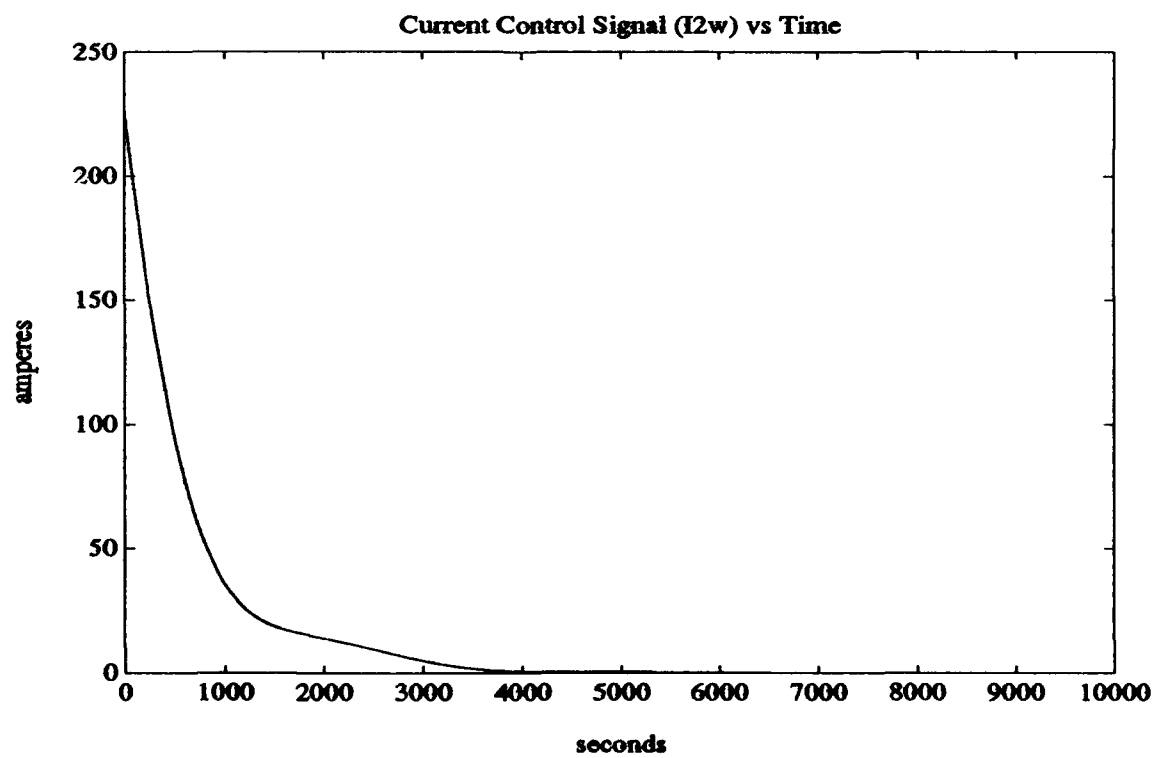
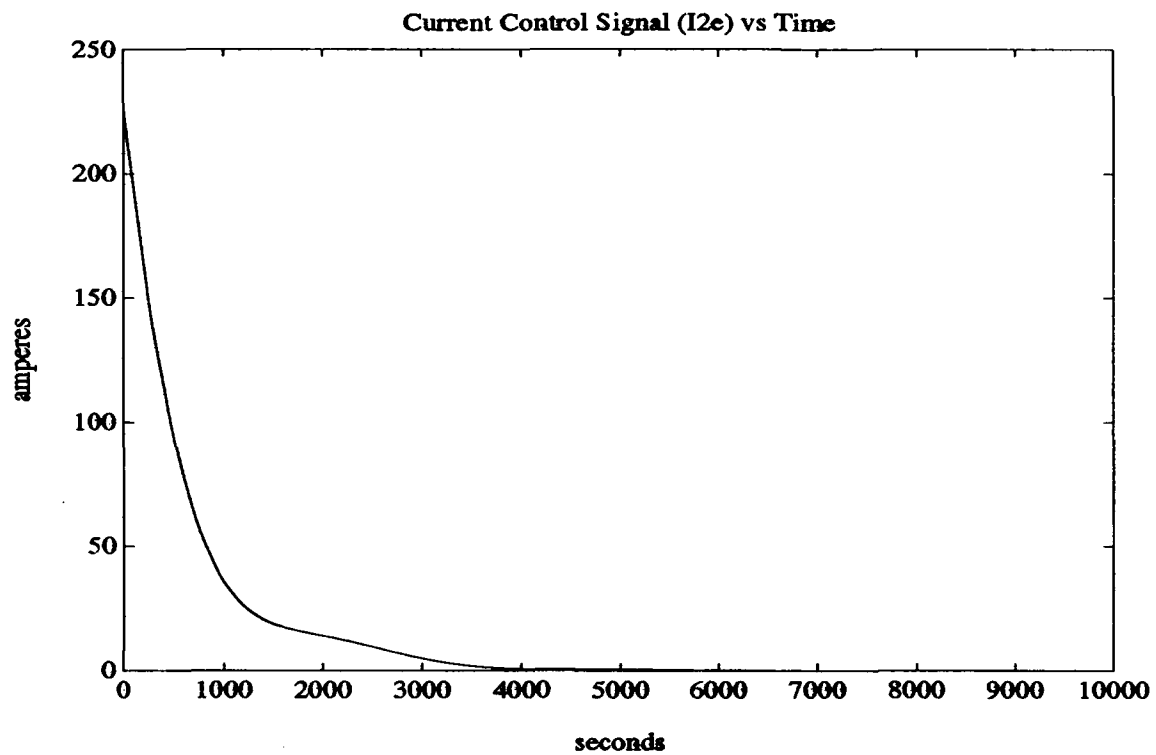


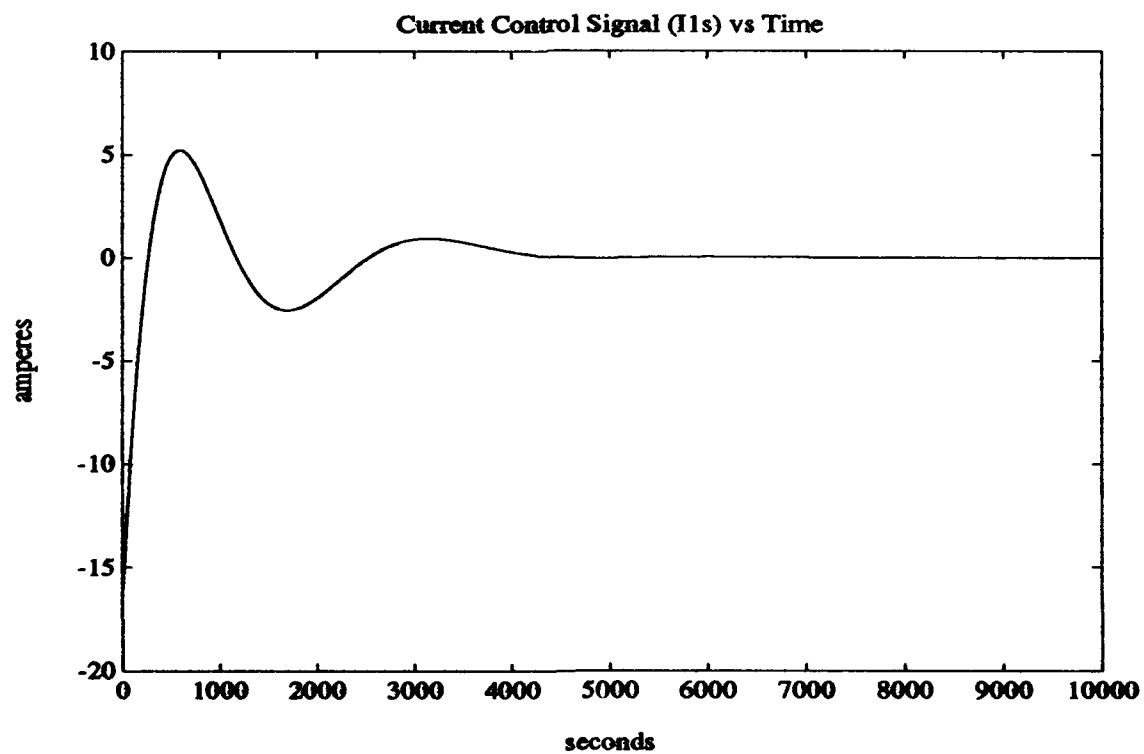
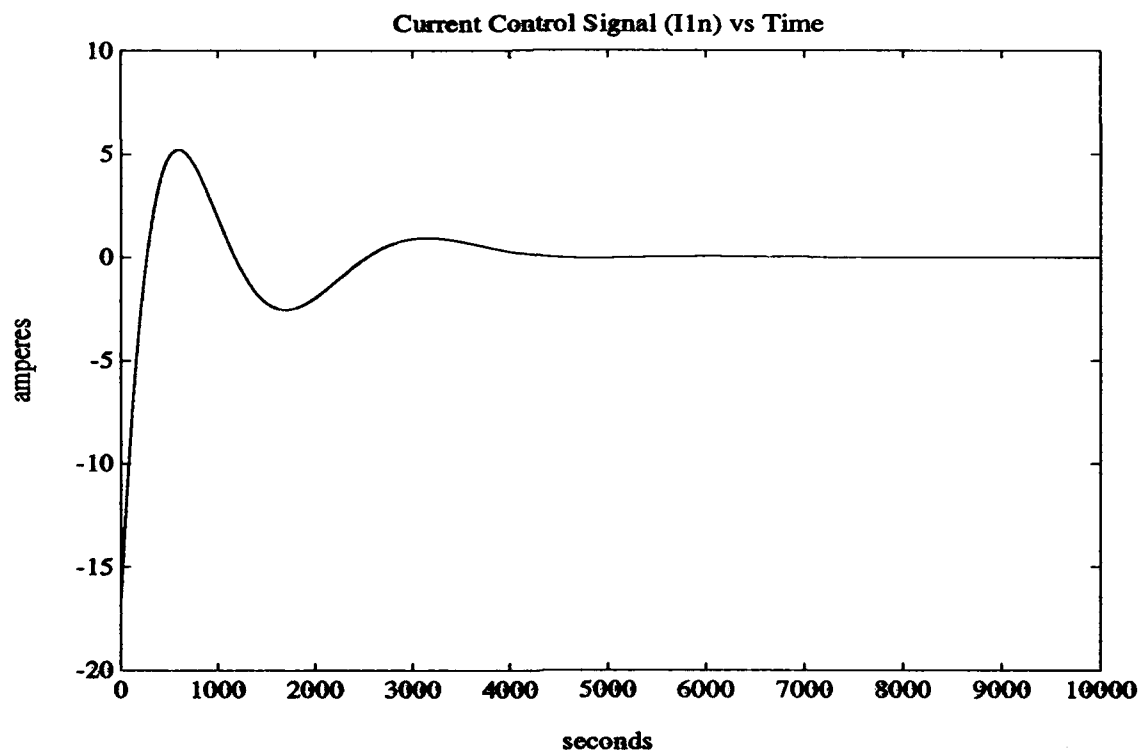


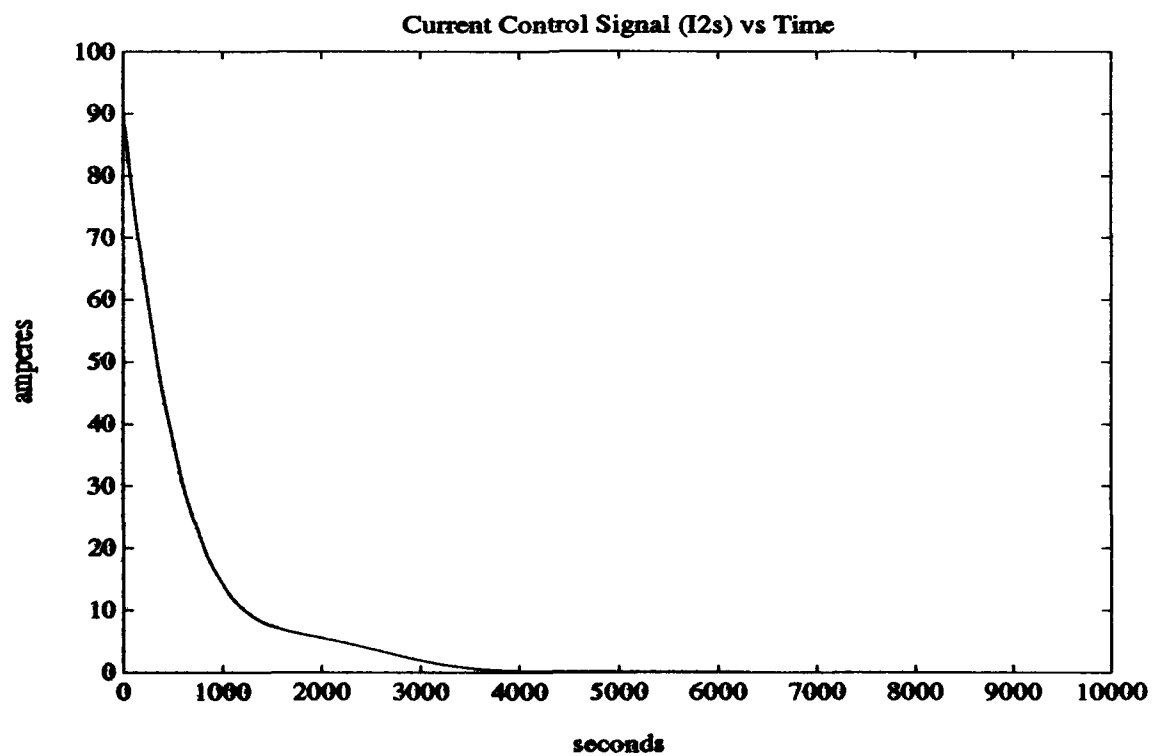
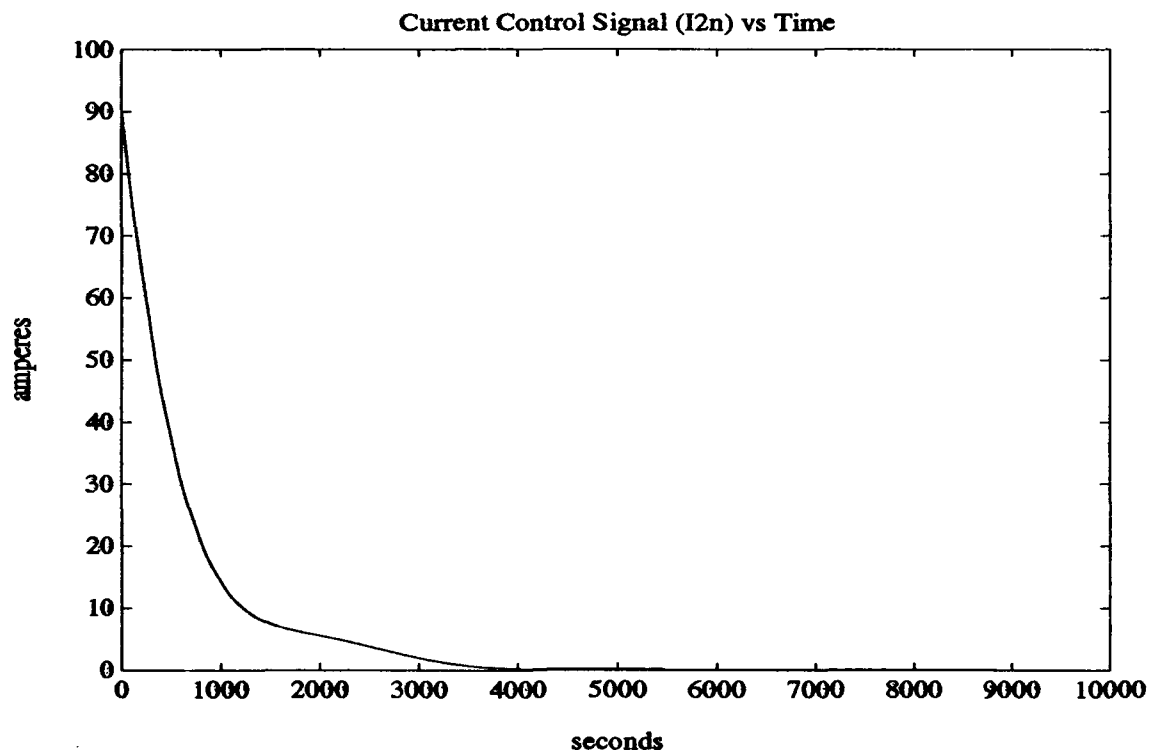


128









126

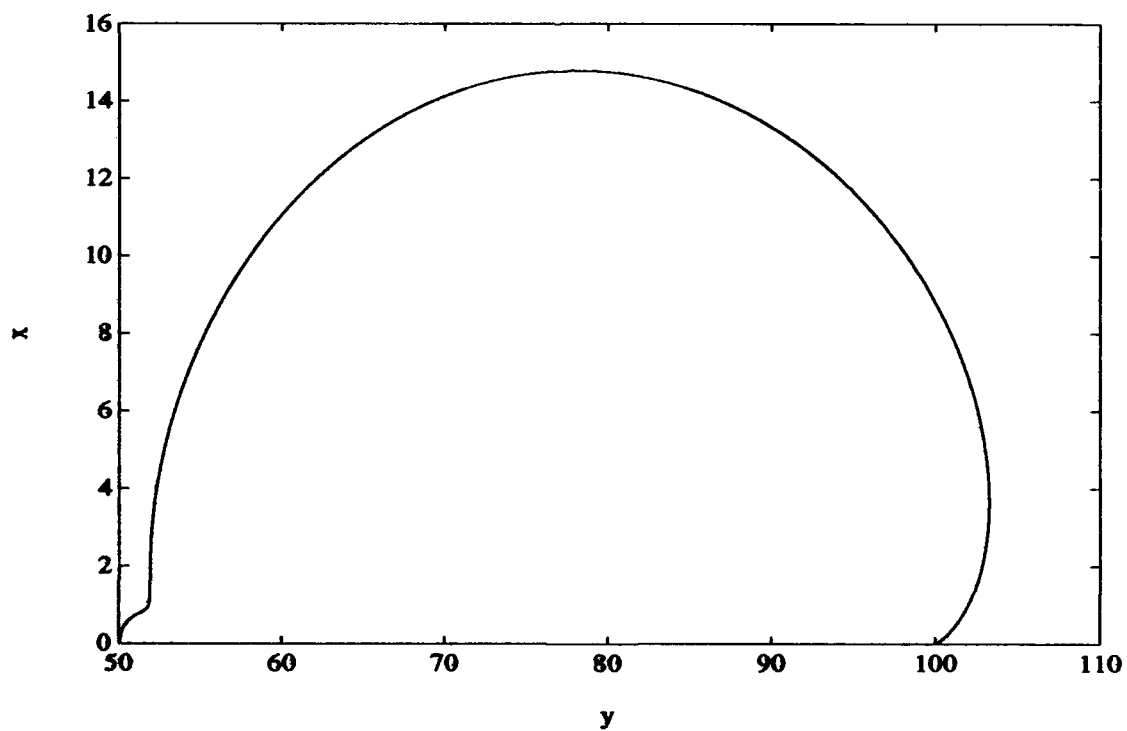
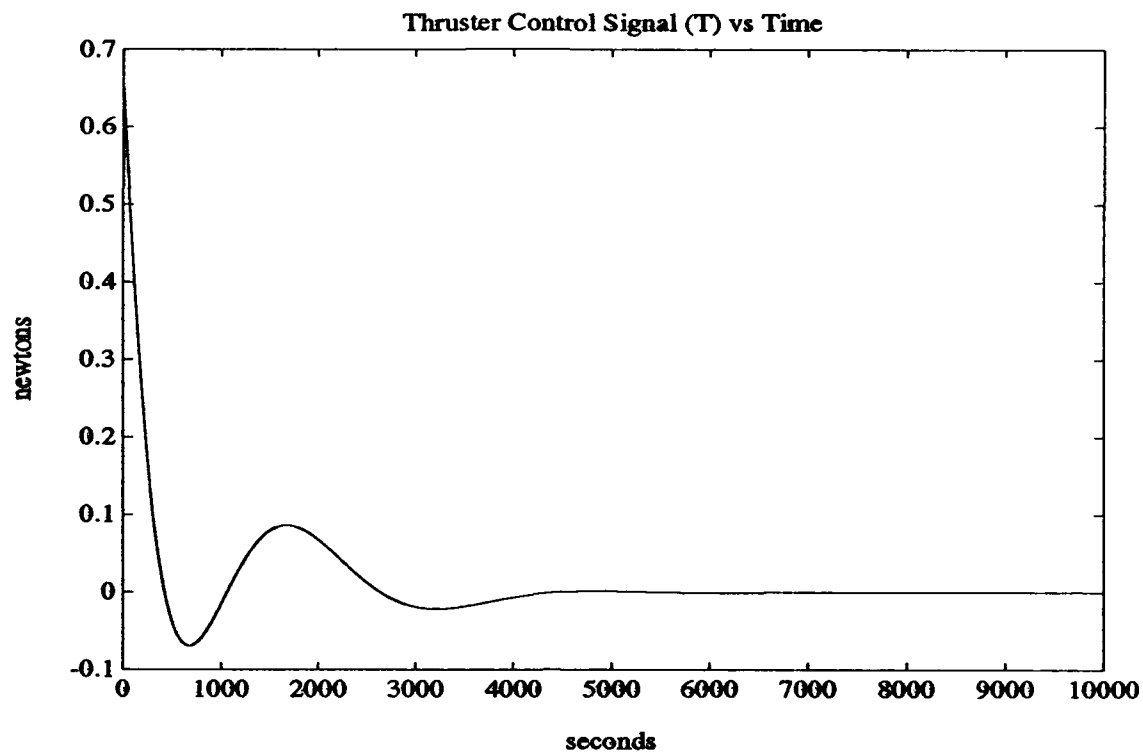


**Figure E.2. V-BAR Tracking Vehicle Trajectory in the X-Y Plane**

## Appendix F. *Controller Design Program Listing*

```
disp(' ');
disp('Welcome to the POTV Controller Design and Performance Program.');
```

disp(' ');

format short e

%define constants

G=6.67259e-11; %gravitational constant

Me=5.976e24; %mass of the earth in kg

re=6.378e06; %mean equatorial radius of earth in meters

m=8.1e15; %magnetic dipole moment of the earth in Tesla

d=-78.5\*pi/180; %latitude of austral magnetic pole in radians

h=46.88; %length of ET modeled as a cylinder in meters

a=4.206; %radius of ET modeled as a cylinder in meters

%user enters tower lengths

altitude=input('Altitude of reference orbit (kilometers) ? ');

w=input('Trig angle (u-theta-g-lambda) to work with (degrees) ? ');

Met=input('Mass of ASSET excluding towers (kg) ? ');

p=input('Linear mass density of conductor towers (kg/m) ? ');

l1=input('Length of vertical (x) in-plane conductors (meters) ? ');

l2=input('Length of horizontal (y) in-plane conductors (meters) ? ');

lt=input('Length of nonconducting cross support towers (meters) ? ');

lc1=input('Length of vertical (x) cross conductors (meters) ? ');

lc2=input('Length of horizontal (y) cross conductors (meters) ? ');

%unit conversions

r0=re+altitude\*1000; %orbital radius of reference orbit in meters

w=w\*pi/180; %convert trig angle to radians



```

%calculations
n=sqrt(G*Me/r0^3); %orbital mean motion (reference orbit)
disp('Orbital mean motion (rad/sec) =');
disp(n);
Mtot=Met+2*p*(l1+l2+lc1+lc2+lt); %Mass of entire POTV system in kg
disp('Total system mass (kg) =');
disp(Mtot);

Iet=Met*([(a^2/2) 0 0;0 ((3*a^2+h^2)/12) 0;0 0 ((3*a^2+h^2)/12)]);
Il1=2*l1*p*([0 0 0;0 ((l1^2/12)+((l1+h)/2)^2) 0;0 0
((l1^2/12)+((l1+h)/2)^2)]);
Il2=2*l2*p*([(l2^2/12)+((l2/2)+a)^2) 0 0;0 0 0;0 0
((l2^2/12)+((l2/2)+a)^2)]);
Ilt=2*lt*p*([(lt^2/12)+((lt/2)+a)^2) 0 0;0 ((lt^2/12)+((lt/2)+a)^2) 0;
0 0 0]);
Ilc1=2*lc1*p*([(lt+a)^2) 0 0;0 ((lc1^2/12)+(lt+a)^2) 0;0 0 (lc1^2/12)]);
Ilc2=2*lc2*p*([(lc2^2/12)+(lt+a)^2) 0 0;0 (lt+a)^2 0;0 0 (lc2^2/12)]);
I=Iet+Il1+Il2+Ilt+Ilc1+Ilc2; %Moment of inertia matrix in kg*m^2
A=I(1,1); %principle moments of inertia
B=I(2,2);
C=I(3,3);
disp('Principle moment of inertia A (kg-m^2) =');
disp(A);
disp('Principle moment of inertia B (kg-m^2) =');
disp(B);
disp('Principle moment of inertia C (kg-m^2) =');
disp(C);

%set up system matrices F,G,H,J (open-loop)
%system matrix

```

```

Fsys=[0 1 0 0 0 0 0 0 0 0 0;
(3*n^2) 0 0 (2*n) 0 0 0 0 0 0 0;
0 0 0 1 0 0 0 0 0 0 0;
0 (-2*n) 0 0 0 0 0 0 0 0 0;
0 0 0 0 0 1 0 0 0 0 0;
0 0 0 0 (-n^2) 0 0 0 0 0 0;
0 0 0 0 0 0 1 0 0 0 0;
0 0 0 0 0 0 (-n^2)*(C-B)/A 0 0 (-n*(-A-B+C)/A) 0 0;
0 0 0 0 0 0 0 0 1 0 0;
0 0 0 0 ((3*n^2)*(A-C)/(r0*B)) 0 0 (-n*(A+B-C)/B) ((4*n^2)*(A-C)/B) 0 0 0;
0 0 0 0 0 0 0 0 0 0 1;
0 (3*n/(2*r0)) ((3*n^2)*(B-A)/(r0*C)) 0 0 0 0 0 0 0 ((-3*n^2)*(B-A)/C) 0];

```

%input matrix

```

Gsys=(1/r0^3)*([0 0 0 0 0 0 0 0 0;
0 0 (-m*l2*sin(d)/Mtot) (-m*l2*sin(d)/Mtot) 0 0 (-m*lc2*sin(d)/Mtot)
(-m*lc2*sin(d)/Mtot) 0;
0 0 0 0 0 0 0 0;
(m*l1*sin(d)/Mtot) (m*l1*sin(d)/Mtot) 0 0 (m*lc1*sin(d)/Mtot)
(m*lc1*sin(d)/Mtot) 0 0 0;
0 0 0 0 0 0 0 0;
(m*l1*cos(d)*sin(w)/Mtot) (m*l1*cos(d)*sin(w)/Mtot)
(-2*m*l2*cos(d)*cos(w)/Mtot) (-2*m*l2*cos(d)*cos(w)/Mtot)
(m*lc1*cos(d)*sin(w)/Mtot) (m*lc1*cos(d)*sin(w)/Mtot)
(-2*m*lc2*cos(d)*cos(w)/Mtot) (-2*m*lc2*cos(d)*cos(w)/Mtot) (r0^3/Mtot);
0 0 0 0 0 0 0 0;
0 0 (-m*l2^2*cos(d)*cos(w)/A) (m*l2^2*cos(d)*cos(w)/A)
(-m*lt*lc1*sin(d)/A) (m*lt*lc1*sin(d)/A) 0 0 0;
0 0 0 0 0 0 0 0;
(-m*l1^2*cos(d)*sin(w)/(2*B)) (m*l1^2*cos(d)*sin(w)/(2*B)) 0 0 0 0
(-m*lt*lc2*sin(d)/B) (m*lt*lc2*sin(d)/B) 0;

```

```

0 0 0 0 0 0 0 0 0;
(m*l1^2*sin(d)/(2*C)) (-m*l1^2*sin(d)/(2*C)) (m*l2^2*sin(d)/(2*C))
(-m*l2^2*sin(d)/(2*C)) 0 0 0 0 0];

%output matrix (selects positions and attitude angles only)
Hsys=[1 0 0 0 0 0 0 0 0 0 0;
0 0 1 0 0 0 0 0 0 0 0;
0 0 0 0 1 0 0 0 0 0 0;
0 0 0 0 0 0 1 0 0 0 0;
0 0 0 0 0 0 0 0 1 0 0;
0 0 0 0 0 0 0 0 0 0 1 0];

Jsyz=zeros(6,9); %no fed-through control signals

%test controllability and observability
disp(' ');
Mc=ctrb(Fsys,Gsys);
if rank(Mc)==12,
    disp('The (Fsys,Gsys) system is completely controllable.');
```

```

else
    disp('The (Fsys,Gsys) system has uncontrollable modes!');
```

```

end
disp(' ');

Mo=obsv(Fsys,Hsys);
if rank(Mo)==12 ,
    disp('The (Fsys,Hsys) system is completely observable.');
```

```

else
    disp('The (Fsys,Hsys) system has unobservable modes!');
```

```

end

```

```

%derive LQR compensator K
%user enters state and control signal weightings

%normalized state weighting matrix
q=input('Weighting on the state weighting matrix Q ? ');
Q=q*([1 0 0 0 0 0 0 0 0 0 0 0;
0 1 0 0 0 0 0 0 0 0 0 0;
0 0 1 0 0 0 0 0 0 0 0 0;
0 0 0 1 0 0 0 0 0 0 0 0;
0 0 0 0 1 0 0 0 0 0 0 0;
0 0 0 0 0 1 0 0 0 0 0 0;
0 0 0 0 0 0 r0 0 0 0 0 0;
0 0 0 0 0 0 0 r0 0 0 0 0;
0 0 0 0 0 0 0 0 r0 0 0 0;
0 0 0 0 0 0 0 0 0 r0 0 0;
0 0 0 0 0 0 0 0 0 0 r0]);

r=input('Weighting on the control weighting matrix R ? ');
R=r*eye(9); %equal weighting on each control

K=lqr(Fsys,Gsys,Q,R);

%derive non-square pre-filter M using optimal pseudo-inverse
M=-pinv(Hsys*inv(Fsys-Gsys*K)*Gsys);

%setup closed-loop system matrices
Fcl=Fsys-Gsys*K;
Gcl=Gsys*M;
Hcl=Hsys;
Jcl=zeros(6);

```

```

%linear simulation of states due to initial condition and reference cmd
rx=input('What is the value of x to attain and track (m) ? ');
ry=input('What is the value of y to attain and track (m) ? ');
rz=input('What is the value of z to attain and track (m) ? ');
rpsi1=input('What is the value of psi1 to attain and track (rad) ? ');
rpsi2=input('What is the value of psi2 to attain and track (rad) ? ');
rpsi3=input('What is the value of psi3 to attain and track (rad) ? ');
x0=input('What is the initial value of x (m) ? ');
y0=input('What is the initial value of y (m) ? ');
z0=input('What is the initial value of z (m) ? ');
psi10=input('What is the initial value of psi1 (rad) ? ');
psi20=input('What is the initial value of psi2 (rad) ? ');
psi30=input('What is the initial value of psi3 (rad) ? ');
X0=[x0 0 y0 0 z0 0 psi10 0 psi20 0 psi30 0]';
tmax=input('How long of a time response to plot ? ');
ntinc=input('Number of time increments (data points) ? ');
t=0:(tmax/ntinc):tmax;
tleng=length(t);
r=zeros(tleng,6); %construct reference command
r(:,1)=rx*ones(tleng,1);
r(:,2)=ry*ones(tleng,1);
r(:,3)=rz*ones(tleng,1);
r(:,4)=rpsi1*ones(tleng,1);
r(:,5)=rpsi2*ones(tleng,1);
r(:,6)=rpsi3*ones(tleng,1);
[y,x]=lsim(Fcl,Gcl,Hcl,Jcl,r,t,X0); %outputs and states
u=(M*r'-K*x)'; %control vector includes 8 currents and thrusters
f=(Gsys*u)'; %forces

plot(t,y(:,1));

```

```

title('Vertical In-Plane Position (x) vs Time');
xlabel('seconds');
ylabel('meters');
meta x;
pause;

plot(t,(Mtot*f(:,2)));
title('Force in Vertical Direction (x) vs Time');
xlabel('seconds');
ylabel('Newtons');
meta fx;
pause;

plot(t,y(:,2));
title('Horizontal In-Plane Position (y) vs Time');
xlabel('seconds');
ylabel('meters');
meta y;
pause;

plot(t,(Mtot*f(:,4)));
title('Force in Horizontal (y) Direction vs Time');
xlabel('seconds');
ylabel('Newtons');
meta fy;
pause;

plot(t,y(:,3));
title('Out-of-Plane Position (z) vs Time');
xlabel('seconds');
ylabel('meters');

```

```

meta z;
pause;

plot(t,(Mtot*f(:,6)));
title('Force in Out-of-Plane (z) Direction vs Time');
xlabel('seconds');
ylabel('Newtons');
meta fz;
pause;

plot(t,y(:,4));
title('Yaw Angle (psi1) vs Time');
xlabel('seconds');
ylabel('radians');
meta psi1;
pause;

plot(t,(A*f(:,8)));
title('Moment About x-Axis vs Time');
xlabel('seconds');
ylabel('N-m');
meta mx;
pause;

plot(t,y(:,5));
title('Roll Angle (psi2) vs Time');
xlabel('seconds');
ylabel('radians');
meta psi2;
pause;

```

```

plot(t,(B*f(:,10)));
title('Moment About y-Axis vs Time');
xlabel('seconds');
ylabel('N-m');
meta my;
pause;

plot(t,y(:,6));
title('Pitch Angle (psi3) vs Time');
xlabel('seconds');
ylabel('radians');
meta psi3;
pause;

plot(t,(C*f(:,12)));
title('Moment About z-Axis vs Time');
xlabel('seconds');
ylabel('N-m');
meta mz;
pause;

plot(t,u(:,1));
title('Current Control Signal (I1u) vs Time');
xlabel('seconds');
ylabel('amperes');
meta i1u;
pause;

plot(t,u(:,2));
title('Current Control Signal (I1d) vs Time');
xlabel('seconds');

```



```
plot(t,u(:,7));  
title('Current Control Signal (I2n) vs Time');  
xlabel('seconds');  
ylabel('amperes');  
meta i2n;  
pause;
```

```
plot(t,u(:,8));  
title('Current Control Signal (I2s) vs Time');  
xlabel('seconds');  
ylabel('amperes');  
meta i2s;  
pause;
```

```
plot(t,u(:,9));  
title('Thruster Control Signal (T) vs Time');  
xlabel('seconds');  
ylabel('newtons');  
meta t;
```

```
ylabel('amperes');
```

```
meta iid;
```

```
pause;
```

```
plot(t,u(:,3));
```

```
title('Current Control Signal (I2e) vs Time');
```

```
xlabel('seconds');
```

```
ylabel('amperes');
```

```
meta i2e;
```

```
pause;
```

```
plot(t,u(:,4));
```

```
title('Current Control Signal (I2w) vs Time');
```

```
xlabel('seconds');
```

```
ylabel('amperes');
```

```
meta i2w;
```

```
pause;
```

```
plot(t,u(:,5));
```

```
title('Current Control Signal (I1n) vs Time');
```

```
xlabel('seconds');
```

```
ylabel('amperes');
```

```
meta i1n;
```

```
pause;
```

```
plot(t,u(:,6));
```

```
title('Current Control Signal (I1s) vs Time');
```

```
xlabel('seconds');
```

```
ylabel('amperes');
```

```
meta i1s;
```

```
pause;
```

## *Bibliography*

1. Bate, Roger R. and others. Fundamentals of Astrodynamics. New York: Dover Publications, 1971.
2. Drell, S. D. and others. "Drag and Propulsion of Large Satellites in the Ionosphere: An Alfven Propulsion Engine in Space," Journal of Geophysical Research, Vol. 70, No. 13, 3131-3145, July 1965.
3. Franklin, Gene F. and others. Feedback Control of Dynamic Systems (Second Edition). Reading MA: Addison-Wesley, 1991.
4. Haislip, James N. Jr. and others. An Aluminum Salvage Station for the External Tank (ASSET). MS thesis, AFIT/GSE/ENY/90D-02. School of Engineering, Air Force Institute of Technology, Wright-Patterson AFB OH, December 1990.
5. Hall, William M. National Aeronautics and Space Administration. An Introduction to Shuttle/LDEF Retrieval Operations: The R-BAR Approach Option. NASA TM 78668. February 1978.
6. Hayt, William H. Jr. Engineering Electromagnetics (Fourth Edition). New York: McGraw-Hill, 1981.
7. Hess, Wilmot N. The Radiation Belt and the Magnetosphere. Waltham MA: Blaisdell Publishing Company, 1968.
8. Jahn, Robert G. Physics of Electric Propulsion. New York: McGraw-Hill, 1968.
9. Kaplan, Marshall H. Modern Spacecraft Dynamics & Control. New York: John Wiley & Sons, 1976.
10. Likins, Peter W. Elements of Engineering Mechanics. New York: McGraw-Hill, 1973.
11. Maciejowski, Jan M. Multivariable Feedback Design. Wokingham, England: Addison-Wesley, 1989.
12. Mathematica. Sun Workstation. Computer Software. Wolfram Research. 1991.
13. National Aeronautics and Space Administration. "Space Station Freedom Fact Sheet." March 1992.
14. National Aeronautics and Space Administration. Space and Planetary Environment Criteria Guidelines for Use in Space Vehicle Development, 1982 (Volume 1). NASA Technical Memorandum 82478. January 1983.
15. Penzo, Paul A. and Paul W. Ammann. National Aeronautics and Space Administration. Tethers in Space Handbook (Second Edition). Contract Number: NASW-4341, May 1989.
16. PRO-MATLAB. Sun Workstation. Computer Software. The Mathworks Inc. 1990.
17. Ridgely, D. Brett. Assistant Professor of Aerospace Engineering, Air Force Institute of Technology, Wright-Patterson AFB OH. Conversation. September 1992.
18. Rimrott, F. P. J. Introductory Attitude Dynamics. New York: Springer-Verlag, 1989.

19. Spiegel, Murray R. Mathematical Handbook of Formulas and Tables. New York: McGraw-Hill, 1968.
20. Strang, Gilbert. Linear Algebra and its Applications. San Diego: Harcourt Brace Jovanovitch. 1986.
21. Tascione, Thomas F. Introduction to the Space Environment. Malabar FL: Orbit Book Company, 1988.
22. Thomson, William T. Introduction to Space Dynamics. New York: Dover Publications, 1986.
23. Waltman, Paul. A Second Course in Elementary Differential Equations. Orlando: Academic Press, Inc., 1986.
24. Wiesel, William E. Spaceflight Dynamics. New York: McGraw-Hill, 1989.
25. Wiesel, William E. Professor of Astronautical Engineering, Air Force Institute of Technology, Wright-Patterson AFB OH. Conversation. 18 August 1992.

### *Vita*

Captain Richard E. Lawrence Jr. was born on August 7, 1965 at Andrews Air Force Base, Maryland. He graduated from AuSable Valley Central School in Clintonville, New York in 1983 and received a Bachelor of Science degree in Electrical Engineering from Clarkson University in 1987. His first Air Force assignment was at Tyndall AFB, Florida where he served as the chief of the telemetry support section of the 83rd Fighter Weapons Squadron. He entered the School of Engineering, Air Force Institute of Technology, in May 1991. Rick and his wife Stephanie were married in May 1986 and have two children: Phillip and Rachel.

Permanent address: 2829 Bahns Dr.  
Beavercreek, Ohio 45434

REPORT DOCUMENTATION PAGE			Form Approved OMB No. 0704-0188	
<small>Public reporting burden for this collection of information is estimated to average 1 hour per response, including the time for reviewing instructions, searching existing data sources, gathering and maintaining the data needed, and completing and reviewing the collection of information. Send comments regarding this burden estimate or any other aspect of this collection of information, including suggestions for reducing this burden, to Washington Headquarters Services, Directorate for Information Operations and Reports, 1215 Jefferson Davis Highway, Suite 1204, Arlington, VA 22202-4302, and to the Office of Management and Budget, Paperwork Reduction Project (0704-0188), Washington, DC 20503.</small>				
1. AGENCY USE ONLY (Leave blank)		2. REPORT DATE December 1992		3. REPORT TYPE AND DATES COVERED Master's Thesis
4. TITLE AND SUBTITLE AN ELECTROMAGNETICALLY-CONTROLLED PRECISION ORBITAL TRACKING VEHICLE (POTV)			5. FUNDING NUMBERS	
6. AUTHOR(S) Richard E. Lawrence Jr., Capt, USAF				
7. PERFORMING ORGANIZATION NAME(S) AND ADDRESS(ES) Air Force Institute of Technology WPAFB OH 45433-6583			8. PERFORMING ORGANIZATION REPORT NUMBER AFIT/GA/ENY/92D-05	
9. SPONSORING / MONITORING AGENCY NAME(S) AND ADDRESS(ES) N/A			10. SPONSORING / MONITORING AGENCY REPORT NUMBER	
11. SUPPLEMENTARY NOTES				
12a. DISTRIBUTION / AVAILABILITY STATEMENT Approved for public release; distribution unlimited			12b. DISTRIBUTION CODE	
13. ABSTRACT (Maximum 200 words) <p>A propulsion configuration is defined for a precision orbital tracking vehicle (POTV) that employs electrodynamic forces to control vehicle attitude and position with respect to another spacecraft. A pair of electrically powered thrusters assist the POTV in position control. The vehicle can maintain continuous standoff at close range from another spacecraft in any direction, has docking capability, and has gross orbital transfer capability. These capabilities and the specific design derived for the POTV have been defined by the requirements of a postulated space facility (ASSET) that salvages structural aluminum from the external fuel tank of the space shuttle. Precision control of the POTV is achieved by an electrical conductor configuration that makes current-produced thrust continuously available for independent control of components of vehicle attitude and translation. A robust tracking controller is designed that guarantees stability and compensates for modelling error.</p>				
14. SUBJECT TERMS Tethering, Spacecraft Docking, Tracking, Space Shuttle External Tank			15. NUMBER OF PAGES 142	
			16. PRICE CODE	
17. SECURITY CLASSIFICATION OF REPORT Unclassified	18. SECURITY CLASSIFICATION OF THIS PAGE Unclassified	19. SECURITY CLASSIFICATION OF ABSTRACT Unclassified	20. LIMITATION OF ABSTRACT UL	